Flood Prevention Guayaquil

A feasibility study on local stormwater storage and the effect of sea branch closure to prevent pluvial and coastal flooding

Multidisciplinary Project

Floor Molenaar
Tom Pak
Hanna de Pous
Bart-Jan van der Werff

Delft University of Technology

TU Delft Delft University of Technology

Flood Prevention Guayaquil

ESPOL "Impulsando la sociedad del conocimiento"

Boskalis

rhs.

TU Delft | Deltas, Infrastructures & Mobility Initiative

TU Delft | Global Initiative

Flood Prevention Guayaquil

A feasibility study on local stormwater storage and the effect of sea branch closure to prevent pluvial and coastal flooding

Multidisciplinary Project

by

Floor Molenaar

Tom Pak

Hanna de Pous

Bart-Jan van der Werff

Student numbers:	Floor Molenaar	4242769
	Tom Pak	4222237
	Hanna de Pous	4146417
	Bart-Jan van der Werff	4248724
Project duration:	February 12, 2018 – April 6, 2018	
Project Supervisors:	Dr. ir. E. Mosselman	TU Delft
	Dr. J. Gebert	TU Delft
	Dr. ir. M. C. ten Veldhuis	TU Delft
	Dr. ir. M. E. Arias Hidalgo	ESPOL-FICT

An electronic version of this report is available at `http://repository.tudelft.nl/`.

TU Delft Delft University of Technology

Flood Prevention Guayaquil

ESPOL "Impulsando la sociedad del conocimiento"

Boskalis

rhs.

TU Delft | Deltas, Infrastructures & Mobility Initiative

TU Delft | Global Initiative

Preface

This project was set up as a collaboration between TU Delft and ESPOL-FICT, as part of the Civil Engineering Master's degree at TU Delft. Our very special thanks go out to dr. ir. Mijail Arias Hidalgo, our supervisor in Guayaquil, who not only supplied us with an immense data set, introduced us to various authorities, and translated all of our interviews, but also taught us many things about his city and culture. Our thanks also go out to dr. ir. Erik Mosselman, who provided us with contacts in Guayaquil and supervised our project from The Netherlands during the preparation as well as the execution.

We are very grateful for our cooperation with Boskalis. A special thanks go out to ir. Willem Kuiper and ir. Johan Henrotte, who delivered useful input, data and feedback throughout the project.

Our thanks also go out to dr. Julia Gebert and dr. ir. Marie-Claire ten Veldhuis, who supervised our project from the Geo-Engineering and Watermanagement departments, respectively.

Local authorities INOCAR, INAMHI, EMAPAG and the Municipalidad de Guayaquil have been so kind to receive us at their office and answer all of our questions regarding the city and the problems she faces. They also provided us with many data sets; without them, there would not have been a project!

This project is supported by the TU Delft Deltas, Infrastructures & Mobility Initiative, TU Delft Global Initiative and Rinny Huizinga Stichting. We thank them for making this project possible.

Floor Molenaar, Tom Pak, Hanna de Pous, Bart-Jan van der Werff
Guayaquil, April 2018

Abstract

The city of Guayaquil suffers from regular floods. During the wet season, typically from late December until late April or early May, multiple floods per week can occur. Mainly the excessive rainfall in combination with high tide penetrating into the city results in a high flood risk, but some flood-prone areas can also flood in case of spring tide only.

The main objective of this research is to investigate the possibility of reducing pluvial and coastal flooding in urban areas by constructing a (semi-permanent) barrier in a sea branch, which retains the incoming tide and creates storage for excessive rainfall. In addition, local storage areas spread over the city are considered to delay stormwater runoff into the sea branches. Based on a system analysis and by numerical modelling, several closure locations and their effects are assessed.

Temporary storage of stormwater behind a barrier in a sea branch is a suitable solution to prevent both coastal and pluvial flooding. Based on the results of this research and possible locations of the barriers, a combination of three selected barriers is most opportune, because all catchment areas adjacent to a sea branch can drain their stormwater in a closed-off part behind one of these barriers. In order for these barriers to be effective, they must be closed during low tide prior to heavy rainfall. All three barriers are able to withhold the stormwater volume from their corresponding catchment areas during a 10-year design rainfall event. Even in the event of the highest possible water level during low tide, being neap tide in combination with the storm surge of El Niño, the storage capacities are sufficiently large. Besides the large-scale and small-scale solutions that are currently considered by the local authorities, they are advised to also consider the intermediate-scale solution presented in this study.

Local stormwater storage in the form of water squares in parks and playgrounds is a small-scale solution to reduce pluvial flooding. The storage capacity of these areas is much smaller than the storage capacity behind a barrier, but it is a solution for low-lying urban areas that are not adjacent to a sea branch or river. When the storage capacity of parks and playgrounds in some catchment areas is not sufficient, underground storage basins can also be considered as local storage areas.

The local authorities are advised to set up regulations on return periods for designing flood risk-reducing structures and to assess the economic losses of floods in urban areas, in order to be able to estimate the acceptable cost of these structures.

Contents

List of Figures ix

List of Tables xi

Nomenclature xiii

1 Introduction 1
- 1.1 Area of study . . . 1
- 1.2 Problem statement . . . 2
- 1.3 Context . . . 2
- 1.4 Research objective . . . 3
- 1.5 Reading guide . . . 3

2 System description 5
- 2.1 Development of Guayaquil . . . 5
- 2.2 Drainage system . . . 6
- 2.3 Guayas river basin . . . 6
- 2.4 River discharge . . . 6
- 2.5 Tide . . . 9
- 2.6 Precipitation . . . 10
- 2.7 El Niño and La Niña . . . 11
- 2.8 Wind . . . 12

3 Methodology 13
- 3.1 Stormwater . . . 13
- 3.2 Hydrodynamic modelling . . . 13
- 3.3 Local storage . . . 14

4 Stormwater 15
- 4.1 General assumptions and determinations . . . 15
  - 4.1.1 Return periods . . . 15
  - 4.1.2 Rainfall duration typical storm . . . 15
- 4.2 Constant design rainfall . . . 16
- 4.3 Rainfall during El Niño . . . 18
- 4.4 Barrier locations . . . 19
- 4.5 Catchment area . . . 20
- 4.6 Stormwater accumulation . . . 21

5 Hydrodynamic model set-up 23
- 5.1 Boundary conditions . . . 24
  - 5.1.1 Tide . . . 24
  - 5.1.2 River discharge . . . 24
- 5.2 Bathymetry . . . 26
- 5.3 Model validation . . . 27
- 5.4 Observation points and cross-sections . . . 29

6 Local storage 31
- 6.1 Water squares . . . 31
  - 6.1.1 Specifications . . . 33
  - 6.1.2 Suitable locations . . . 33
  - 6.1.3 Infiltration . . . 34
  - 6.1.4 Backwashing . . . 34
  - 6.1.5 Pumping . . . 34

6.1.6 Storage capacity . . . 35
6.2 Underground basins . . . 35
6.2.1 Operation and maintenance . . . 36
6.2.2 Suitable locations . . . 36
6.2.3 Airport . . . 37
6.2.4 Feasibility . . . 37

7 Results **39**
7.1 Simulation approach . . . 39
7.2 Design criteria . . . 40
7.2.1 Storage capacity of a sea branch . . . 40
7.2.2 Storage area in parks and squares . . . 41
7.2.3 Rainfall . . . 41
7.3 Case scenarios . . . 41
7.3.1 CS01 - Reference scenario . . . 41
7.3.2 CS02 - Situation after barrier construction . . . 42
7.3.3 CS03 - Mean discharge . . . 45
7.3.4 CS04 - Neap tide . . . 46
7.3.5 CS05 - El Niño . . . 47
7.3.6 CS06 - El Niño during neap tide . . . 48
7.4 Conclusions . . . 50

8 Discussion **51**
8.1 Stormwater . . . 51
8.2 Hydrodynamic modelling . . . 52
8.3 Local storage . . . 53

9 Conclusions and Recommendations **55**
9.1 Conclusions . . . 55
9.2 Recommendations . . . 55

Bibliography **57**

A Flood-prone areas **61**

B Satellite Images **63**
B.1 Guayaquil . . . 64
B.2 La Trinitaria . . . 65

C Catchment areas **67**
C.1 Typical runoff parameters . . . 67
C.2 Pipelines . . . 69

D Local authorities **71**
D.1 Instituto Nacional de Meteorología e Hidrología (INAMHI) . . . 71
D.2 Instituto Oceanográfico de la Armada (INOCAR) . . . 71
D.3 Risk Management Department of the Municipality of Guayaquil . . . 72
D.4 Empresa Pública Municipal de Agua Potable y Alcantarillado de Guayaquil (EMAPAG-EP) . . . 72

E Probability distributions **73**

F Design rainfall **75**
F.1 Locations meteorologic measuring stations . . . 75
F.2 Intensity per 24 hours . . . 76
F.3 Intensity per duration . . . 76

G Design discharge **79**

H Local storage **83**
H.1 Locations and sizes of possible local storage areas . . . 84
H.2 Soil profiles of park locations . . . 86

List of Figures

1.1 Map of Guayaquil (Google, ndb) . . . 1
1.2 Photographs of floods in Guayaquil (API, 2016; José Morán, 2016; Cedeño, 2018) . . . 2

2.1 Urdesa in 1952 . . . 5
2.2 Average river discharge per month (based on data from INAMHI) . . . 7
2.3 Guayas river discharge: Average and El Niño 1997-1998 (based on data from INAMHI) . . . 8
2.4 Annual variation Daule river (based on data from INAMHI) . . . 8
2.5 Water depth at Puerto Nuevo tidal station . . . 9
2.6 Tidal amplitudes and phase lags in the estuary (Barrera Crespo, 2016) . . . 9
2.7 Average rainfall (based on data from INOCAR) and temperature (based on data from INAMHI) . . . 10
2.8 Relation between average daily rainfall and average Guayas river discharge . . . 11
2.9 Ocean-atmospheric outline of El Niño and La Niña (INOCAR, 2016) . . . 11
2.10 Wind direction and velocities in Guayaquil (Suárez Changuán, 2010) . . . 12

3.1 Definition of water level (ζ) and water depth (h) (Deltares, 2015) . . . 14
3.2 Conceptual example of an unstructured grid (Kernkamp et al., 2011) . . . 14

4.1 Average rainfall per hour of the day . . . 16
4.2 Probability distribution of the duration of a storm . . . 17
4.3 IDF curves for the city of Guayaquil . . . 18
4.4 Possible barrier locations in the sea branches (Google, ndb) . . . 19
4.5 Division of the city into catchment areas, based on altitude and stormwater pipe maps (Google, ndb) . . . 21

5.1 Unstructured grids of the sea branches and Guayas river . . . 23
5.2 Discharge stations for the Daule river and the tributaries of the Babahoyo river (based on ArcGIS Pro render) . . . 25
5.3 Boundaries and sources in the Delft3D-FM model . . . 26
5.4 Bathymetry relative to MSL and tidal gauges in the Delft3D-FM model in meters . . . 27
5.5 Measured and computed water levels at Puerto Nuevo tidal station . . . 28
5.6 Observation points and cross-sections in the Delft3D-FM model . . . 29

6.1 Bellamy water square (Gemeente Rotterdam, 2012; Straatbeeld, 2014) . . . 32
6.2 Benthem water square (De Urbanisten, 2013) . . . 33
6.3 Stormptrap underground stormwater basin (Stormtrap, 2016). . . . 36

7.1 Cumulative discharge through a cross-section . . . 40
7.2 Water level in the Estero Salado near Febres Cordero during regular tide . . . 41
7.3 Water depth in the Port of Guayaquil after modelled construction of barriers . . . 43
7.4 Water level in the Estero Salado near Febres Cordero after modelled construction of barriers . . . 43
7.5 Cumulative discharge through the cross-section of barrier 5 after modelled construction of possible barriers . . . 44
7.6 Water depth in the Port of Guayaquil for 10-year discharge and mean annual discharge . . . 45
7.7 Water level in the Estero Salado near Febres Cordero during neap tide . . . 46
7.8 Water level in the Estero Salado near Febres Cordero for El Niño . . . 47
7.9 Water level in the Estero Salado near Febres Cordero for El Niño during neap tide . . . 48
7.10 Wetted cross-sectional area of barrier 1 . . . 49

8.1 Missing bathymetry data in the inner estuary . . . 52

A.1 Areas prone to flooding (Municipalidad de Guayaquil, 2015) 62

B.1 Old satellite images of Guayaquil (Google, nda) 64
B.2 Old satellite images of La Trinitaria district (Google, nda) 65

C.1 Characterisation of ground cover in urban areas (Butler and Davies, 2004) 67
C.2 Part of the system of pipelines in Guayaquil (based on ArcGIS Pro render) 69

F.1 Locations of used rainfall stations (based on ArcGIS Pro render) 75
F.2 PDF and CDF of Bellavista (1 hour) 76
F.3 PDF and CDF of Bellavista (2 hour) 77
F.4 PDF and CDF of Bellavista (4 hour) 77
F.5 PDF and CDF of Bellavista (8 hour) 77
F.6 PDF and CDF of Bellavista (12 hour) 77
F.7 PDF and CDF of Bellavista (24 hour) 78
F.8 IDF curve per measuring station 78

G.1 PDF and CDF of Daule river 80
G.2 PDF and CDF of Zapotal river 80
G.3 PDF and CDF of Vinces River 80
G.4 PDF and CDF of San Pablo river 81
G.5 PDF and CDF of Chimbo river 81

H.1 Locations of possible underground basins (Google, ndb) 84
H.2 Locations of possible water squares (Google, ndb) 85

List of Tables

2.1 Average river discharge (m^3/s) per month (based on data from INAMHI) 7

4.1 IDF curve values of Guayaquil 18
4.2 Stormwater accumulation per catchment area 22

5.1 Tidal components in the Gulf of Guayaquil (Barrera Crespo, 2016) 24
5.2 Overview discharge data 25
5.3 Discharge $[m^3/s]$ per return period 26
5.4 Difference between MLWS and MSL for different regions (INOCAR, 2018b) 27
5.5 Measured and computed tidal components from Puerto Nuevo tidal station 28

6.1 Local storage per catchment area 34
6.2 Underground basins areas 37

7.1 Stored stormwater per barrier during regular conditions 42
7.2 Possible combinations of barriers 44
7.3 Stored stormwater for barrier 5 with different barrier combinations 45
7.4 Stored stormwater per barrier during mean river discharge 46
7.5 Stored stormwater per barrier during neap tide 47
7.6 Stored stormwater per barrier during El Niño 48
7.7 Stored stormwater per barrier during El Niño and neap tide 49

C.1 Typical values of runoff coefficient in urban areas (Urban Water Resources Council, 1992) 67
C.2 Runoff coefficient per catchment area 68

F.1 Daily maximum rainfall per return period 76
F.2 RMSE per duration for Bellavista rainstation 76

G.1 RMSE discharge 79

H.1 Sizes of possible water squares 85
H.2 Coordinates of soil profiles 86
H.3 Soil profiles near the possible water square locations 87

Nomenclature

α	Scale parameter
$\hat{y}$	Fitted data point
∇	Spatial gradient
$\overline{x}$	Time-average of measured data points
$\overline{y}$	Time-average of computed data points
∂	Partial derivative
$\vec{u}$	Depth-averaged velocity vector
ζ	Water level elevation
A	Catchment area
C	Runoff coefficient
c_f	Bed friction coefficient
d	External forces in the system
$F_x(x)$	Integrated function of x
$f_x(x)$	Function of x
g	Gravitational acceleration
h	Time-averaged water depth
i	Precipitation intensity
k	Shape parameter
n	Number of samples
q	Specific discharge (sources and sinks in the system)
t	Time
u	Location parameter
V	Total accumulated volume of water
x	Computed data point
y	Measured data point
CDF	Cumulative density function
CS01	Reference case scenario
CS02	Barrier case scenario
CS03	Mean discharge case scenario
CS04	Neap tide case scenario
CS05	El Niño case scenario
CS06	El Niño during neap tide case scenario
Delft3D-FM	Delft3D Flow Flexible Mesh

EMAPAG-EP	Empresa Municipal de Agua Potable y Alcantarillado de Guayaquil EP
ENSO	El Niño southern oscillation
GEV	Generalised Extreme Value
HW	High water
HWS	High water slack
IDF	Intensity density frequency
INAMHI	Institucional Nacional de Meteorología e Hidrología
INOCAR	Instituto Oceanográfico de la Armada
MLWS	Mean low water surface
MSL	Mean sea level
PDF	Probability density function
POT	Peaks over threshold
RMSE	Root-mean-square error

1 Introduction

1.1. Area of study

The Gulf of Guayaquil (see Figure 1.1) is the largest estuarine ecosystem on the Pacific coast of South America. More than 20 rivers discharge into the Gulf of Guayaquil. The gulf has a shelf boundary with a width of more than 200 km. The tidal signature reaches far into the inner estuary, known as the Guayas river estuary. The city of Guayaquil is located at the northern point of this estuary. In the southwest of the city, a relatively large sub-estuary, the Estero Salado (meaning 'salty estuary'), enters the city, where it bifurcates into multiple sea branches. The Guayas river forms at the confluence of the Babahoyo and Daule rivers, on the east side of the city. It is the major source of freshwater (Twilley et al., 2001). An overview is shown in Figure 1.1.

The city of Guayaquil, located in the southwest of Ecuador, is the biggest city in the country. It houses over 2.3 million residents and is the country's economic heart. The city was established in the 16th century. The area was mainly water-dominated at first, having multiple sea branches reaching deep into the city. Over the years, residents have filled up those sea branches and covered them for urbanization purposes. The city has expanded rapidly and is also heavily industrialised. Nowadays, only a few branches remain.

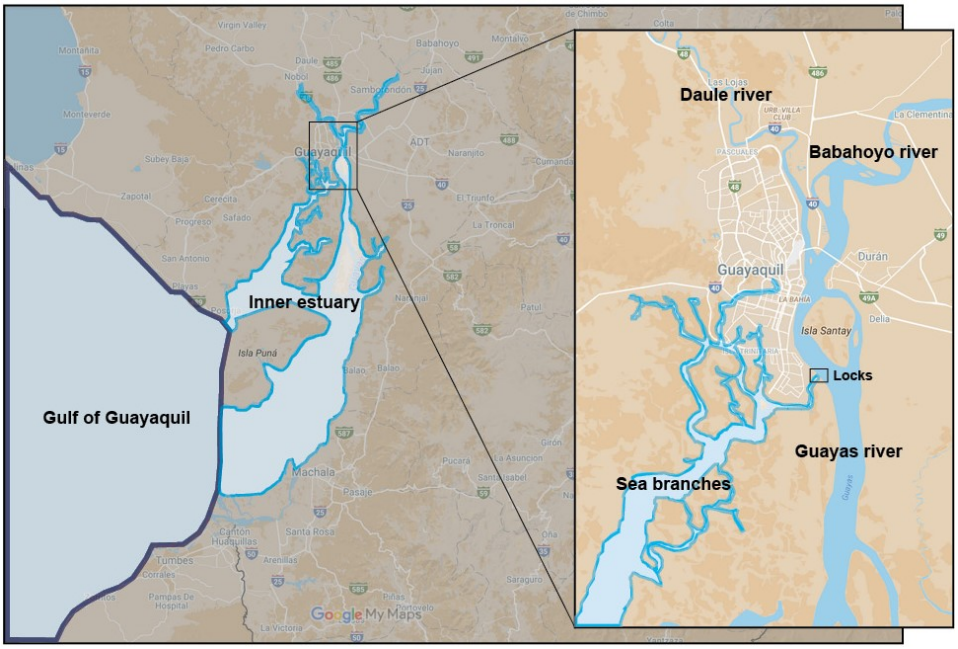

Figure 1.1: Map of Guayaquil. Zooming in, the confluence of the Daule and Babahoyo into the Guayas river is seen. Locks separate the sea branches from the river (Google, ndb)

The port of Guayaquil is the main port of Ecuador and its productive activities represent over 20% of the country's global economy (Vera-Grunauer et al., 2006). It is located about 70 km north of the Gulf of Guayaquil. Container ships export mostly banana, cacao, coffee, and shrimps. The route from the port to open sea, however, is long and passes mangrove-like areas. Plans for a new deepwater port near the coast are being made which will increase the capacity and the draft of the port (DP World, 2016).

1.2. Problem statement

The city of Guayaquil suffers from regular floods. During the wet season, typically from late December until late April or early May, multiple floods per week can occur, although the exact frequency is not known. The high flood risk is mainly caused by pluvial flooding due to excessive rainfall in combination with coastal flooding due to the high tide penetrating into the city. However, some flood-prone areas can also flood in case of spring tide only (Betancourt et al., 2013). An overview of the flood-prone areas within Guayaquil is shown in Appendix A.

Figure 1.2 gives an impression of different flooding events in 2016 and 2018. Streets are flooded and water can enter houses. The daily activities of citizens are significantly affected during a flooding.

The floods have multiple causes. Due to the rapid expansion of the city, most of the area is covered in concrete, leaving no infiltration areas for rainwater. Secondly, space once occupied by sea branches is now filled up and turned into urban areas, so less space is reserved to retain the water inside the city. When rainfall occurs during high tide, the sea branch is already filled and the runoff water makes the water in the branches overflow its banks. On top of that, the stormwater system cannot drain the low lying areas: During high tide, the stormwater system backwashes and water flows onto the streets. In some areas, the amount of drains is insufficient, leading to accumulation of rainwater on the streets.

The described problems are worsened by an El Niño event. During such an event, mean water levels are higher and rainfall intensities increase. Also, predicted sea level rise due to climate change threatens to further increase the city's flooding problems (CAF, 2017).

Because of the complexity of the flooding problems, an integral solution is needed. An optimal measure accounts both for the inflow of the tidal sea as well as for processing excessive rainfall. As stated in Stenfert et al. (2017), a possible measure is closing off one or multiple sea branches during high tide or extreme weather events, creating storage area and reducing water levels at the same time.

Figure 1.2: Photographs of floods in Guayaquil. Left: January 25, 2016 (API, 2016), middle: February 2, 2016 (José Morán, 2016), right: February 19, 2018 (Cedeño, 2018)

1.3. Context

Different studies into the hydrological and hydrodynamic system have been carried out over the past years. Stenfert et al. (2017) executed an overall analysis on floods and its critical points within the city of Guayaquil. They briefly considered different measures to reduce the risk of flooding.

A study of Garcés Santander (2017) into the perception of citizens in flood-prone areas shows that there is no clear insight into the causes of the flood problems. Only a minority of people in the city relate flooding to the high tide in combination with intense rainfall periods. The prevailing idea is that garbage on the street is the major cause of the problems because they clog the stormwater pipes. From interviews conducted, it is clear

that citizens experience multiple negative effects of the floods: Damage to property and assets, reduction of sales, and health problems.

A study funded by The Corporacion Andina de Fomento (CAF) (2017), a development bank in Latin America, provides a broad analysis on the vulnerabilities of the city of Guayaquil due to climate change. In this study, areas with an increased flood risk are identified.

Local authority Empresa Municipal de Agua Potable y Alcantarillado de Guayaquil (EMAPAG) has recently initiated two studies into barriers in the inner estuary: A small-scale barrier to be placed in the Brazo Represado to create storage area for stormwater, and a large-scale barrier to close off the entire inner estuary to prevent the high tide from forcing its way into the city (M. Orta, personal communication, March 27, 2018).

1.4. Research objective

The main objective of this research is to investigate the possibility of reducing pluvial and coastal flooding in urban areas by constructing a (semi-permanent) barrier in a sea branch, which retains the incoming tides and creates storage for excessive rainfall. In addition, local storage areas spread over the city are considered to delay stormwater runoff into the sea branches. Based on a system analysis and by numerical modelling, several closure locations and their effects are assessed in this research.

1.5. Reading guide

Chapter 2 describes the current hydrologic and hydrodynamic conditions in the city and the estuary. Chapter 3 contains the methodology. The report consists of three parts, which are elaborated upon in Chapters 4, 5 and 6. In Chapter 4, the catchment areas in the city and the design values for rainfall are determined. Chapter 5 explains the Delft3D-FM model set-up and the design values for the discharge in the rivers. Chapter 6 explains and quantifies the possibility of local storage in parks around the city. Chapter 7 shows the results for different case scenarios. The discussion in Chapter 8 gives a critical view on the results and limitations of this research, after which the final conclusions and recommendations are summarised in Chapter 9.

2

System description

2.1. Development of Guayaquil

Over the past decades, the city of Guayaquil has expanded rapidly. From 2001 to 2010, the city experienced a population increase of 1.55% per year (Brinkhoff, 2018). Even though the numbers include the complete Municipality of Guayaquil, the increase in residents mainly took place within the urban limits of the city.

Using satellite images of the city of Guayaquil, one can see a clear growth of urban areas (Google, nda). The photographs (see Appendix B) depict Guayaquil in the years 1984 and 2016, respectively. Development has taken place mostly in the northwest part of the city. Large neighbourhoods now cover areas that previously consisted of forests. Where the city was first concentrated next to the Guayas, it now reaches north along the Daule river. As can be seen, the city has doubled in size since 1984.

A particularly interesting development can be observed in La Trinitaria neighbourhood, located in the southwest part of Guayaquil, see Appendix B.2. Over the past years, La Trinitaria grew up to its limits. Satellite images show the expansion of the neighbourhood in 2000 and 2017. Large areas that were once occupied by sea branches have been taken up by the urban district. Parts of sea branches have been greatly reduced in width, as is visible in the furthermost right branch. In addition, no open space is left between the water and the settlements, placing buildings closer and closer to the waterfront.

A clear evolution can also be observed in the port district further south. Great parts of the sea branches have been reclaimed in order to develop the port.

Old photographs show exactly what satellite images already suggest: Much more space used to be reserved for the sea branch, and its banks were covered by wide regions of mangroves. Pictured here is the Urdesa neighbourhood in the year 1952, which is currently a vibrant residential and commercial area.

Figure 2.1: Urdesa in 1952 (city archives)

Concluding, the combination of reducing the size of the branches plus moving buildings closer to the water has exposed both persons and goods at a higher flood vulnerability.

2.2. Drainage system

The city of Guayaquil has a complicated stormwater system. Most of the pipelines follow the street pattern. However, pipe systems that discharge to different waters turn out to be interwoven. A map of the stormwater system is shown in Appendix C.2. Unfortunately, no information on pipe diameters is provided to the authors.

A major problem the city faces is water backwashing through the stormwater pipes during high tide (Betancourt et al., 2013). When this coincides with heavy rainfall, the rainwater is not able to drain and the streets are flooded. Being aware of this problem, EMAPAG (Municipal Division in charge of Water Resources) installed so-called 'duck-peak' valves on 20 pipes in the city to prevent backwashing. According to ir. Juan Ramírez-Ponce, Director of the Municipal Risk Department (personal communication, March 14, 2018), the measure seems to have some positive effects and will be extended to a greater amount of valves throughout the city.

In addition, a large amount of garbage in the drainage system causes a reduction of the runoff. As a prevention procedure, the municipality thoroughly cleans the drainage system every year prior to the rainy season (Juan Ramírez-Ponce, personal communication, March 14, 2018).

Another point of attention is the amount of drains on large highways. During intense rainstorms, the drains may be too far apart, leading to water accumulating in between them.

2.3. Guayas river basin

North of the city, two large rivers are approaching, see Figure 1.1. The Babahoyo river flows from northeastern direction and is fed by tributaries rising in the Andes Mountains, while the Daule river flows from northwestern direction. At Duran, located east of Guayaquil, the two rivers confluence to form the Guayas river, which has a length of about 65 km before discharging into the Pacific Ocean. The tidal effect can be observed over large distances, for approximately 120 km upstream of Guayaquil in the Daule river and approximately 93 km upstream of Guayaquil in the Babahoyo river (Castro et al., 2009). More information on the tides can be found in Section 2.5.

In different areas in the Guayas river system, increases in sedimentation are currently leading to problems with navigability of ships. Sedimentation is caused by the flood-dominant tide transporting sediment landward, see Section 2.5. In addition, there is also an increase in the potential risk of flooding in the lower areas around the margins of the rivers, especially in the northern part of Guayaquil and the cities of Daule and Babahoyo (Barrera Crespo, 2016).

The Guayas river discharges into the Pacific Ocean while the inner estuary originates from this ocean. The Guayas and the sea branches are interconnected at different locations above Isla Puná. There is a lock system located near the Puerto Nuevo, in the south of the city, see Figure 1.1. At the moment of writing, these locks are closed and no actual connection is present between the Estero Cobina and Guayas river.

However, there are plans for restoring this lock system, in a joint corporation between the Port Authority of Guayaquil and EMAPAG (M. Orta, personal communication, 27 March, 2018). When the lock will be restored, the discharge between the Estero Cobina and the Guayas river will remain approximately 0 m^3/s. Therefore, this alteration is not taken into account in this research. The lock system will enable a frequent transport route and, according to González (2017), it possibly provides an additional tide control mechanism helping to reduce flood problems in the area.

2.4. River discharge

The discharge data of five gauging stations in the Daule and Babahoyo river is obtained from the Ecuadorian National Institute of Meteorology and Hydrology (INAMHI). These gauges measure the discharge in the Daule river and in four tributaries of the Babahoyo river: the Zapotal, Vinces, San Pablo, and Chimbo river. Daily discharge measurements are available from 1963 to 2015. The dataset is not complete as for some years no data are available or measurements for specific days or months are missing.

In the year 1988, the Daule Peripa Dam was constructed, having a large influence on the discharges in the Daule river and therefore in the Guayas river as well. Only the discharge rates of the Daule river after 1988 are used because only the current situation is taken into account.

The average discharge rate per month for all five rivers is given in Table 2.1. In Figure 2.2 the average river discharge per month is plotted to give a clear view on the monthly variations. Large differences in discharge occur comparing the wet season with the dry season. High discharges during the wet season are expected between February and April and the minimum between August and October.

Table 2.1: Average river discharge (m^3/s) per month (based on data from INAMHI)

	Daule	Vinces	Zapotal	Chimbo	San Pablo
Jan	213.43	233.98	183.33	25.03	68.94
Feb	445.13	480.85	414.14	64.37	148.51
Mar	598.10	504.67	462.67	76.23	162.65
Apr	613.21	530.99	402.42	80.78	152.28
May	401.24	313.06	238.21	56.66	89.78
Jun	180.78	125.95	107.00	17.33	35.91
Jul	154.33	61.76	55.88	7.44	17.23
Aug	124.44	39.28	36.21	3.56	8.67
Sep	106.33	23.64	27.88	1.73	3.43
Oct	96.77	20.72	23.11	6.94	3.34
Nov	126.72	19.49	20.52	3.85	2.26
Dec	148.71	35.70	27.25	4.76	14.08
Wet season	552.15	505.50	426.41	73.80	154.48

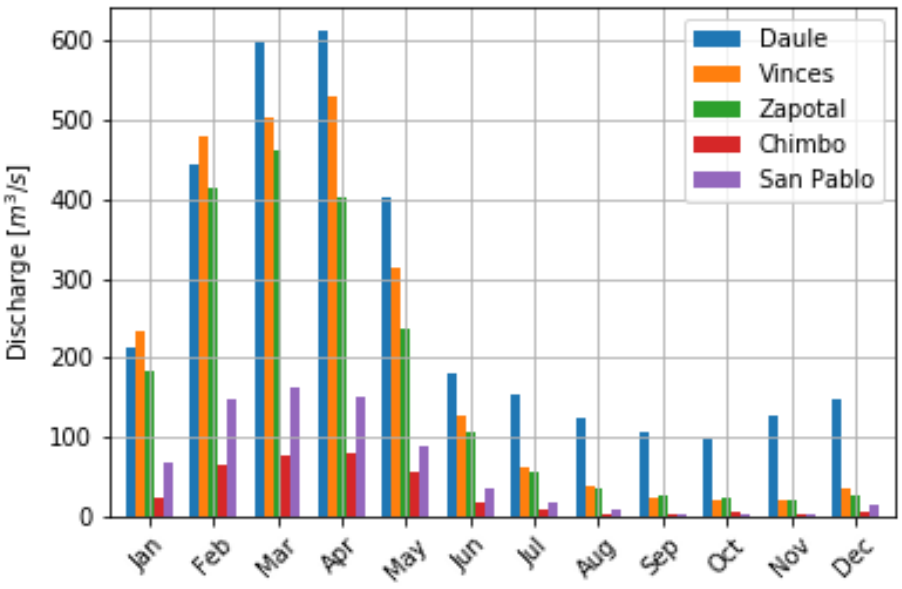

Figure 2.2: Average river discharge per month (based on data from INAMHI)

During an El Niño event, the river discharges significantly increase, as can be seen in Figure 2.3 for the Daule river. Unfortunately, there are no discharge measurements available of all of the Babahoyo tributaries, so this comparison cannot be made for the Babahoyo river.

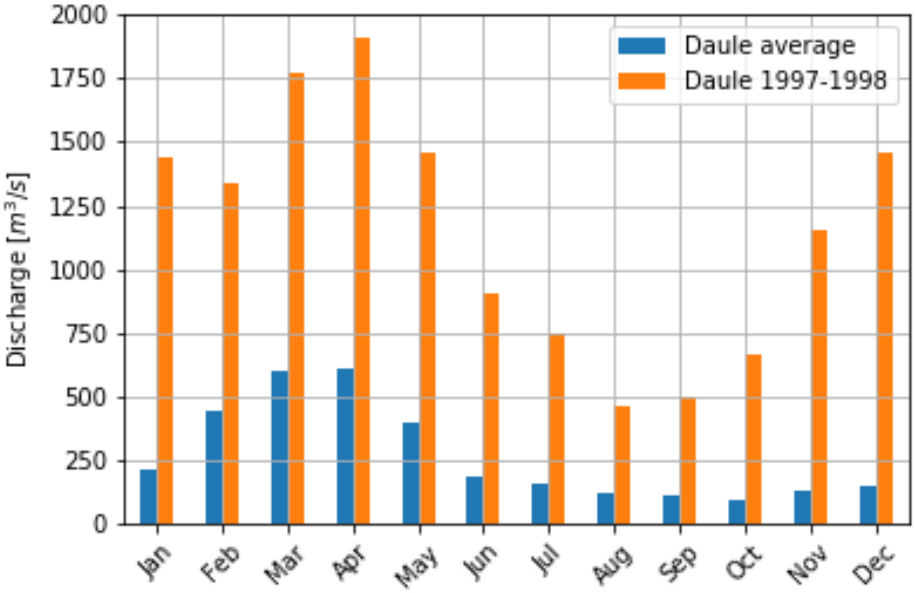

Figure 2.3: Guayas river discharge: Average and El Niño 1997-1998 (based on data from INAMHI)

In Figure 2.4 the variation pver different years of the Daule river discharge per month is visualised using data from 1989-2014. As can be seen, large variations are present, especially during the wet season. Multiple El Niño events are included in this dataset.

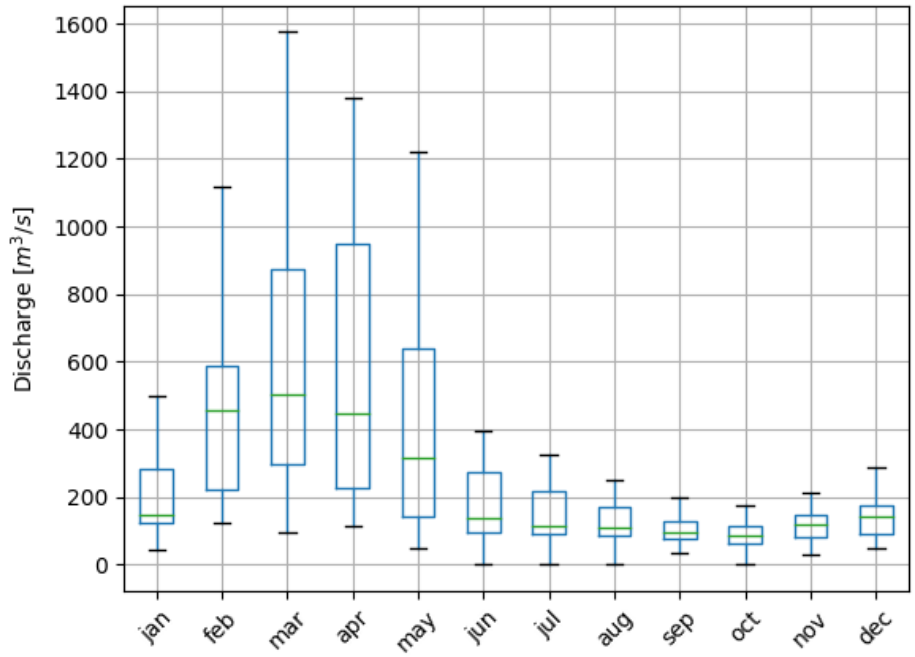

Figure 2.4: Annual variation Daule river (based on data from INAMHI)

2.5. Tide

The entrance of the outer estuary is more than 200 km in width and convergences further upstream. The tidal amplitude increases as the wave propagates landward, because convergence has a larger effect than friction (Barrera Crespo, 2016; Betancourt et al., 2013). The water level elevation in Puerto Nuevo is shown in Figure 2.5 and shows a maximum tidal wave height of approximately 4.5 m. The tidal environment is semi-diurnal (i.e. two high tides per day), see also Subsection 5.1.1.

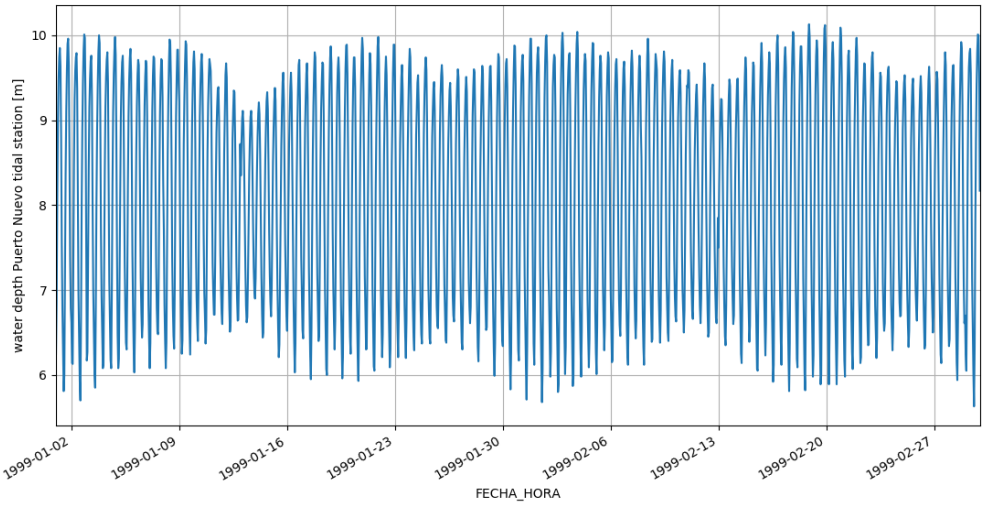

Figure 2.5: Water depth at Puerto Nuevo tidal station

Large variations of the water level makes the influence of the tide within the city clearly noticeable. As explained in Section 2.3, the tidal signature reaches far into the inner estuary.

Because the phase lag between high water (HW) and high water slack (HWS) is approximately 1 hour, the tidal system is considered to be flood dominant (Barrera Crespo, 2016). This implies that the rising period is faster than the falling period and maximum tidal flood velocities are higher than maximum tidal low tide velocities. Because sediment transport is related to the flow velocity, there is a net landward sediment transport in the inner estuary, slowly filling up the sea branches.

The tidal amplitudes and phase differences in the estuary are visualised in Figure 2.6.

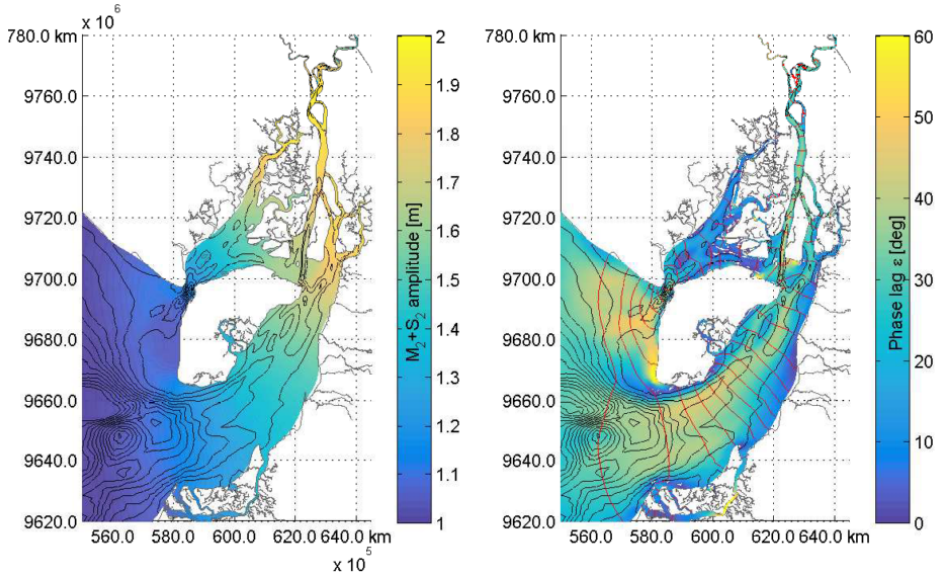

Figure 2.6: Tidal amplitudes and phase lags in the estuary (Barrera Crespo, 2016)

2.6. Precipitation

The ocean currents El Niño (warm front) and Humboldt (cold front), as well as the Andean Mountains, have a large impact on the climate in Guayaquil. The city therefore experiences a strong wet and dry season. However, the temperature is more or less constant over the year. The wet season is short, usually lasting from January till early May. In an average year about 90% of the rainfall falls between December and April, with maximum values in February and March (CAF, 2013).

As can be seen in Figure 2.7, the wet season is intense. In March, the wettest month, 280 mm of rain falls on average. In comparison, the annual rainfall in The Netherlands is about 880 mm (Rijksoverheid, 2016). Rainfall of 80 to 120 mm/day is not unusual and even up to 200 mm per day is measured, according to data provided by Instituto Oceanográfico de la Armada (INOCAR).

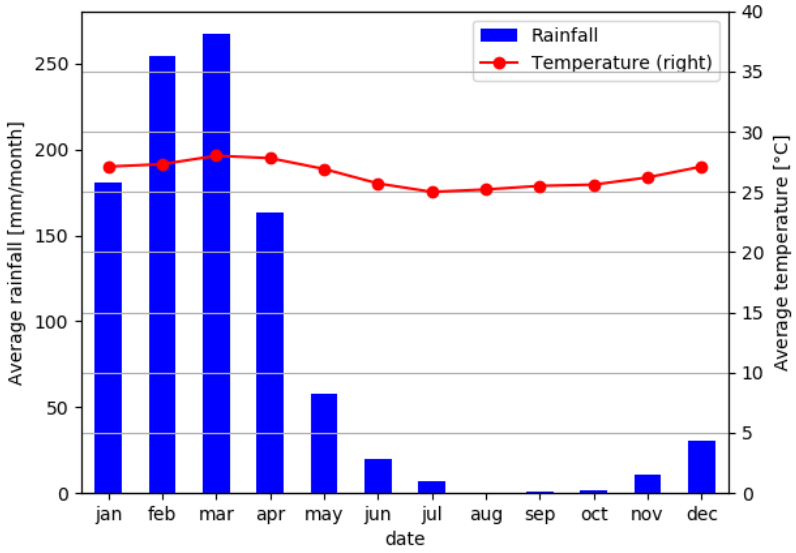

Figure 2.7: Average rainfall (based on data from INOCAR) and temperature (based on data from INAMHI)

Rainfall data from three different institutions is obtained: INOCAR, INAMHI and EMAPAG. The measuring stations are located in different parts of the city. Comparing data of the different stations shows that rainfall events can differ over small distances within the city. Typical rainfall events are short, intense and therefore local. In addition, vegetation within the city differs greatly, which might lead to microclimatic zones (Ing. Jaime Fuentes, personal communication, March 13, 2018).

Both the river discharges and the precipitation show a clear wet and dry season. In Figure 2.8 the monthly averaged Guayas river discharge is compared with the monthly averaged rainfall, using data from 2012-2014. Discharge data of the Daule river and four tributaries of the Babahoyo river is summed to estimate the Guayas river discharge. Rainfall data from INOCAR is used. From this figure, it can be concluded that high discharges and high precipitation rates are likely to coincide, possibly leading to an increased flood risk.

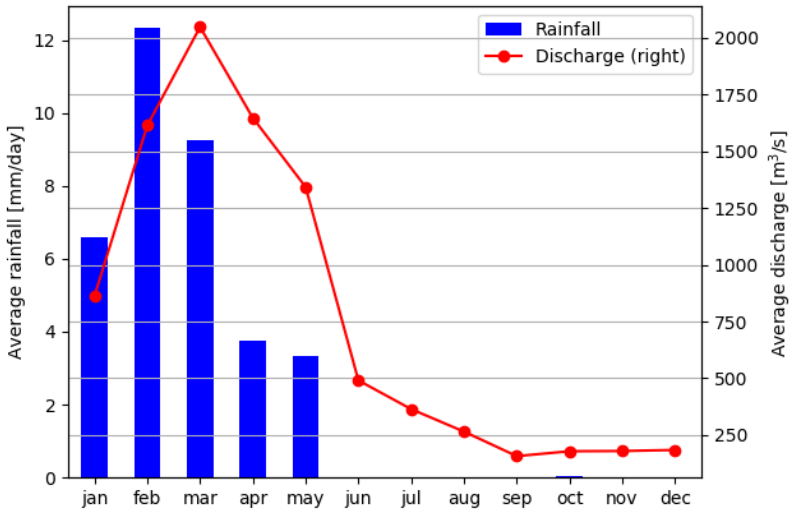

Figure 2.8: Relation between average daily rainfall and average Guayas river discharge

2.7. El Niño and La Niña

The ENSO phenomenon (El Niño Southern Oscillation) is known as one of the largest global scale and most severe climatic events. El Niño and La Niña can be seen as opposite phases, where El Niño is the warm phase and La Niña the cold phase of this phenomenon (NOAA, 2017).

El Niño causes the influx of unusually warm surface water to the southeast Pacific Ocean, which triggers a change in the climate patterns at several places on earth. It can cause heavy rainfalls, prolonged droughts and major floods, especially in Latin America. In the coastal areas of Ecuador, it prompts heavy rainfalls. The rainfall associated with El Niño can be twice the amount of rainfall of a regular year. In addition, an increase in water levels in the Gulf of Guayaquil can occur. The left image of Figure 2.9 shows the atmospheric outline of El Niño. Ecuador suffered from El Niño in the following years: 1972-1973, 1982-1983, 1997-1998, and 2009-2010, leading to an increased flood risk. During the 1997-1998 event, a water level increase up to 42 cm was reported (CAF, 2000).

Each El Niño is unique in strength, duration, and how it affects the global weather and is therefore hard to predict. El Niño episodes typically occur at irregular intervals of three to five years. However, in the historical record, this interval has varied from two to seven years. It lasts 9 months to 2 years. The average return period length is 5 years (NOAA, 2017).

According to INOCAR (2011), the La Niña phenomenon can lead to a decrease of rainfall in Ecuador. However, in other regions in South America (i.e. Northern Colombia) an increase in rainfall can be noticed. The atmospheric outline of La Niña is shown in the right image of Figure 2.9. Because of the scope of this project, the La Niña phenomenon is not further taken into account.

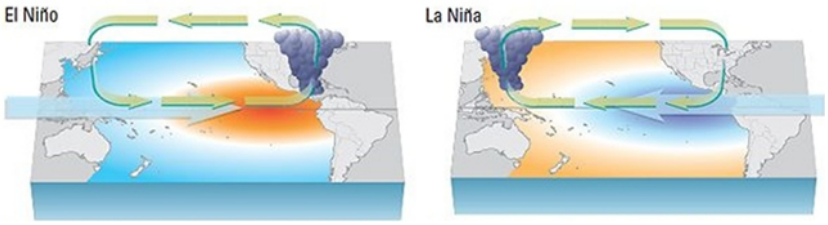

Figure 2.9: Ocean-atmospheric outline of El Niño and La Niña (INOCAR, 2016)

There is no consensus on whether climate change will have any influence on the occurrence, strength or duration of El Niño events (NOAA, 2017).

Because of the extreme rainfalls that can occur during an El Niño event in Ecuador, it is important to take this phenomenon into account when determining design precipitation rates and water levels.

2.8. Wind

The effect of wind on water waves could influence potential solution designs. Suárez Changuán (2010) shows that the wind direction is predominantly from the southwest and the maximum wind velocity is 8 m/s, see Figure 2.10. With a fetch of approximately 70 km from El Morro Channel to Puerto Nuevo, the significant wave height can increase to a maximum of 0.8 m using the method of Sverdrup-Munk-Brettschneider (Schiereck, 2012). However, the complex geometry and the many bifurcations of the sea branches will significantly reduce the wave height once it enters the city. This means the tidal wave height in the inner estuary is much larger than the wave height and that wind waves will be neglected in the rest of this study.

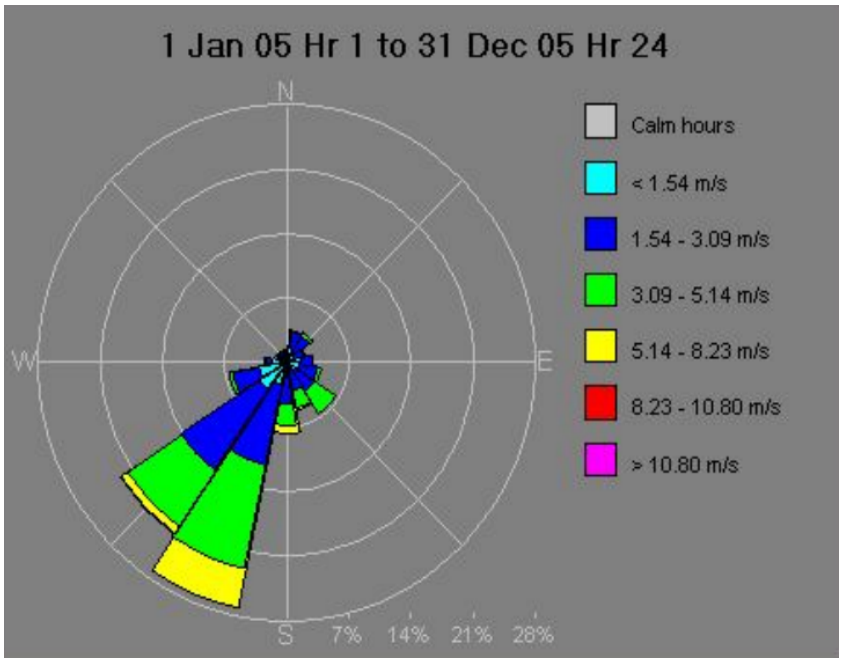

Figure 2.10: Wind direction and velocities in Guayaquil (Suárez Changuán, 2010)

3

Methodology

The project is divided into three parts: The stormwater analysis, modelling a barrier in one of the sea branches, and an investigation into small-scale local storage. These subjects are all fully elaborated on in the corresponding chapters. In this section, the methods used in each of these chapters are briefly explained in order to form a clear overview of this research project.

The sea branch will be closed using a semi-permanent barrier, see Section 4.4. However, the exact type, construction method as well as the costs will not be considered within this research. Neither the technical feasibility nor the risk of failure of the barrier itself will be taken into account. It is assumed that the barrier will be able to obstruct high tidal water levels, for example during spring tide or El Niño.

During this project, multiple interviews with local authorities are conducted. A brief description of those authorities can be found in Appendix D.

3.1. Stormwater

Rainfall data is provided by multiple authorities. These different datasets are compared for validation before the design rainfall is determined, using statistical distributions as Gumbel, Weibull, and Fréchet to obtain Intensity Duration Frequency (IDF) curves. From these IDF curves, the rain intensity per duration and return period can be read.

The city is divided into catchment areas, using altitude maps and local stormwater system maps. This is needed to be able to determine where the rainwater will flow. A runoff coefficient is determined per area to calculate the total amount of runoff generated per catchment area. With this, the needed dimensions of the storage basin can be determined.

3.2. Hydrodynamic modelling

In order to determine the effects of a possible closure of part of the sea branches, a hydrodynamic model in Delft3D Flow Flexible Mesh (Delft3D-FM) is used. Delft3D-FM solves the two- and three-dimensional shallow water (Navier-Stokes) equations. The delta of Guayaquil is modelled in a 2D depth-averaged model since morphology or stratified flows of fresh and salt water are not of importance for this research. The 2D-shallow water equation describes the conservation of mass and momentum, shown in Equation (3.1) and (3.2) respectively.

$$\frac{\partial \zeta}{\partial t} + \nabla(h+\zeta)\vec{u} = q \tag{3.1}$$

$$\frac{\partial \vec{u}}{\partial t} + \vec{u}\nabla\vec{u} + g\nabla\zeta + \frac{c_f}{h+\zeta}|\vec{u}|\vec{u} = d \tag{3.2}$$

Where ∇ is the spatial gradient: $\nabla = \partial/\partial x + \partial/\partial y$, $\vec{u}$ is the depth-averaged velocity vector, ζ is the water level elevation (as visualised in Figure 3.1), h is the time-averaged water depth, and c_f is the bed friction coefficient. On the right side of the equations, q and d are the sources and external forces in the system, respectively.

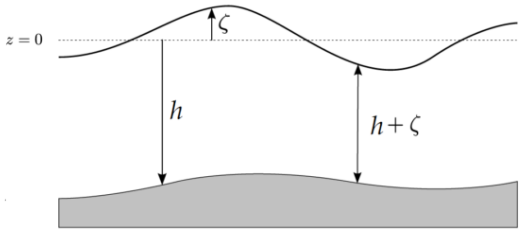

Figure 3.1: Definition of water level (ζ) and water depth (h) (Deltares, 2015)

Delft3D-FM runs on unstructured grids. The main advantage of an unstructured grid relative to a structured grid is an increased spacial freedom, because grid cells can be placed in random sequence and grid cells can take multiple shapes, like triangular or pentagonal. A conceptual example of an unstructured grid is shown in Figure 3.2. The layout of the grid can follow the land boundaries of the area more flexibly, without creating losses of energy due to the generation of staircase boundaries.

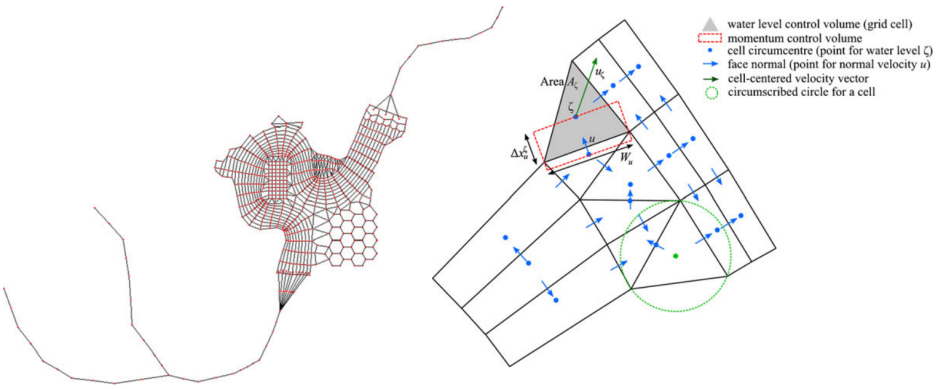

Figure 3.2: Conceptual example of an unstructured grid (Kernkamp et al., 2011)

The complicated geometry of the estuary and the delta of Guayaquil requires a high flexibility in the shape and resolution of grid cells. The set-up of the model is explained in Chapter 5.

Different boundary conditions need to be implemented. At the open sea, the boundary is an astronomical tide. To determine the boundary conditions located at the Daule and Babahoyo rivers, a probabilistic analysis is conducted to compute the design discharge.

The Delft3D-FM model is used to assess the impact on the estuary when one or multiple sea branch closures are constructed at certain locations. The optimal location for a closure requires that there are no increased water levels in the city outside the closed-off area. If the probability of a flood outside the closed-off area has increased, the corresponding closure location will be disregarded in future analyses.

3.3. Local storage

Flooding due to rainwater accumulation in the lower parts of neighbourhoods will not be resolved by placing a barrier in the sea branches; water is unable to drain towards it. Therefore, a preliminary study into local solutions in the form of underground basins and water squares is performed. Requirements for these type of solutions are drawn up based on reference projects, after which possible suitable locations are determined within flood-prone areas. Finally, global storage capacities are determined.

4

Stormwater

A thorough analysis of the rainfall over the city needs to be executed in order to determine if the created storage areas will be sufficient. In this section, some general assumptions are explained, after which a constant design rainfall and catchment areas are elaborated on. Finally, water accumulation per catchment area can be estimated.

4.1. General assumptions and determinations

4.1.1. Return periods

One uncertainty that remains throughout the project is the design return period. The return period chosen for computing the design values is based on a balance between costs and benefits. The main question is what society and the client see as an acceptable return period for an event, in this case the floods. At the moment of writing, there are no guidelines for return periods of barriers within the city (R. Ponce, personal communication, March 14, 2018). Ponce stated that a return period of around 5 to 10 years would be suitable for a project like this. A higher return period will lead to higher project costs and will, therefore, reduce the economic feasibility of the project. On the other hand, for the design of stormwater pipes, return period guidelines are available for the city. For commercial areas and roads with heavy traffic, a return period of 5 to 10 years is suggested (Interagua, 2010a).

The floods mainly cause material damage. Interviews with citizens show that part of the people accept one flood per year and others think no flood is acceptable (Garcés Santander, 2017). In addition, this study shows that the magnitude of the flooding is also important. Lower flood levels are more acceptable because they lead to less damage.

So taking the social and especially the economic feasibility into account, this project group proposes a solution with a return period equal to the highest return period for stormwater pipes, namely 10 years.

4.1.2. Rainfall duration typical storm

From the data, it appears that heavy rainstorms usually have a duration shorter than 4 hours, see Figure 4.2. Ir. Jaime Fuentes (Environmental Engineering) from INOCAR (personal communication, March 13, 2018) confirmed that rain shower duration is about 3 hours on average, although it might take up to a longer period. By closing off a part of the sea branch during low tide, water should be maximally be retained up to 12 hours, which is the time difference between two low tides. The worst case that the basin should be able to handle is, therefore, a rainstorm of 12 hours.

4.2. Constant design rainfall

Rainfall data is provided by INOCAR, INAMHI, and EMAPAG. The goal is to combine all data and determine a design rainfall event for different return periods for the complete city of Guayaquil. However, data sets from different authorities do not completely match. This is due to two reasons:

1. The rain is measured in different time steps and for different time spans; INOCAR and INAMHI provide data over many years starting from 1962, in mm/day. EMAPAG provides data over only the last 9 years but measures every hour.
2. The measuring stations are located in different parts of the city and due to the character of the rain showers and the large size of the city, the rainfall can greatly differ per location. Typical rainfall events are short, intense and therefore local. Besides, vegetation within the city differs greatly, which might lead to microclimatic zones within the city (Ing. Jaime Fuentes, personal communication, March 13, 2018)

First, the data from INOCAR and INAMHI are analysed since they cover the largest time span and are thus more reliable to determine longer return periods. An Extreme Value Analysis is performed using the Gumbel, Weibull and Fréchet distributions, see Appendix E. It is concluded that the Gumbel distribution fits the data best. The best fit was determined by analysing both the root-mean-square error (RMSE) and the plot itself. The RMSE is defined as:

$$RMSE = \sqrt{\frac{\sum_{i=1}^{n} \left(\hat{y}_i - y_i\right)^2}{n}} \tag{4.1}$$

where $\hat{y}_i$ is the fitted value, y_i is the measured value, and n is the number of samples.

It must be noted that this rainfall data, measured daily from 00.00h to 00.00h, contains one big disadvantage for this particular research. In reality, most of the rain showers seem to start in the evening. These daily rainfall measurements are here cut off at 00:00h, while the maximum 'total rainfall per 24 hours' may be much higher. Resampling is not possible since more specific data is not available. Downscaling of the daily rainfall data is also not possible, because there is no clear daily rainfall pattern based on the hourly rainfall data. Figure 4.1 shows the mean hourly rainfall in mm for every hour of the day, based on the 9 years of data from EMAPAG.

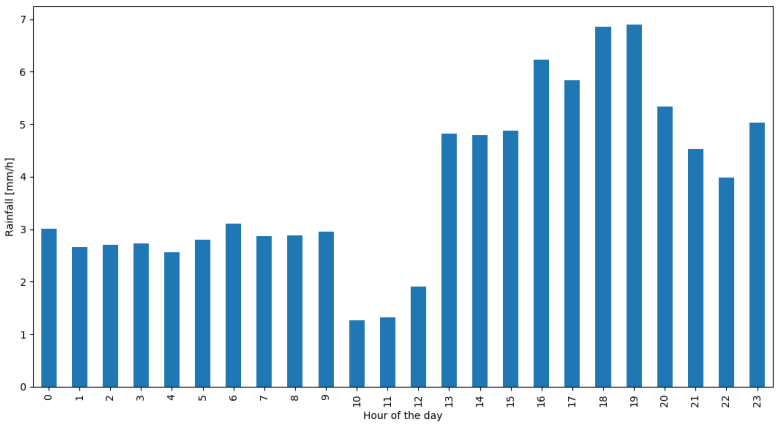

Figure 4.1: Average rainfall per hour of the day

Figure 4.2 shows the probability distribution of the duration of a storm, both with and without a threshold value. These results are based on the data from EMAPAG. This figure does not show that shorter storms are more likely to occur, but that a typical duration of a storm cannot be assigned based on daily rainfall data. It is also possible that multiple (intense) storms occur within one day.

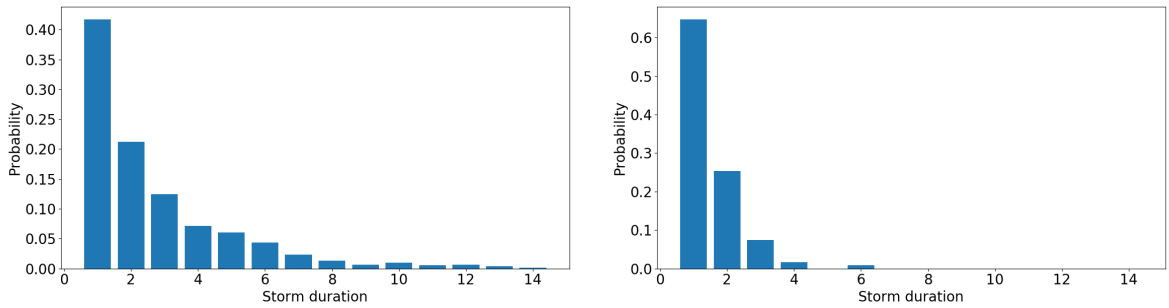

Figure 4.2: Probability distribution of the duration of a storm. On the left: no threshold value. On the right: a threshold value of 10 mm/hour

Because rain showers are independent of each other, one peak per year is not chosen to be the best option to evaluate the data. The Peaks-Over-Threshold method (POT) is considered. The data used for the POT contains all peak flows that are greater than a given threshold flow. The threshold is generally set to include an average of five events per year. Where multiple peak flows occur in a single event, the largest is used for the POT series (Centre for Ecology & Hydrology, 1999) to ensure all showers remain fully independent.

The results from this new analysis, combined with the old results, are found in Appendix F. Due to reasons mentioned above, these new results are considered to represent actual rainfall patterns better.

After determining the intensity per return period for a duration of 24 hours, the EMAPAG data per hour is analysed. To be able to compare it to the INOCAR and INAMHI data, all durations of 24 hours are sampled from 00.00h to 00.00h. EMAPAG provided data from measuring stations all over the city. From these stations, five are selected based on their locations, evenly spread over the area, see Appendix F.1. Since only 9 years of data are available, the POT method is applied again with on average five peaks per year.

Similar to the previous analysis, the Gumbel, Weibull, and Fréchet distributions are fitted and again the Gumbel distribution showed the best fit. While sometimes the RMSE gave a lower value for a different fit, the visual analysis determined that Gumbel fitted the data points better, for example by also taking into account the very outliers. RMSE results are and the plot itself is added in Appendix F.

From a comparison of the intensity per return period, it can be seen that the EMAPAG data from the Bellavista and Progreso station and the INAMHI data fit each other well. All three stations are downtown. On the other hand, the INOCAR data and the stations in the north and south of the city, Juan Montalvo and Trinitaria, show lower intensities per return period. The INOCAR station is located in the south of the city and registers less rainfall in general compared to the other stations. This can be due to, again, the city being widespread and local microclimates.

As the data from EMAPAG is comparable to the long-term data from INAMHI and INOCAR, the data can be considered representative. Of course, it must be mentioned that uncertainty remains and the authors highly advise to always measure rainfall per hour or even shorter time steps in the future. Due to a lack of complete rainfall data for some stations, the average of the different stations is taken as one value for the complete city.

Elaborating on the EMAPAG data, smaller rainfall durations are now analysed. Durations of 1, 2, 4, 8, 12 and 24 hours are sampled. Rainfall intensities are calculated at intervals of 1 hour. For example for a duration of 4 hours, the intensity is calculated from 00:00h to 04:00h, from 01:00h to 05:000h, from 02:00h to 06:00h, etc. This resampling is done for every duration.

Intensity Duration Frequency (IDF) curves are created, see Table 4.1 and Figure 4.3, for return periods of 2, 5, 10, 25, 50 and 100 years using the values found by the Gumbel fit, see Appendix F.3. From these curves, a constant rainfall per duration is determined. To find the design rainfall, return period and duration should be taken into account. Based on a return period of 10 years and a duration of 12 hours, a constant rainfall event of 12.3 mm/h is taken into account, see Table 4.1.

Table 4.1: IDF curve values of Guayaquil

Intensity [mm/hour]	Duration [hours]					
Return period	1	2	4	8	12	24
2 years	49.3	35.4	21.9	12.5	9.0	5.1
5 years	58.9	42.8	26.5	15.1	10.9	5.3
10 years	66.2	48.3	29.9	17.1	12.3	7.1
25 years	76.2	55.5	34.4	19.6	14.2	8.2
50 years	84.1	60.9	37.7	21.5	15.7	9.1
100 years	92.3	66.3	41.1	24.1	17.1	9.9

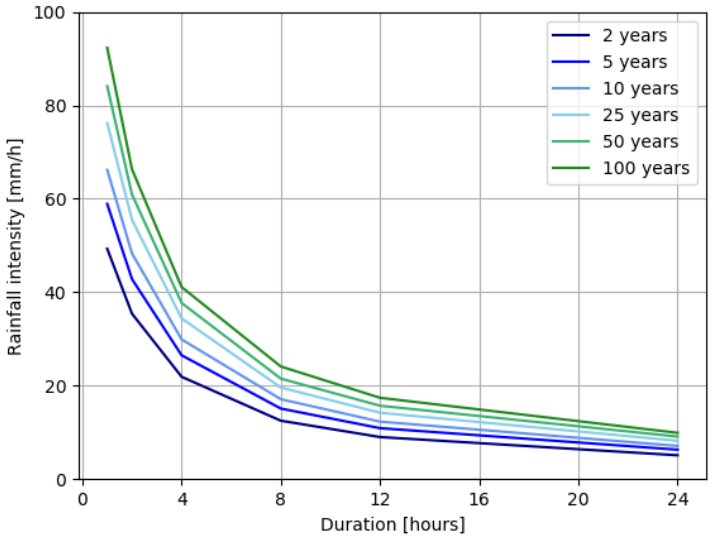

Figure 4.3: IDF curves for the city of Guayaquil

4.3. Rainfall during El Niño

In the previous analysis, no distinction has been made between rainfall during El Niño and regular conditions. This is not yet possible, since in the detailed data set only one El Niño event is included; the 2009/2010 one. This was a relatively 'mild' El Niño event, and one El Niño is not enough to base a complete set of IDF curves on; not enough data points are provided. More El Niño events are included in the longer data sets containing mm/day, but those are not precise enough.

The way the curves are determined now, the 2009/2010 El Niño event is included in the data points. This will lead to slightly higher rainfall intensity values when used for regular periods (not El Niño). However, leaving out these years will lead to insufficient data points for an analysis. In conclusion, the designed IDF curves will be used as an indication, keeping in mind that during regular times, rainfall will be slightly lower and during El Niño rainfall will be significantly higher.

This explanation is substantiated by files provided by Interagua. In their 'Adjustment and Revision of the Masterplan Drinking Water; Sanitary Sewerage and Sewered Pluvial' (Interagua, 2010b), IDF curves are also determined for the city. However, they only lead up to a duration of 2 hours, which is insufficient for this particular project. Comparison of the first 2 hours shows that the Interagua curves, indeed, give slightly lower values.

4.4. Barrier locations

Several possible barrier locations will be considered in this research. Figure 4.4 shows these locations for barriers in the sea branches.

During storm surge in El Niño years and spring tide, water levels can be so high that the barrier must be closed prior to every high tide to prevent floods. More than 50 % of the vessels depend on the tide to enter or leave the port (i.e. they cannot enter or leave the port during low tide) (Roman, 2016). The ports in Guayaquil will become inaccessible during these events if a (closable) barrier south of these ports is constructed. Since there are no floods south of these ports (see Appendix A and the study of CAF (2017)), a closure south of the ports is neither preferred nor necessary. There is no need for vessels to sail north of the barriers, so a semi-permanent barrier is optional at these locations.

Barrier 1, 2, 5, 6, 7 and 9 are located at the end of a sea branch (Brazo Urdesa Miraflores, Brazo Represado, Estero Salado, Estero Puerto Lisa, Estero Mogollón and Estero Cobina, respectively), just behind the bifurcation. Barrier 3 covers the combined domain of barrier 1 and 2, thus closing both the east and west side of Urdesa. Barrier 4 closes half of the Estero Salado at a narrow location of the sea branch. Number 8 consists of two barriers which close off the two entrances of the Estero Del Muerto, without closing of Terminal Fertisa, the port in the south of this sea branch.

Figure 4.4: Possible barrier locations in the sea branches (Google, ndb)

4.5. Catchment area

Based on the altitude map of the city (provided by Interagua) and the possible locations of barriers (see Figure 4.4), the estuary is divided into areas for which the runoff will be determined.

Other locations that might function as storage areas can be container lots, local parks, and playgrounds. For this reason, the rest of the city is also divided into catchment areas. These alternative storage locations are further analysed in Section 6.

The borders of the separate catchment areas are determined using both the altitude map and an overview of the stormwater system of Guayaquil, provided by Interagua (see Appendix C.2). It must be noted that the map of the stormwater system is dated, and thus in some specific areas data is lacking. Here, it is assumed that the stormwater system follows the city streets, as it does in the known areas.

In some parts of the city, the stormwater pipes are clearly disconnected from each other and discharge on different waters. In other parts, however, some pipe systems are intertwined. Here, logical assumptions based on the altitude map are made in order to determine to which part of the sea branch this catchment area belongs.

The division of catchment areas can be found in Figure 4.5. The size of each area can be found in Appendix C, Table C.2.

As can be seen on the catchment area map (Figure 4.5), areas 1 and 4 share a road as the western boundary. Right next to this road, to the west, a mountain slope is present. The slope is fairly steep and water would run off fast. However, this mountainous area is covered with a dense forest. It is assumed that rainwater falling here is retained by the vegetation sufficiently long, i.e. long enough to not reach the sea branch within 12 hours. Therefore, this area is not included in the catchment areas.

For each catchment area, an analysis of the urban development is made based on Butler and Davies (2004). Three types of land coverage are distinguished: Green areas (like parks and forests); residential areas; and city centres. The corresponding runoff coefficients are calculated by analysing satellite images and so determining the area per type, its runoff coefficient and finally the total runoff coefficient for that area, see Appendix C.1.

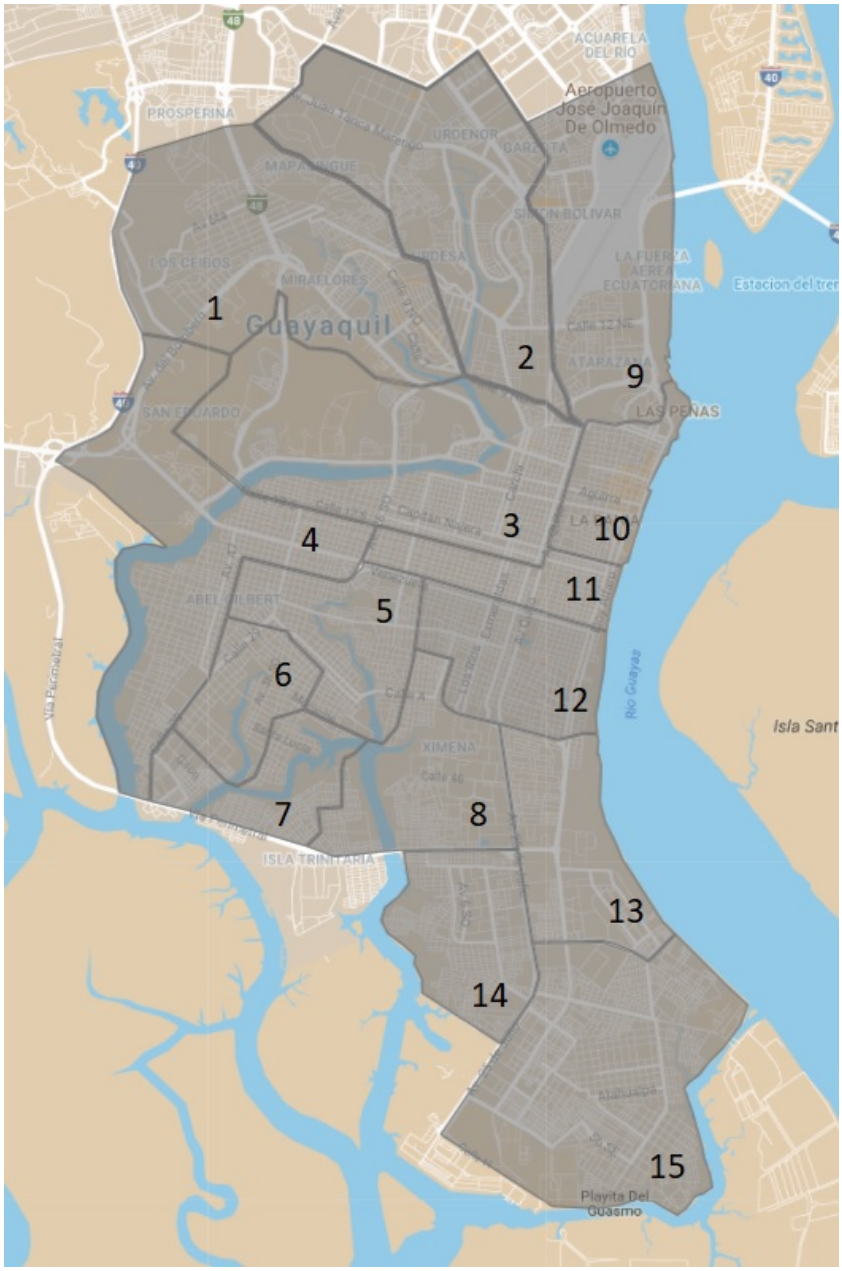

Figure 4.5: Division of the city into catchment areas, based on altitude and stormwater pipe maps (Google, ndb)

4.6. Stormwater accumulation

When the area and runoff coefficient of a catchment area are known, the total amount of rainwater that can fall within a given return period can be determined. In this case, a return period of 10 years is used, as is described in Section 4.1.1. From the IDF curves, the rainfall for a duration of 12 hours and a return period of 10 years, as stated in Section 4.1.2, is determined to be 12.3 mm/hour. The total water accumulation is calculated as follows:

$$V = C \cdot i \cdot A \tag{4.2}$$

where V is the total accumulated volume of water, i is the precipitation intensity in mm/hour, A is the catchment area in km^2, and C is the runoff coefficient.

This calculation neglects the time of concentration. The time of concentration is the time required for surface runoff to flow from the remotest part of the catchment area to the point under consideration Butler and Davies (2004). In this research, assumed is that all water arrives within the 12 hours of closure. This assumption might overestimate the amount of water accumulated in the storage locations, but since most of the streets are impervious, the runoff time will be short.

Table 4.2: Stormwater accumulation per catchment area

Catchment area [#]	Area [km^2]	Runoff coeff [-]	Total water accumulation [m^3]
1	12	0.65	1,151,280
2	11.4	0.76	1,278,806
3	11.9	0.59	1,036,299
4	10.6	0.67	1,048,255
5	4.36	0.75	482,652
6	2.85	0.78	328,114
7	3.3	0.79	384,793
8	5.1	0.75	564,570
9	8.51	0.57	715,963
10	2.66	0.76	298,388
11	2.48	0.59	215,968
12	4.34	0.71	454,814
13	4.79	0.75	530,253
14	4.39	0.73	473,013
15	11.6	0.71	1,215,633

5

Hydrodynamic model set-up

A hydrodynamic Delft3D-FM model is used to determine the effects of a possible closure of part of the sea branches. The aim for the model is to find an optimal location for a closure, so that it will not lead to an increase in flood risk in other areas and determine the storage capacity behind each barrier.

The first version of a Delft3D-FM model of the delta and estuary of Guayaquil has been made by Barrera Crespo (2016) at Deltares. This model is used as a starting point and expanded with more accurate data. The model domain covers the entire Gulf of Guayaquil and reaches about 50 km upstream of the Daule and Babahoyo river. The boundaries are located far from the area of interest, so the hydrodynamic characteristics at the boundaries are uninfluenced by disturbances in the area of interest.

The study of Barrera Crespo (2016) focused on morphological issues in the Guayas river. The unstructured grid in the model had a relatively high resolution in the Guayas river relative to the sea branches. To shift the focus of the model towards the sea branches, the grid in the Guayas river was coarsened, while the grid cells in the sea branches were refined. Grid coarsening has been applied to reduce the computational time. Smaller sea branches, which were not included in the first version, were added to the grid of the model. The width of a sea branch is modelled with a minimum number of three grid cells.

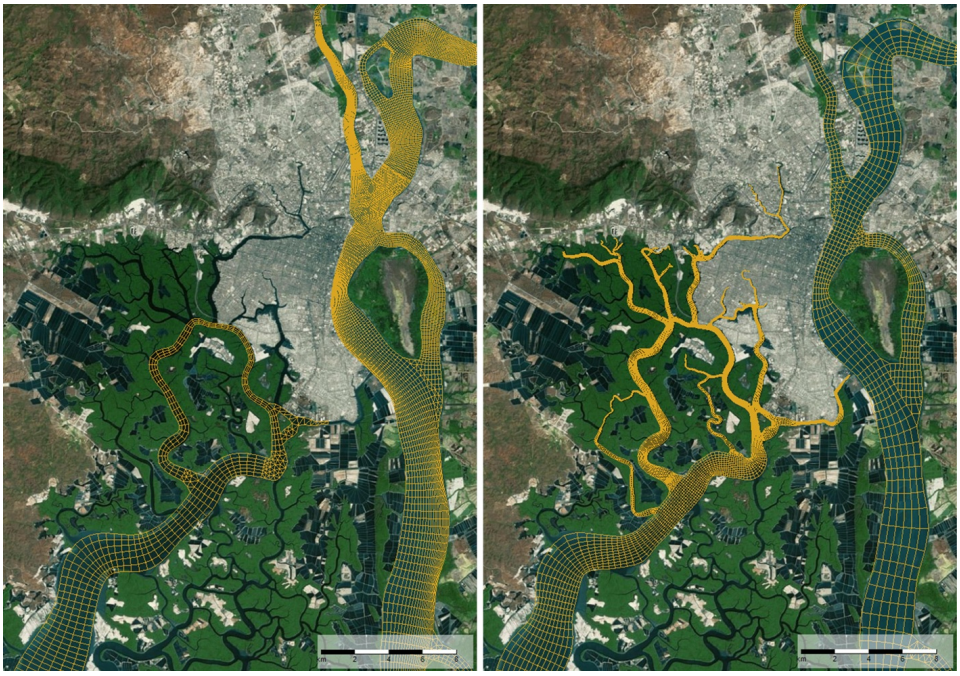

Figure 5.1: Unstructured grids of the sea branches and Guayas river. On the left, the original model. On the right, the adapted model

The new model has a typical grid cell size of approximately 25 m to 150 m around the area of interest. The Gulf of Guayaquil has been unaltered in the new model and has a typical grid cell size of approximately 200 m to 7500 m. A curvilinear grid has been constructed where possible and triangular grid cells were only used when strictly needed due to their lower accuracy. The previous and the new model are shown in Figure 5.1.

5.1. Boundary conditions

The locations of the boundaries were adopted from the previous Delft3D-FM model. The type of boundary condition and numeric values for certain parameters have changed.

5.1.1. Tide

At the open sea boundary in the Gulf of Guayaquil, the previous model used a 'morphological tide' to reduce the computation time when modelling a long time period. This morphological tide averages the real tidal components, while it is able to produce the same morphological changes in the estuary. Because the time period of floods and rainfall is in the order of hours to days, the tide at the sea boundary is changed from a morphological tide to a regular tide. Nevertheless, Barrera Crespo (2016) calculated the tidal components of the Gulf of Guayaquil in his study. He based the offshore tidal components on measurements of the Puerto, Bolívar, Porsoja and Libertad tidal stations. The offshore tidal components are shown in Table 5.1.

Table 5.1: Tidal components in the Gulf of Guayaquil (Barrera Crespo, 2016)

Component	Description	Amplitude [m]	Phase [deg]
Z_0	Mean water level	0	0
M_2	Principal lunar semi-diurnal	0.75	250.16
S_2	Principal solar semi-diurnal	0.22	295.02
N_2	Larger lunar elliptic semi-diurnal	0.16	221.63
K_2	Lunisolar semi-diurnal	0.060	294.68
K_1	Lunar diurnal	0.11	41.15
O_1	Lunar diurnal	0.031	11.91
P_1	Solar diurnal	0.035	40.70
Q_1	Larger lunar elliptic diurnal	0.0012	292.05
M_F	Lunisolar fortnightly	0.012	20.08
M_M	Lunar monthly	0.0071	11.15
M_4	Shallow water overtides of principal lunar	0.0017	130.94
MS_4	Shallow water quarter diurnal	0.0015	134.82
MN_4	Shallow water quarter diurnal	0.0013	88.94

The form factor F gives an indication for the tidal environment. This factor takes into account the two main diurnal tidal components (K_1 and O_1), as well as the two main semi-diurnal tidal components (M_2 and S_2).

$$F = (K_1 + O_1)/(M_2 + S_2) \tag{5.1}$$

Based on the tidal amplitudes of Table 5.1, the form factor for the Gulf of Guayaquil is 0.15. Because $F < 0.25$, the tidal environment in the gulf can be considered semi-diurnal (Bosboom and Stive, 2013).

The boundary at the Gulf of Guayaquil is split into seven boundary points, at the offshore end of the gulf. Each of the seven boundary points describes all tidal components from Table 5.1.

5.1.2. River discharge

Upstream of Guayaquil, the Daule and Babahoyo rivers merge to form the Guayas river. Boundaries are located in both rivers, approximately 50 km upstream of the confluence. The locations of these boundaries are adopted from the previous model, but the numeric value of both discharges have changed. Also, two tributaries of the Babahoyo river, the Chimbo and the Vinces river, have been added as a source.

The previous model uses the monthly averaged discharge in both rivers to model several years. This boundary condition is not suitable to model effects of flooding. For this research, a probabilistic analysis is executed to find a design discharge to implement in the model. In Section 2.4, these monthly averaged discharges are analysed and visualised, giving insight into the discharge fluctuations during the year.

Discharge data is obtained from INAMHI. The discharge at five different gauging stations is known: H0345, H0348, H0365, H0371 and H0390, shown in Figure 5.2. These gauges measure the discharge in the Daule river and in the tributaries of the Babahoyo river. The design discharges of the Zapotal and the San Pablo rivers, with gauging stations H0345 and H0371, are summed up and used as the Babahoyo boundary condition. The design discharges of the Chimbo (gauge H0390) and Vinces river (gauge H0348) are added to the model as a source.

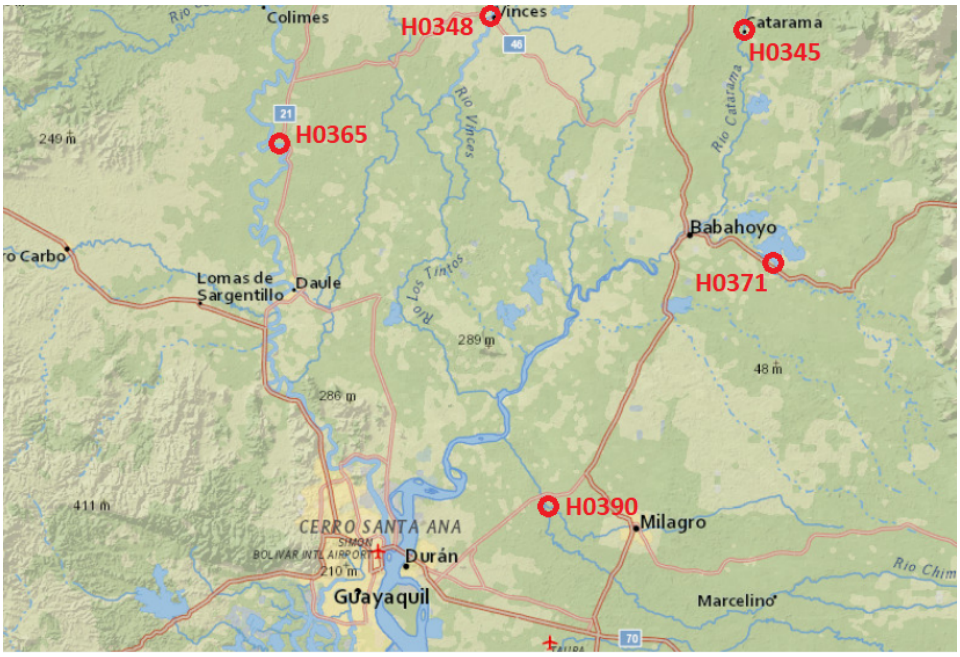

Figure 5.2: Discharge stations for the Daule river and the tributaries of the Babahoyo river (based on ArcGIS Pro render)

The design discharge that is used for the hydrodynamic modelling is computed using extreme value analysis based on the Generalised Extreme Value (GEV) distribution. As stated before, the tidal waves can be observed far upstream because of the convergence. It is therefore important to carefully locate the discharge boundary conditions to exclude interference of the tides.

As stated before, the datasets of the different gauges are neither consistent nor complete. The maximum daily discharge per year is used for fitting the distributions. In Table 5.2 the details of the data used per gauge is shown.

In most cases, at least one strong El Niño event (1997-1998) is included. Only in case of the Chimbo river there is no data available of discharges during an El Niño event. Because of this lack of data, the discharges of the Chimbo river will be underestimated. However, this will be neglected because of the small magnitude of these river discharges.

Table 5.2: Overview discharge data

Gauge	Latitude	Longitude	River associated	Tributary	Years available	No. of years
H0365	01°41’ 46" S	79°59’ 43" W	Daule	-	1989-2015	27
H0345	01°34’ 15" S	79°28’ 56" W	Babahoyo	Zapotal	1972-1997 + 2012-2015	30
H0348	01°32’ 30" S	79°44’ 35" W	Babahoyo	Vinces	1964-2015	52
H0371	01°49’ 55" S	79°26’ 20" W	Babahoyo	San Pablo	1971-2015	42
H0390	02°06’ 09" S	79°41’ 36" W	Babahoyo	Chimbo	2003-2015	13

To compute the design discharge for different rates of return, an extreme value analysis is performed. Different distributions - Gumbel, Weibull and Fréchet - are fitted onto this data and is compared by applying the RMSE method. Theoretical background about the different distributions and the formulas used can be found in Appendix E. The expected discharges for a return period up to 100 years are determined, but it has to be stated that, due to the little amount of data, the discharge rate for high return periods will be less reliable. It can be advised to use more data when available because the analysis can be made more accurate and thus more reliable.

In Table 5.3 an overview of the discharges per return period is shown. These results and an explanation for the chosen distributions can be found in Appendix G.

Table 5.3: Discharge $[m^3/s]$ per return period

	Distribution	Return period [years]								
		2	3	5	10	15	20	25	50	100
Daule	Weibull	1158.95	1352.69	1536.80	1732.69	1829.43	1892.36	1938.45	2069.32	2185.54
Zapotal	Fréchet	844.81	874.39	908.41	953.16	979.34	998.11	1012.81	1059.48	1107.93
Vinces	Weibull	873.90	920.63	961.08	1000.73	1019.22	1030.91	1039.30	1062.43	1082.18
San Pablo	Fréchet	240.50	251.56	264.42	281.56	291.71	299.04	304.81	323.29	342.73
Chimbo	Weibull	137.88	153.74	168.20	183.03	190.17	194.76	198.09	207.42	215.56

As stated in Section 4.1.1, the return period chosen for computing the design discharge is based on a balance between costs and benefits. Therefore, a return period of 10 years is chosen as the starting point within this project. Because high river discharges and high precipitation rates are likely to coincide (see Figure 2.8), the independently computed design values for river discharge and precipitation rates can be used together.

The river discharges are either implemented into the model as a boundary or as a source. The boundary condition of the Daule river is described with the calculated 10-year event of gauge H0365. The boundary at the Babahoyo river is located exactly at the confluence of the Zapotal and the San Pablo river. The boundary condition is described by the sum of those two discharges. The discharges of the Vinces and the Chimbo river are implemented as a source.

The boundary at the Babahoyo river and the source at the Chimbo river are shown in Figure 5.3.

Figure 5.3: Boundaries and sources in the Delft3D-FM model. On the left, the boundary at the Babahoyo river shown in blue. On the right, the source of the Chimbo river shown in red

5.2. Bathymetry

Data about the bathymetry was obtained from the INOCAR and Boskalis. Bed level measurements of several regions of the inner estuary were made between 2009 and 2017. These data are used as input for the Delft3D-FM model. In regions where bathymetry data is not received, the bathymetry of the model of Barrera Crespo (2016) is used.

The obtained data from INOCAR and Boskalis had to be adapted to implement in the Delft3D-FM model. The bed levels were given relative to mean low water surface (MLWS), while the bed level in Delft3D-FM is relative to mean sea level (MSL). Also, the bed levels are positive when they are below the reference level, while a bed level below MSL in Delft3D-FM must be negative. Because the difference between MLWS and MSL are not the same in the whole domain, the domain is divided into multiple regions. The bed levels are then scaled in accordance with the difference in that region, see Table 5.4.

Table 5.4: Difference between MLWS and MSL for different regions (INOCAR, 2018b)

Region	Tidal gauge	Latitude	Longitude	Difference MLWS and MSL
Estero Salado	Puerto Nuevo	02°16' 42" S	79°54' 44" W	2.42 m
Guayas river	Guayaquil-Río	02°11' 43" S	79°52' 47" W	2.33 m
Morro Channel	Porsoja	02°42' 00" S	80°14' 41" W	1.45 m
Jambeli Channel	Puerto Bolívar	03°15' 25" S	80°00' 05" W	1.77 m

The bathymetry of the estuary and the Gulf of Guayaquil, as well as the location of the tidal gauges, are presented in Figure 5.4. For a clear view of the bed levels in the estuary, bed levels in the Gulf of Guayaquil lower than -50 m are limited to -50 m in the figure.

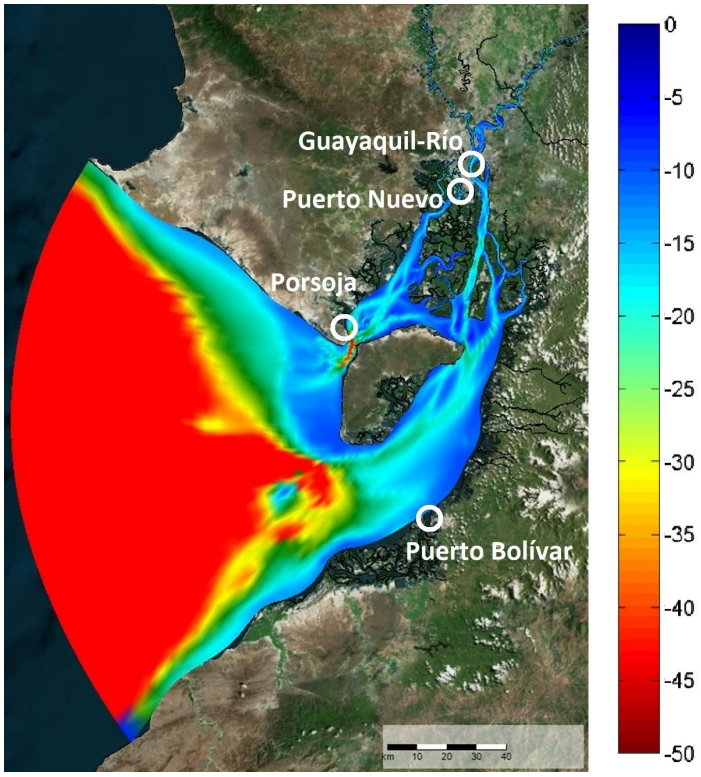

Figure 5.4: Bathymetry relative to MSL and tidal gauges in the Delft3D-FM model in meters

5.3. Model validation

To validate the Delft3D-FM model, the output of the Delft3D-FM model must be compared with the measured water level of a tidal station. The model was run to obtain water level data for 30 days. The computed water levels are compared with measured water levels from INOCAR, who provided hourly measurements in Puerto Nuevo tidal station from 1990 up to 2000. The result is shown in Figure 5.5.

To quantify whether the model accurately reproduces the water levels in the system, the correlation between the measured and the computed water level signals must be computed. Equation (5.2) describes the correlation between the measured and the computed water levels.

$$r_{xy} = \frac{\sum_{i=1}^{n} (x_i - \overline{x})(y_i - \overline{y})}{\sqrt{\sum_{i=1}^{n} (x_i - \overline{x})^2 \sum_{i=1}^{n} (y_i - \overline{y})^2}} \tag{5.2}$$

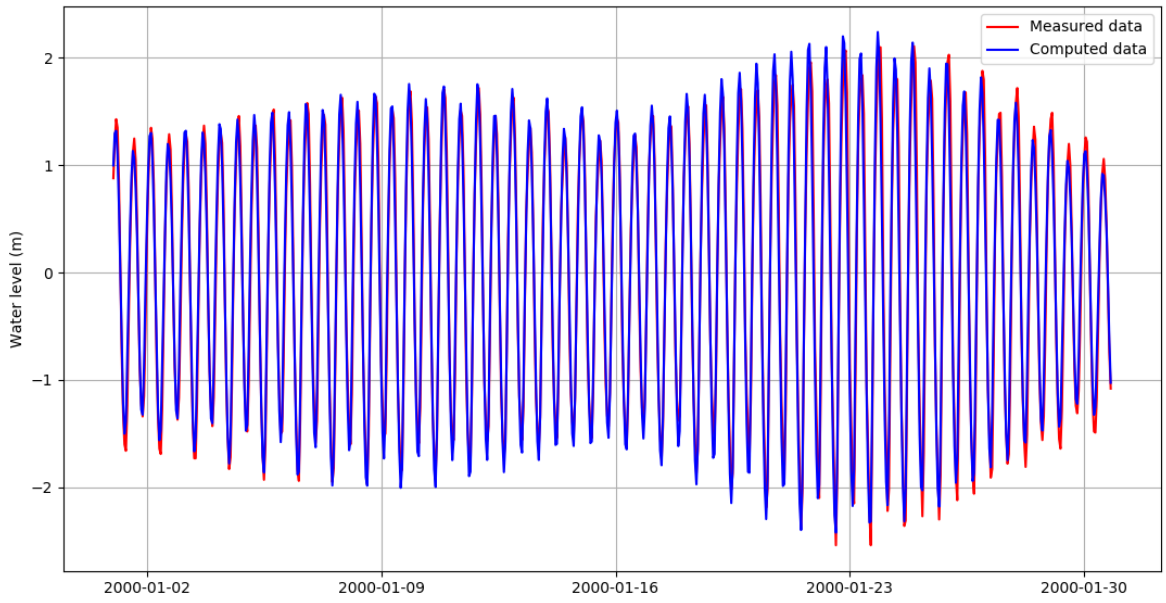

Figure 5.5: Measured and computed water levels at Puerto Nuevo tidal station

where x is the computed data point, $\overline{x}$ is the mean of the computed data points, y is the measured data point, $\overline{y}$ is the mean of the measured data points, and n is the number of measurements.

The correlation between INOCAR's measurements and the Delft3D-FM model output is $r_{xy} = 0.982$, showing a very strong correlation. The RMSE quantifies the error between the two datasets, using Equation (4.1): RMSE = 0.231 m.

Table 5.5 shows a comparison of the primary tidal components of the measured and the computed water levels. Most computed amplitudes and phases agree with the measured ones. The main difference stems from the small components of the tidal signal, for example, the amplitude and phase of the Q_1 tidal component. Because the contribution of the Q_1 tidal component to the water level signal is very small, the model will not be improved to reduce this error.

Table 5.5: Measured and computed tidal components from Puerto Nuevo tidal station

Component	Amplitude			Phase		
	Measured [m]	Computed [m]	Ratio [-]	Measured [deg]	Computed [deg]	Difference [deg]
M_2	1.562	1.587	0.984	180.45	173.77	6.68
S_2	0.851	0.631	1.349	245.15	226.99	18.16
N_2	0.333	0.310	1.074	150.81	153.10	2.29
K_2	0.582	0.316	1.842	274.86	251.79	23.07
K_1	0.122	0.126	0.968	12.89	355.92	16.97
O_1	0.035	0.036	0.972	330.76	343.87	13.11
P_1	0.081	0.052	1.558	308.66	356.64	47.98
Q_1	0.0081	0.0011	7.364	198.61	301.19	102.58
M_F	0.049	0.010	4.900	279.82	325.01	45.19
M_M	0.034	0.014	2.429	10.95	28.74	17.79
M_4	0.085	0.095	0.895	173.00	202.71	29.71
MS_4	0.054	0.045	1.200	248.11	285.48	37.37
MN_4	0.040	0.026	1.538	139.90	193.66	53.76

5.4. Observation points and cross-sections

Figure 5.6 shows the observation points and observation cross-sections in the Delft3D-FM model. The observation points measure the water levels in the parts of the sea branches adjacent to flood-prone areas in the city, see Appendix A. Also, the water depth in the Port of Guayaquil is measured. The observation cross-sections represent the possible barrier locations (see Figure 4.4) and can measure the tidal prism (the volume of water that flows through the cross-section from low tide to high tide), which indicates the storage capacity for stormwater behind the closure. Section 7.1 further explains this calculation.

Figure 5.6: Observation points and cross-sections in the Delft3D-FM model

6

Local storage

Besides floods in urban areas close to the Guayas river and sea branches, floods occur in other low-lying neighbourhoods as well. These areas are not connected with one of the water bodies via land surface. The stormwater accumulates due to gravity and has to be drained through the stormwater pipes. Some pipes are underdimensioned for the highly intense rainfall and cannot drain the water fast enough. Other pipes may backwash during high levels in the Guayas river or sea branches. In both cases, water is unable to drain and floods the streets. To prevent these types of flooding, local storage in these particular urban areas is suggested.

Two types of local storage are proposed in this report, namely water squares and underground basins. For both solutions, some reference projects are introduced, after which suitable locations within Guayaquil will be located and assessed.

6.1. Water squares

The city of Rotterdam in the Netherlands faces challenges similar to those of Guayaquil. More water is coming their way: More frequent rainfall events with longer durations and higher intensities. However, the norms prescribe that only once every two years the streets may flood with a maximum duration of 20 minutes. As a solution, the city is actively combining the design of public spaces with rainwater collection. The municipality is working closely with designers and consultants to see if there is a practical solution to collect, maintain and drain the rainwater in order to disburden its stormwater system (Gemeente Rotterdam & dS+V, 2011). The main problem here is the capacity of the stormwater system. During heavy rainfall, the tubes are not able to process all the water and the streets start to flood: Inundation. Expansion of the tubes is expensive, and underground space is getting limited.

One option to reduce the pressure on the stormwater is the realization of so-called water squares. These are existing squares which are lowered with 1 to 2.5 meters and which can flood during severe rainfall, serving as temporary water storage area. When the rainstorm fades away, the water is slowly fed into the stormwater system, disburdening it during the actual rainstorm.

Bellamyplein
Two of these water squares are already realised in Rotterdam. The first one is the Bellamyplein, designed in 2012 by architect Rik de Nooijer and commissioned by the municipality of Rotterdam. The conditions were optimal, as the square is located in one of the lowest lying parts of the area plus the local stormwater system needed replacement and the municipality was planning on redesigning the area. By combining financial means, it was possible to realise an integral solution for local water problems (Rotterdam Climate Initiative, nd).

Due to its low lying location, water is guided from the surrounding streets relatively easily. Water from roofs is also collected and led to the plaza.

The square itself consists of a lower laying middle part, which can be reached through a small number of steps.

In dry weather conditions, it serves as a meeting place for residents or a playing area for children. As soon as it starts raining heavily, the lower part will start to flood (see Figure 6.1). When it rains 10 mm, the water will raise up to 15 cm within the square. With heavier rainstorms, the water will be collected into an extra storage area underneath the square after reaching the 15 cm on the square. When this extra storage basin is filled as well, the square will start to fill up more. It is expected that the water will exceed the 15 cm about 15 times a year and that a water depth of 50 cm is reached once per year. After a rainstorm, a small part of the water is infiltrated while the rest is directed to the stormwater system within 24 hours (Gemeente Rotterdam, 2012). Total costs of the project are estimated to have been around €2 million to redesign the complete square, of which €725,000 for the water square specifically (Hoogheemraadschap van Delfland, 2012).

Figure 6.1: Bellamy water square. Above, the filling sequence during heavy rain (Gemeente Rotterdam, 2012). Below, photographs of the finished. square (Straatbeeld, 2014)

Benthemplein

The second experience presented here is the Benthemplein, also in Rotterdam. This complex design was created by architects De Urbanisten and was finished in 2013. It consists of two 1 meter deep basins and one deep basin of 2.5 meters. The shallow basins fill up during every rainstorm, the deep one only during very intense rainfall. Water is collected from neighbouring streets and roofs, and led to the square through steel gutters, which double as elements for skaters. The deep basin has been designed as a basketball field, making the square attractive to the students of the adjacent school. Many steps lead to the field, creating space to sit and relax. In this way, the square keeps its function as a recreational place and serves as a storage basin during rainy days. It can store up to 1,700 m^3.

The square comes with a sophisticated drainage system. The first water from every rainfall is collected in the shallow basins and directly pumped into the stormwater system. According to Daniel Goedbloed, advisor for the municipality, this is necessary because the first water is the most polluted. It washes in all dirt from the street, like leaves and plastic. The pump is stopped after an hour (Visscher, 2013). After every rainstorm, the basins need to be cleaned (Amsterdam Rainproof, 2014).

After the rain stops, water is partially infiltrated into the ground using the infiltration crates placed below the square. The other part of the water is pumped into the nearby Noordsingel (Visscher, 2013). Total costs of the project have been estimated around €4 million.

Figure 6.2: Benthem water square. Left: Overview of the design of the square. Middle and right: Steel gutters transport rainwater towards the basins. (De Urbanisten, 2013)

6.1.1. Specifications

From the reference projects, some conditions needed for a water plaza can be summarised:

- The area suffers from floods due to heavy rainfall
- It is favourable to have a square located in a low lying area
- The square has to maintain its social function after the redesign
- Areas which already need stormwater system renewal are financially attractive, since funds and design can then be combined

Other points to consider are maintenance, pollution and infiltration. In the two Rotterdam cases, the responsibility for maintenance lays with the municipality. However, no clear data on costs have been found. Pollution will prove to be a big problem in Guayaquil. Plastic lingers throughout the streets, and debris is already blocking some of the stormwater systems. To prevent this from happening at a water square, clever measures have to be implemented in the design. To demonstrate the infiltration capacity of the soil, soil samples need to be taken and analysed.

6.1.2. Suitable locations

Looking at the specifications, finding a suitable location is based on technical and 'other' aspects. As a starting point, the location has to be situated in a flood prone area. Technical requirements consist of altitude of the location, size of the location and availability of a stormwater system. Other requirements are economic viability of the construction (combining it with renewal of stormwater pipes) and the usefulness of the area to the local community. Unfortunately, no data on stormwater system renewal plans is available to the research group. Only parks and playgrounds will be considered as potential locations, ensuring usefulness to the community.

In order to find a location, an altitude map of the city is combined with a map provided by the Municipality of Guayaquil, containing marked areas which are prone to flooding. The latter can be found in Appendix A.

A suitable square has a size that is large enough to handle the desired water volume. In total 29 locations are selected in three flood-prone areas: In the Samanes Park area, from the Urdesa neighbourhood to Las Peñas, and spread over the south part of the city. The locations are indicated on a map in Appendix H.1. The volume of each area is indicated in Table 6.1.

Besides areas fitting the criteria, some areas are also chosen because of their location next to the sea branches. These locations can function as a potential extension of the sea branches, diverting water from here to the squares during heavy rainfall. Examples are parks 5 and 27.

Another option is lowering existing parking lots and connecting them to the stormwater system. This option is now left out, because another requirement of a water square is that rainwater should not be able to damage assets on the squares. With car parks, this is difficult: Parked cars can start floating when the square fills up. Warning signs should be put up and a very precise weather prediction system is needed for people to remove

their vehicle in time. These areas, therefore, belong to a different sector of water storage and are thus left out of this section.

In Section 4.5 the city is divided into different catchment areas. It is, therefore, useful to determine how much storage the parks can contribute to each area. This is shown in Table 6.1

Table 6.1: Local storage per catchment area

Catchment area	Local storage [m^3]	Catchment area	Local storage [m^3]
1	13,910	8	39,300
2	59,030	9	1,590,000
3	35,600	10	36,500
4	71,300	11	-
5	59,020	12	11,100
6	8,060	13	-
7	3,180	14	-

6.1.3. Infiltration

In the reference projects, some water is infiltrated into the ground after collection. This would even further reduce the burden on the stormwater system. To determine if this is also possible in Guayaquil, soil profiles near the possible parks will now be analysed.

A dataset containing 585 soil profiles throughout Guayaquil is provided by ESPOL. It is an assembly of data obtained from various projects and by various companies and authorities. It includes x- and y-coordinates in PSAD56, and data on depth ranges of 0-2 m, 2-4 m, 4-6 m, 6-8 m and 8-10 m. The dataset actually continues up to a depth of 50 m, but since the constructions will be relatively shallow, these depths are left out of the analysis. Data provided are for example liquid and plastic limit, gravel, and sand and fines content. About half of the data points are missing, either due to not having sampled deeper or due to errors made.

For each possible park, the nearest soil profile is taken and assumed to be comparable. The distance to the measuring point is added in the overview table in Appendix H.2.

A distinction is made between grava (gravel), arena (sand) and finos (fines) with the help of a sieving test, carried out during the different projects. All material retained at sieve #4 (4.75 mm) is labelled as gravel. This was not found at any of the parks. All material retained on sieve #200 (0.075 mm) is labelled sand, and everything passing this as fines. To be able to distinct clay from silt, the Plasticity Index will be calculated per data point. Global infiltration rates based on the Minnesota Stormwater Manual (Minnesota Stormwater Steering Committee, 2017a) are then also added to the general overview table in Appendix H.2.

From the table, it is clear that infiltration rates are very low due to the high fine content. Thus, It is probably not profitable to install a complete infiltration installation under each park. All water should, therefore, be discharged into the stormwater system after a rainstorm.

6.1.4. Backwashing

One of the main problems in Guayaquil is backwashing of the storm system during high tides. At the water squares, this is highly undesirable. Backwashing stormwater onto sport or playing areas will endanger the health of the children playing there and should be avoided at all times. Therefore, the pipes that discharge onto the sea branches must be provided with valves. EMAPAG-EP nowadays already started installing 'duck-peak' valves on these stormwater pipes, to prevent high tide to backwash into the city (Martha Orta, personal communication, March 27, 2018) and are planning to install more around the city.

6.1.5. Pumping

In the reference projects, pumping is used to move the water from the basin into the stormwater system during the first hour of rain and after the rainstorm has finished. Purchasing and maintaining those pumps will greatly increase the costs of the square, but might be a necessity. After the rainfall event, the water should be

removed from the square to recover the social function of the locations and to avoid creating a pool ideal for pathogens and waste to accumulate. Since part of the water will be below the water level in the sea branches and the river, water should be pumped out.

6.1.6. Storage capacity

Of course, the given total area is not equal to the exact area that can be lowered. Space is needed for stair steps, trees, etc. Looking at reference projects, some space is also used for architectural aspects, giving the squares a modern look. However, all of this is not necessary. For the sake of simplicity, it is assumed that these squares will be lowered equally throughout the square, and only contain a staircase at the entrances of the park. Any extra assets are only needed increase the look of the square, but will decrease the rainwater storage capacity.

These local storage areas can be used as independent storage facilities. However, they can also be used in combination with the storage capacity in the sea branches. Once the model of the barrier produces results, it can be determined if extra storage is needed to disburden the complete area. When this is known, the depth of the water squares can also be determined.

If used as an independent storage to prevent flooding on a very local scale, the depth of a square can be 1 to 2.5 meters deep, based on the reference projects.

6.2. Underground basins

Another option that can be explored is the installation of underground basins. Constructions alike have already been installed around the world, and sophisticated techniques are readily available.

The principle of underground basins is to temporarily store stormwater from surrounding impervious areas in very large underground chambers or pipe systems during intense rainfall events. Afterwards, the water can be released at a controlled rate, to mimic pre-development conditions. In this way, it is possible to manage and control the volume and time of stormwater runoff. This avoids the harmful effects of high stormwater runoff, such as erosion and flooding (District, 2014). Sometimes, stored water can even be infiltrated to recharge groundwater, but only if soil types are suitable and the groundwater level is located below the water storage.

Underground basins are an excellent solution that have limited impact on the neighbourhood. Since the solution is out-of-sight, it is not affecting appearances with large constructions. Underground basins have fewer restrictions based on the level of public safety as well. This is a major advantage over open ponds (Minnesota Stormwater Steering Committee, 2017b).

Many types of underground detention basins are available, like the designs as shown in Figure 6.3. Storage basins can be as large as 350,000 m^3, which are already build in Tokyo (Takahashi, 2017). These types of storage basins can be kept in mind when further expanding the city of Guayaquil. Also, they could be implemented below parks or parking lots as a major solution to the stormwater problems. However, these solutions will be far more expensive than the small scale solutions proposed earlier.

Figure 6.3: Stormptrap underground stormwater basin (Stormtrap, 2016).

6.2.1. Operation and maintenance

Infiltration systems can be installed to drain the basin. Based on a database with ground profiles of the city provided by ESPOL, it can be concluded that some clayey sand layers are around. Small-scale infiltration might have been possible, but the groundwater table is located between 2.6 m and 1.0 m below ground level in the north and even higher in the center and south of the city, making infiltration impossible (CAF, 2013). Therefore, the basin should be emptied using gravity and additionally by pumping. Installing pumps increases the costs of construction, operation, and maintenance, but is a necessity.

Water from the streets will flush into the basins. This water may contain high loads of sediment and floatables. Bar screens should be installed to keep out the largest waste and protect the catch basins. The bar screens should be cleaned regularly to avoid clogging at the entrance. By cleaning and sweeping the catchment area, the sediment and floatables loading can be reduced.

Accumulated floatables and sediments within the system are the main concern for maintenance. The basin should be cleaned at least once per year. Preferably, the area is manually cleaned instead of flushing the system. Flushing might lead to garbage piling up at the end of the installation. When flushing is still chosen, great care has to be taken to protect downstream waters from contamination (Axler et al., 2009).

6.2.2. Suitable locations

Underground storage is usually implemented close to locations where land availability is scarce and no space can be reserved for natural water retention areas. Downtown Guayaquil is densely populated and therefore area is limited. For the creation of storage space here, people should be relocated and this is highly undesirable.

Installing basins is ideal beneath open areas like parking lots, paved roadways and large green areas, just outside crowded neighbourhoods. These areas are easily accessible for construction, and therefore have a low impact on the neighbourhood during construction.

Suitable locations within Guayaquil are selected based on three criteria: Size of the location, distance from flood-prone areas, and impact of construction. To be able to store large amounts of water, the underground basin should be of significant size. Besides this, building such constructions is expensive, so small basins are economically less attractive. Another point of interest is the construction. The soil should be replaced, so it is advised to implement underground structures in combination with rehabilitation activities.

Based on these criteria, several locations around the city are selected as possible solution locations. Amongst them are parking lots, larger parks like Samanas and Parque Forestal, and the container lots near the port. All of the locations are indicated on a map in Appendix H.1 and the areas are shown in Table 6.2.

Table 6.2: Underground basins areas

Number	Local storage area [m^2]
1	1,230,000
2	1,720,000
3	17300
4	6060
5	27,000
6	109,000
7	34,300
8	184,000
9	209,000
10	92,000

6.2.3. Airport

A special location that can be considered for stormwater storage is the current airport of Guayaquil, indicated as location 2 on the map in Appendix H.1. Given economic growth anticipated for the Guayaquil region, the existing airport in Guayaquil is expected to reach capacity around 2024. There is little space for extension, so a complete new airport is being built 30 kilometers from the city centre (LeighFisher, nd). It is expected to open in 2024, at which point the current airport will be abandoned.

The current airport covers an area of 1.7 million m^2. There are no plans for the redesign yet, which makes this location highly suitable for underground storage basins. When a new layout is designed, water storage could form an integral part. The airport is situated far from residential areas and covers a lot of ground, creating possibilities for a very large underground basin. The depth of the basin can be based on the needed storage capacity. With this area size, it would be possible to detain all stormwater throughout the city. Of course, investments should then also be made in altering the stormwater system, leading them towards the storage basin.

6.2.4. Feasibility

The selected areas are of great size and have a high potential for stormwater storage. Assuming an average depth of 10 m, a total capacity of 36 million m^3 can be stored. This would be sufficient to store the excessive rainfall within the whole city. Not even all of the area has to be used for underground storage, since less capacity is needed.

However, there are also disadvantages. Costs of such basins are high. The project build in Tokyo was estimated around $ 2 billion. Smaller projects will lead to less expenses, but costs will still be considerably high. Besides this, large projects like these will cause great nuisance when executed close to residential areas or roads.

Concerning the redesign of the current airport area, this location offers many opportunities. Stormwater storage can be integrated in the total design plan in many ways, of which an underground storage basin forms one. However, at this point in this research, too little is known to draw solid conclusions. An economic feasibility study has to be performed in order to determine how large the costs of such a project can and may be. Also, other requirements already imposed on the airport area should be investigated to see if they can be combined with this type of storage. Besides this, when a storage volume big enough for ***all*** stormwater in the city is designed (which is possible), the stormwater system should be immensely altered to drain all the water towards the storage area. This will bring along even more costs.

Combining these outcomes, it can be concluded that underground storage basins form a potential solution for the pluvial flooding problems of the city of Guayaquil. However, too little is known about financial means to further investigate the possibilities at this point, considering that the design size of such basins is probably based on costs. Therefore, these underground storage basins are not further taken into account in this report.

7

Results

In this chapter, the large scale solutions are further analysed with the help of the Delft3D-FM model (as introduced in Chapter 5). Barriers will be modelled at different locations in the inner estuary. The goal for the barriers is to block the tide in the closed-off area and to create storage area for stormwater. The effects of the barriers will be analysed for different scenario's, like during neap tide or an El Niño event.

This chapter incorporates results from the previous chapters with the results from the Delft3D-FM simulations. The amount of potential storage area, determined with the model simulations, will be compared to the needed stormwater storage area determined in Chapter 4. Doing this, one can determine if all of the surplus of stormwater can be stored in the sea branch area. This will prove whether or not this solution is viable.

7.1. Simulation approach

From the model validation from the Chapter 5, it can be said that the model can reproduce water levels in the sea branches. Therefore, the model should be able to accurately predict changes in water levels after changes in the sea branches or boundaries are implemented. The impacts on several locations in the sea branches will be quantified after implementing one of the case scenarios. The approach is as follows:

- Simulations will be run for two days, using a time step of 5 minutes. The first day will be taken as spin-up time. The water levels are calculated for the second day, which is January 1st, 2018, where the tidal amplitude is average.
- The initial water level for all points is 0 m above MSL, except far upstream in the Daule and Babahoyo river, where the bed level is above 0 m. All simulations are performed with this initial water level, except for the El Niño case scenario.
- A total of six case scenarios will be analysed, namely:

  CS01 - Reference scenario: The boundaries at the Daule river and at the tributaries of the Babahoyo river consist of the discharge in a 10-year event, according to Table 5.3. The tidal component from Table 5.1 will be implemented at the seaward boundary. This scenario is simulated without any barrier in the sea branches.

  CS02 - Situation after barrier construction: To check whether a barrier in one of the sea branches affects the water level in the rest of the estuary and to check the possibility of constructing multiple barriers, multiple simulations will be done. One of the barriers from Figure 5.6 is implemented per simulation. Other conditions will be similar to the reference scenario **CS01**.

  CS03 - Mean discharge: To quantify the impact of the river discharges on the water levels in the sea branches, the model will be run for mean annual discharges in the Daule river and the tributaries of the Babahoyo river. No sea branch closures will be implemented in this simulation.

CS04 - Neap tide: This scenario uses the same boundaries as **CS01**, but the date of the simulation will be changed such that neap tide will enter the estuary. During neap tide, the water level during low tide is higher than during a regular tide. This means the storage capacity in the sea branch is smaller after closing the barrier. The chosen date is March 27th, 2018.

CS05 - El Niño: During the El Niño phenomenon, the mean water level in the estuary can increase up to 42 cm. This scenario uses the same conditions as **CS01**, except for a change in the initial water level and the Z_0 tidal component at the Gulf of Guayaquil. An increase in mean water level results in a lower storage capacity in the closed-off parts of the sea branches. Due to the lack of rainfall data during El Niño (see Section 4.3), the design rainfall from **CS01** is used.

CS06 - El Niño during neap tide: This case scenario combines the conditions of **CS04** and **CS05**. This case can be considered the worst case scenario for storage capacity in the sea branches. The combination of El Niño with neap tide gives the highest low tide levels possible.

The results of the case scenarios will be presented in the next sections.

7.2. Design criteria

7.2.1. Storage capacity of a sea branch

The storage capacity of the closed-off part of the sea branch follows from the change in cumulative discharge through a cross-section at the location of the barrier, without implementing the barrier itself. The tidal prism of that cross-section (the volume of water that flows through a cross-section from low tide to high tide during a regular tide) is a good indication of the volume of water that is expected to fit into the closed-off area, given that there is no overtopping of the dykes along the sea branches during a regular tide. The exact berm heights are unknown, so in reality the storage capacity could be larger.

The volume of water that flows *seaward* through the cross-section is measured. This means high values in the figure indicate low tide and low values indicate high tide, see Figure 7.1.

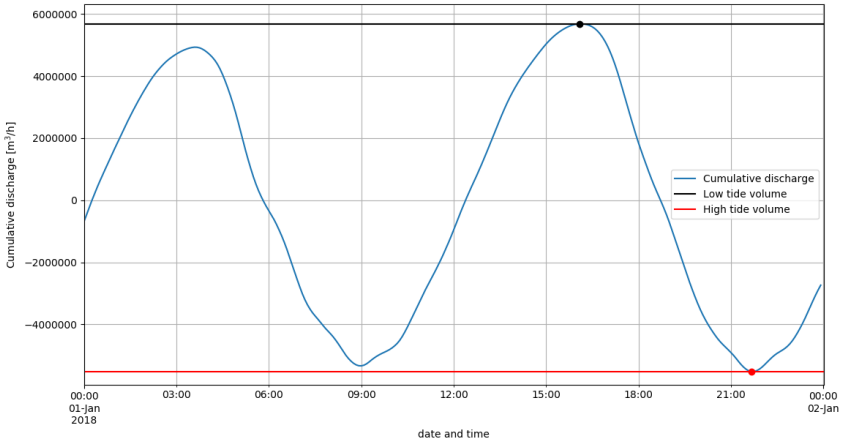

Figure 7.1: Cumulative discharge through a cross-section

During neap tide (**CS04**) and El Niño (**CS05**), the low tide level has increased relative to the reference scenario. For both scenarios, the high tide levels will not be taken into account. During neap tide, the high tide levels are lower, giving a lower tidal prism and a lower storage capacity than is actually the case. Tide levels during El Niño can be very high and can result in overtopping of the dykes along the sea branches during high tide. The storage capacity for case scenarios **CS04**, **CS05** and **CS06** consists of the difference in cumulative discharge between low tide of that case scenario and high tide of the reference case scenario (**CS01**)

7.2.2. Storage area in parks and squares

Although the reconstructed parks are only able to solve very local flooding, they can contribute (slightly) to the total system and are therefore added to the water balance of each scenario. A depth of 2 meters for each park is used. Smaller parks will probably be designed to be shallower and larger parks deeper, so a supposed average is taken. The total storage capacity is calculated using the areas given in Table 6.1.

7.2.3. Rainfall

In the different scenarios the total rainfall does not change. No distinction is made between El Niño rainfall and regular rainfall. This has to do with the available rainfall data, as described in Section 4.3. In the current data set, the latest El Niño event of 2009/2010 is included among the 'regular' rainfall data. Although this was a 'mild' El Niño, it will give rainfall values which are slightly too high for regular conditions. For El Niño conditions, these values will be far too low.

7.3. Case scenarios

7.3.1. CS01 - Reference scenario

The reference case scenario uses the 10-year design rainfall for a duration of 12 hours from Table 4.1, the 10-year design discharges from Table 5.3, and the tidal components from Table 5.1.

Figure 7.2 presents the water level elevation in the Estero Salado during regular tide. The tidal wave height is approximately 4 m.

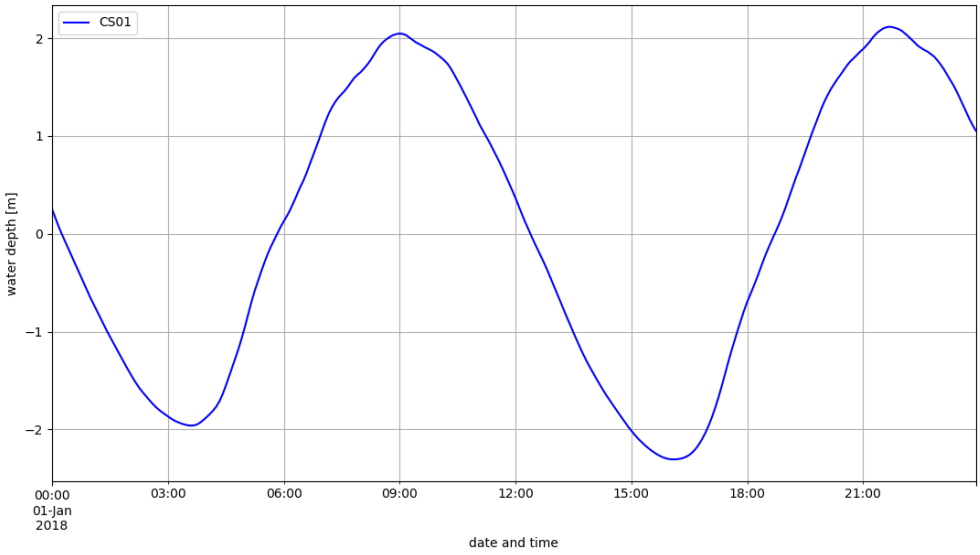

Figure 7.2: Water level in the Estero Salado near Febres Cordero during regular tide

The total amount of stormwater that can be stored per barrier location can be estimated. The total volume of stormwater that can be stored temporarily is the sum of the storage capacities in the local storage areas in parks and the storage capacity of the closed-off sea branch. The volume of stormwater that falls during a design rainstorm is presented in Table 4.2, the volume of stormwater that can be stored locally is the area of each park (found in Table H.1) times 2 meters, and the storage capacity of the sea branch from the cumulative discharge through the cross-section in Delft3D-FM (see Subsection 7.2.1). Again, the barrier itself will not be implemented in the model, but the volume of water that passes the cross-section from low tide to high tide gives the storage capacity of that barrier if it was constructed in reality. A table containing the total overview

is presented in Table 7.1. An overview of barrier locations can be found in Figure 4.4 and the catchment areas can be found in Figure 4.5.

Per barrier location, the storage capacity of the sea branch and parks in the area are subtracted from the volume of accumulated stormwater. If the last column indicates a score of 100 %, it means that all stormwater from the catchment areas corresponding with that barrier location can potentially be stored within the parks and the closed-off sea branch. If this percentage is small than 100 %/, the storage capacity will be insufficient.

Table 7.1: Stored stormwater per barrier during regular conditions

Barrier [#]	Catchment areas [#]	Stormwater [m^3]	Storage capacity sea branch [m^3]	Storage capacity parks [m^3]	Potential stormwater storage [%]
1	1	1,151,280	446,806	27,820	41
2	2	1,278,806	421,890	59,030	38
3	1+2	2,430,086	982,591	72,940	43
4	1+2+3	3,466,386	4,058,313	108,540	100
5	1+2+3+4	4,514,641	11,208,368	179,840	100
6	5	482,652	553,982	59,020	100
7	6	328,115	484,500	8,060	100
8	5+6+7+8	1,760,130	4,635,889	70,260	100
9	15	1,680,144	3,725,835	0	100

Based on Table 7.1, the storage capacity of barrier 4, 5, 6, 7, 8 and 9 are sufficiently large to store all stormwater in their corresponding catchment areas. For the other barriers, only a part of the stormwater can be stored and floods are likely to occur during the design rainfall. Therefore, a basin that only collects the stormwater from the Urdesa-region is not recommended.

However, the fact that a certain volume of stormwater can fit behind a barrier does not mean that this will happen in reality: Flow paths are unknown and water may be accumulating in lower areas, not able to flow towards the sea branch. Also, after a while, the stormwater pipes may be below the sea branch water level and stop discharging the rainwater. It is important to remember that the water balances made in the next sections are a simple, global estimation in order to see if this project can be feasible.

7.3.2. CS02 - Situation after barrier construction

When considering a barrier, possible water level changes in the estuary must be taken into account. A constructed barrier can affect the tidal prism and water levels in the entire estuary, potentially reducing the storage capacity for another closed-off sea branch or increasing the water levels in an already flood-prone area. The water depth in the Port of Guayaquil must also be considered, since a decrease in water depth during high tide means a shorter operation period for moored vessels.

A barrier is modelled in Delft3D-FM as a thin dam which is permanently closed. Figure 7.3 shows the water depth in the Port of Guayaquil after the modelled construction of one of the barriers. It can be concluded that the impact on the water depth is negligibly small, as the smallest decrease in water depth is less than 2 cm.

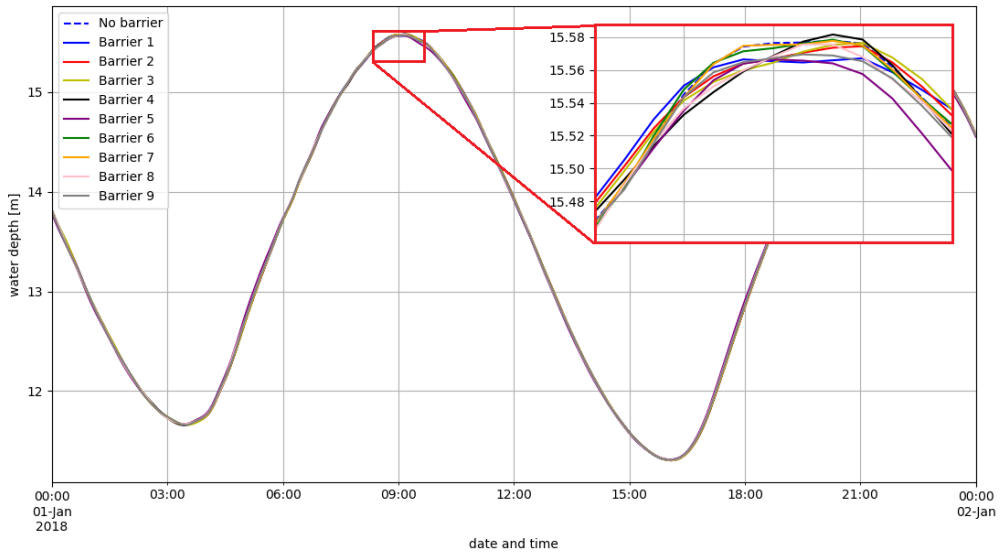

Figure 7.3: Water depth in the Port of Guayaquil after modelled construction of barriers (relative to MSL)

The water levels in other observation points along the sea branches also do not vary a lot. Figure 7.4 shows that the water level in the Estero Salado does not change significantly after implementing one of the barriers. The highest change in water level is approximately 4 cm. The water level is 0 m after construction barrier 5, because the observation point will be located within the closed-off area.

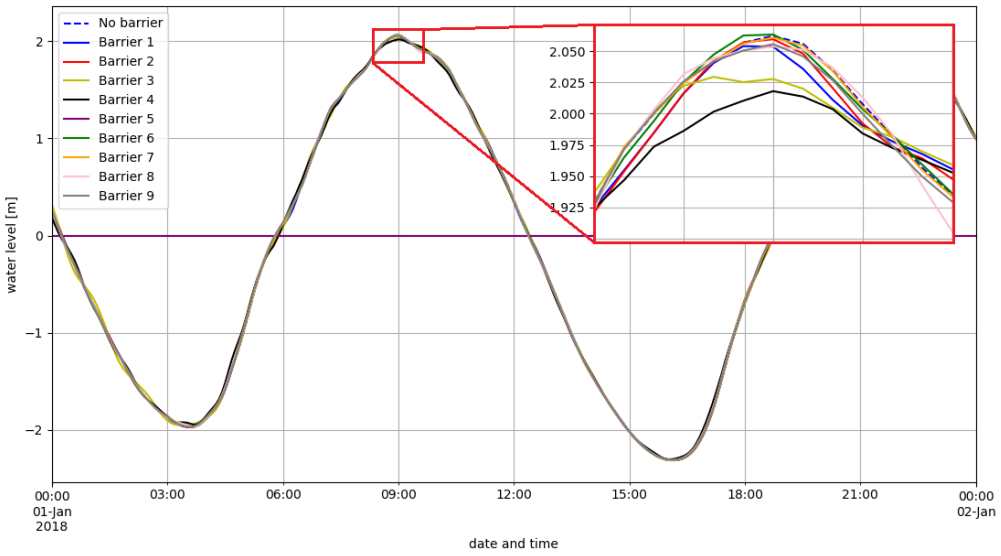

Figure 7.4: Water level in the Estero Salado near Febres Cordero after modelled construction of barriers

In order to be able to protect multiple parts of the city, multiple barriers must be considered. Apart from changes in water levels, changes in storage capacity must be assessed. Multiple simulations will be carried out to see if the storage capacity in a sea branch changes when another barrier already has been constructed. The possible combinations of barriers are shown in Table 7.2. In this table, a combination of barriers is presented as one number (e.g. 16 means a combination of barrier 1 and barrier 6).

Table 7.2: Possible combinations of barriers

Barrier	Combinations
1	16, 17, 18, 19, 167, 169, 179, 189, 1679
2	26, 27, 28, 29, 267, 269, 279, 289, 2679
3	36, 37, 38, 39, 367, 369, 379, 389, 3679
4	46, 47, 48, 49, 467, 469, 479, 489, 4679
5	56, 57, 58, 59, 567, 569, 579, 589, 5679
6	67, 69, 679
7	79
8	89

Figure 7.5 shows the cumulative discharge through barrier 5 for different combinations of other barriers. From this figure, it seems that a modelled barrier in one of the sea branches does not or merely affect the storage capacity for another barrier.

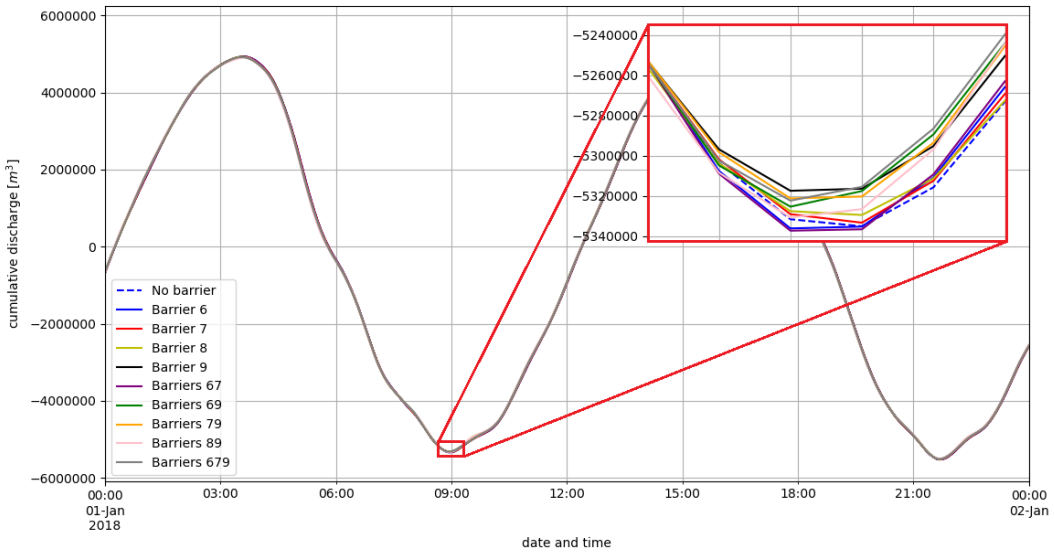

Figure 7.5: Cumulative discharge through the cross-section of barrier 5 after modelled construction of possible barriers. The possible barriers stem from Table 7.2

The results of the simulations from Figure 7.5 are shown in Table 7.3. The data on rainfall and storage capacity in parks is the same as used in Table 7.1. The park storage capacity and sea branch storage capacity are subtracted from the volume of rainfall belonging to the catchment areas of barrier 5.

Table 7.3: Stored stormwater for barrier 5 with different barrier combinations

Barrier [#]	Combined with barrier [#]	Storage capacity sea branch [m^3]	Difference [%]	Potential stormwater storage [%]
5	-	11,208,368	0.00	100
5	6	11,207,582	0.01	100
5	7	11,207,341	0.01	100
5	8	11,202,944	0.05	100
5	9	11,199,932	0.08	100
5	6+7	11,199,325	0.08	100
5	6+9	11,192,346	0.14	100
5	7+9	11,191,451	0.15	100
5	8+9	11,187,870	0.18	100
5	6+7+9	11,191,106	0.15	100

This table confirms that a barrier does not negatively affect the storage capacity of another barrier and that the total storage capacity is simply the sum of the barriers' individual storage capacities. This means that multiple storage areas can be created at once without having a negative impact on each other.

7.3.3. CS03 - Mean discharge

CS01 uses the 10-year design discharges together with the 10-year design rainfall, because Figure 2.8 has shown that rainfall and river discharge are correlated. The impact of these discharges on the water levels in the sea branches will be assessed by changing the 10-year design discharge to the annual mean discharge, presented in Table 2.1. All other conditions are kept the same as in **CS01**. Figure 7.6 shows the water depth in the Port of Guayaquil for the 10-year design discharge and the mean annual discharge.

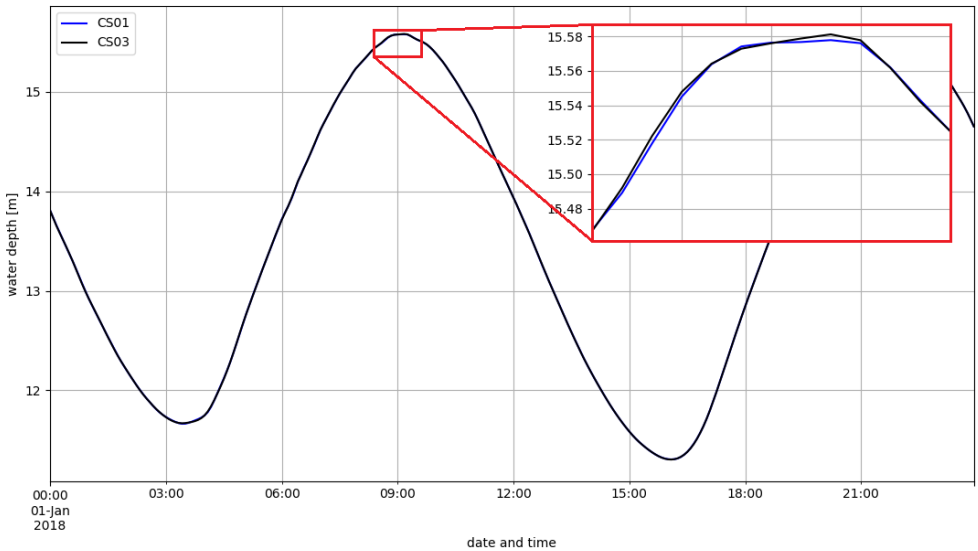

Figure 7.6: Water depth in the Port of Guayaquil for 10-year discharge and mean annual discharge (relative to MSL)

The difference in water height is very small, meaning that the effect of the river discharges to the water level in the sea branches is negligible. To confirm this, the percentage of stored stormwater is calculated and presented in Table 7.4.

Table 7.4: Stored stormwater per barrier during mean river discharge

Barrier [#]	Catchment areas [#]	Stormwater [m^3]	Storage capacity sea branch [m^3]	Storage capacity parks [m^3]	Potential stormwater storage [%]
1	1	1,151,280	446,855	27,820	41
2	2	1,278,806	421,854	59,030	38
3	1+2	2,430,086	982,755	72,940	43
4	1+2+3	3,466,386	4,058,443	108,540	100
5	1+2+3+4	4,514,641	11,210,477	179,840	100
6	5	482,652	554,163	59,020	100
7	6	328,115	484,626	8,060	100
8	5+6+7+8	1,760,130	4,636,456	70,260	100
9	15	1,680,144	3,727,117	0	100

The impact from the discharge to the water levels and storage capacities in the sea branches is indeed negligibly small. In the following cases, only the discharges corresponding to the reference case (**CS01**) will be considered.

7.3.4. CS04 - Neap tide

During neap tide, the tidal wave height reduces from 4 to 3 m. This means the water level during low tide is approximately 0.5 m higher than during regular tide. The simulation date is changed from January 1st, 2018 to March 27th, 2018. Figure 7.7 shows the difference in tidal wave height between regular tide (**CS01**) and neap tide (**CS04**). In this figure, the tidal signal corresponding to neap tide has been shifted such that high tide and low tides of the two signals are at the same time.

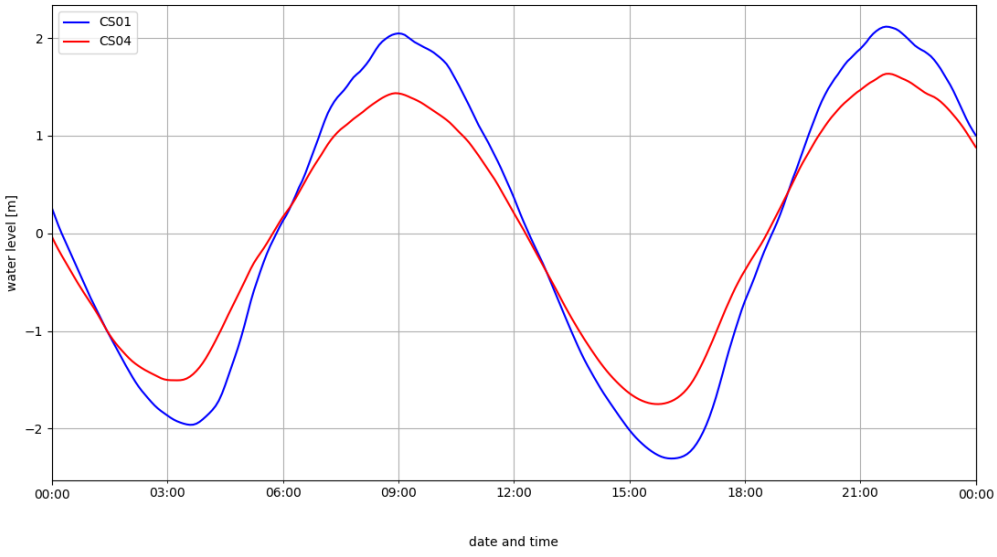

Figure 7.7: Water level in the Estero Salado near Febres Cordero during neap tide

The storage capacity during neap tide is lower than during low tide, because the lowest water level in the closed-off area is 0.5 m higher during neap tide than during regular tide.

To compute the storage in the sea branch, the neap low tidal level and regular high tidal level are taken as boundary conditions. The storage area of the parks does not change compared to **CS01**.

Table 7.5: Stored stormwater per barrier during neap tide

Barrier [#]	Catchment areas [#]	Stormwater [m^3]	Storage capacity sea branch [m^3]	Storage capacity parks [m^3]	Potential stormwater storage [%]
1	1	1,151,280	431,508	27,820	40
2	2	1,278,806	398,126	59,030	36
3	1+2	2,430,086	932,920	72,940	41
4	1+2+3	3,466,386	3,645,660	108,540	100
5	1+2+3+4	4,514,641	9,977,573	179,840	100
6	5	482,652	499,356	59,020	100
7	6	328,115	429,555	8,060	100
8	5+6+7+8	1,760,130	4,110,358	70,260	100
9	15	1,680,144	3,393,371	0	100

Similar to **CS01** and **CS03**, barrier 4, 5, 6, 7, 8 and 9 are capable of storing the stormwater from their entire catchment area.

7.3.5. CS05 - El Niño

During El Niño, the total water level can rise up to a level of 42 cm, due to storm surge. Figure 7.8 shows the water level during El Niño compared to the water level of **CS01**.

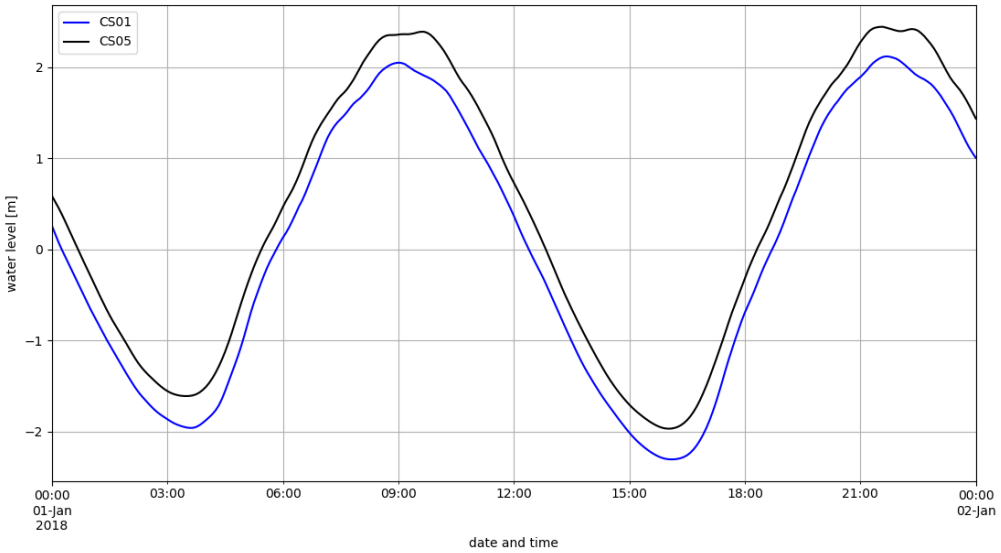

Figure 7.8: Water level in the Estero Salado near Febres Cordero for El Niño

Storm surge leads to a low tide level that is 42 cm higher than during regular conditions, resulting in a decrease of storage capacity in the closed off parts of the sea branches. The results of the computation are found below in Table 7.6.

Table 7.6: Stored stormwater per barrier during El Niño

Barrier [#]	Catchment areas [#]	Stormwater [m^3]	Storage capacity sea branch [m^3]	Storage capacity parks [m^3]	Potential stormwater storage [%]
1	1	1,151,280	442,977	27,820	41
2	2	1,278,806	409,795	59,030	37
3	1+2	2,430,086	959,918	72,940	43
4	1+2+3	3,466,386	3,822,270	108,540	100
5	1+2+3+4	4,514,641	10,476,639	179,840	100
6	5	482,652	520,226	59,020	100
7	6	328,115	450,891	8,060	100
8	5+6+7+8	1,760,130	4,309,769	70,260	100
9	15	1,680,144	3,520,993	0	100

It can be concluded that in the case of storage area, intense rainfall during neap tide (**CS04**) is a worse case scenario than during El Niño (**CS05**). However, as discussed in Section 4.3, the design rainfall values depicted here correspond to regular conditions, and not El Niño conditions. In reality, rainfall here will be much more intense and it is unsure if all of this can be stored in the sea branch.

7.3.6. CS06 - El Niño during neap tide

The combination of El Niño with neap tide is expected to give the lowest possible storage capacities for the sea branches, because the two phenomena result in very high water levels during low tide. This scenario combines the change in simulation date of **CS04** with the changes to the boundary and initial conditions of **CS05**. The result of the Delft3D-FM simulation is shown in Figure 7.9.

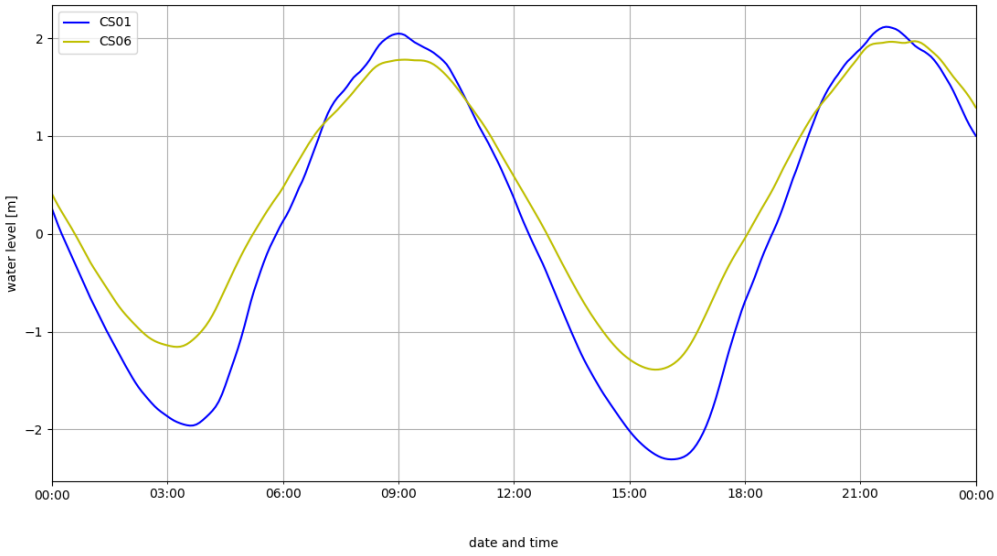

Figure 7.9: Water level in the Estero Salado near Febres Cordero for El Niño during neap tide

The volume of unstored stormwater and the percentage of stored stormwater are presented in Table 7.7

Table 7.7: Stored stormwater per barrier during El Niño and neap tide

Barrier [#]	Catchment areas [#]	Stormwater [m^3]	Storage capacity sea branch [m^3]	Storage capacity parks [m^3]	Potential stormwater storage [%]
1	1	1,151,280	393,507	27,820	37
2	2	1,278,806	376,363	59,030	34
3	1+2	2,430,086	864,529	72,940	39
4	1+2+3	3,466,386	3,336,042	108,540	99
5	1+2+3+4	4,514,641	9,110,929	179,840	100
6	5	482,652	463,133	59,020	100
7	6	328,115	392,754	8,060	100
8	5+6+7+8	1,760,130	3758021	70,260	100
9	15	1,680,144	3,141,720	0	100

The volumes of unstored rainwater are lower than all previous case scenarios, as was expected. The storage capacity behind barrier 4 is just too low to withhold the stormwater volume from the 10-year design rainfall. The storage areas behind barrier 5, 6, 7, 8 and 9 are still sufficiently large, even during neap tide and an increased mean water level.

For most barriers, the decrease in storage capacity for the combination of El Niño and neap tide (**CS06**) is more or less equal to the sum of the storage capacity decreases of these individual events (**CS04** and **CS05**). Notable is the difference between the results of **CS04** (Table 7.5), **CS05** (Table 7.6) and **CS06** (Table 7.7) for barrier 1. A significantly smaller amount of stormwater can be stored when a combination of El Niño and neap tide occurs. This can be explained by the cross-section of the barrier locations: The wetted cross-sectional area takes a giant leap when combining El Niño and neap tide conditions, especially during low tide. The wetted cross-sectional areas for the reference scenario (**CS01**), neap tide (**CS04**), El Niño (**CS05**), and El Niño during neap tide (**CS06**) of barrier 1 are shown in Figure 7.10. Clearly visible is the large difference in cross-sectional area around 3:30 PM.

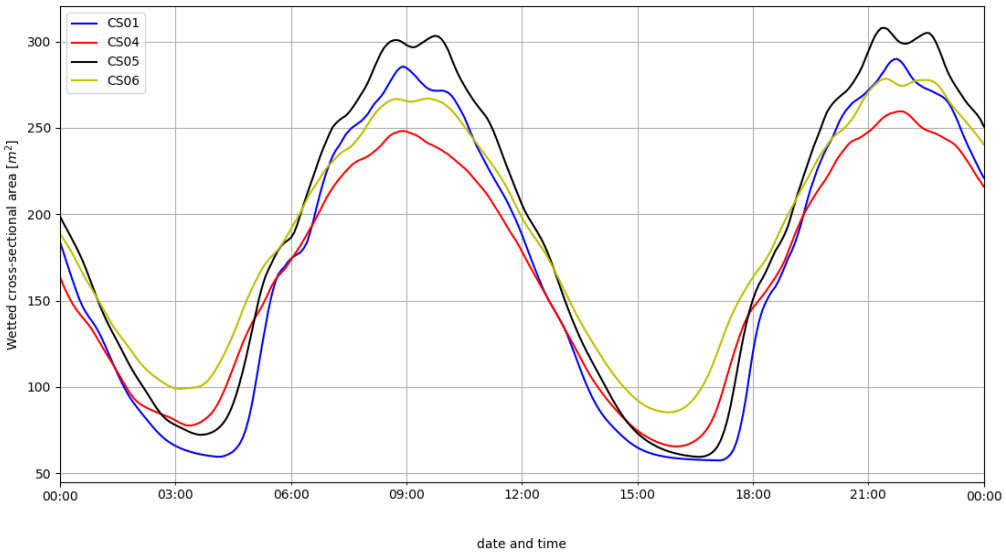

Figure 7.10: Wetted cross-sectional area of barrier 1

7.4. Conclusions

Based on the results from the sections above and the locations of the barriers from Figure 4.4, a combination of barrier 5, 8 and 9 would be most opportune. All catchment areas adjacent to a sea branch will drain their stormwater in a closed-off part behind one of these barriers. Also, all three barriers are able to withhold the stormwater volume from their corresponding catchment areas during the 10-year design rainfall, even during neap tide in combination with the storm surge from El Niño.

8

Discussion

In this study the possibility of reducing pluvial and coastal flood risk in urban areas by creating storage for excessive rainfall and retaining the incoming tide by a sea branch closure is analysed. In addition, other storage areas spread over the city to collect stormwater runoff are considered. The results and the limitations of the study are discussed in this chapter. Due to lack of time and lack of data, several simplifications and assumptions were made throughout this research, leading to a number of limitations.

8.1. Stormwater

To provide insights into the amount of stormwater that has to be retained, rainfall data is analysed to determine a constant design rainfall. With help of local authorities, a return period of 10 years is chosen to compute a constant design rainfall.

In the current scenarios a constant design rainfall is assumed with a return period of 10 years. In reality, this rainfall intensity only causes flooding when it coincides with high tide. Intense rainfall events during low tide generally do not cause flooding along the sea branches. Therefore, the probability of flooding during such an event is overestimated in this research and a higher return period can be expected.

Another limitation of the constant design rainfall determination is the spatial rainfall averaging. In this study, the rainfall data throughout the city is being averaged to one value. However, due to its widespread character, this is not entirely right. Microclimates within the city of Guayaquil are present. On average, more rain falls in the northern part of the city. More research should be done on microclimates and, based on that, the city could be divided into areas with similar rainfall characteristics. This would highly increase the precision of the total stormwater determination.

Rainfall data is obtained from several institutions, going back to the year 1962. However, most of these datasets contain intensities in mm/day. Measurements in mm/hour start only from 2011 onwards. For this particular research, mm/day is not specific enough, since critical rainfall shower durations are in the order of hours. Since no data is provided on the rainfall distribution over the day, downscaling of data is not an option. Therefore, the few years of data in mm/hour are compared to the large dataset of mm/day to see if they are representable. It shows similarities to some extend on the total rainfall per day and is therefore used, but this is far from optimal. Once detailed data over a longer period is available, this analysis has to be redone.

A further study should be executed on the urban stormwater system. Although, as concluded in this report, there is sufficient volume to store the stormwater in the sea branches, the stormwater system design might be an obstruction. Adjustments in the amount and sizes of stormwater pipes and drains might therefore be needed.

Due to the small number of measurement years, no clear trend in rainfall patterns and water levels due to climate change can be observed. Therefore, the findings of this report only refer to the current situation. Some conclusions may change when hydrologic or hydrodynamic conditions change in the future. CAF (2017) introduced the impact of climate change on the city of Guayaquil.

8.2. Hydrodynamic modelling

With help of a hydrodynamic Delft3D-FM model the effects of a closure at different locations are analysed.

First, the boundary conditions that are determined imply several limitations. To compute the design discharge, a probabilistic analysis based on measured discharge rates is conducted. This analysis is based on the maximum annual discharge, but due to the limited amount of years these rates are not accurate. In addition, it is important to state that only four tributaries of the Babahoyo are used as boundary conditions and that there are more small tributaries that are not taken into account. This may lead to an underestimation of the Babahoyo discharge. Because of the fact that measurements are performed only once a day, there is no clear vision on the possible influence of the tidal waves at the discharge gauging stations. However, model results show that there is no significant influence of the river discharge on water levels in the sea branches.

The bathymetry data used in the Delft3D-FM model is incomplete. Figure 8.1 shows the parts (in white) in the inner estuary where data is missing. The bed levels of these parts consist of a prismatic cross-section, using average bed levels of similar parts in the estuary. Although the model proved to be very accurate during validation, bathymetry data on these parts is required to improve the model. Also, barriers in these areas were not regarded because of the lack of bed level data.

Figure 8.1: Missing bathymetry data in the inner estuary

After the research, it turned out that the difference between MLWS and MSL must be complemented with the difference between the tidal gauge and MLWS to use for the bathymetry data from INOCAR. However, this difference lies below low tide. It does not directly influence the modelled storage capacities in the sea branches, but it may influence the tidal amplitudes in the estuary. A Delft3D-FM run with the new bed levels shows that the difference in water levels is negligibly small. For future research, the bed levels from data from INOCAR must be increased with 0.69 m in the Guayas river and with 3.32 m in the sea branches.

Within this research only the location of a possible barrier is analysed. The exact type, construction method, as well as the costs are not considered. A more detailed design of a barrier has to be made in order to balance costs and benefits. The technical feasibility and the risk of failure of the barrier itself have to be analysed as well.

8.3. Local storage

Using lowered parks and playgrounds to temporarily store rainwater is a solution that has proven to work on a very local scale in other countries. However, the available altitude maps of the city of Guayaquil are not precise enough to exactly determine the volume of water that will flow into the squares. The provided stormwater system map does not contain altitude levels, making it difficult to determine how the stormwater will flow through the system. To be able to make a design for the water square, more detailed maps are necessary. Only then, the suitable depth can be determined for each square as well, making storage calculations more precise.

Another problem is the exact costs of such a project. In the reference projects costs were high, but this could be due to the fact that architects designed the plazas to look modern; details are not known. In Guayaquil, the squares could be designed in a more practical way, saving costs. Being only a very local solution, the water squares would probably be implemented more often when the costs are relatively low. To be able to make a balance between costs and benefits, a more detailed design of the water squares has to be made first.

Concerning the underground storage basins, conclusions can only be drawn when an economic feasibility study is performed. The size of the basins, especially the depth, will determine the greatest part of the costs. Budget restrictions will probably define the dimensions, and those dimensions are needed to determine how much stormwater can be stored. Thus, more research should be executed before further commenting on this solution - which is full of potential.

9

Conclusions and Recommendations

9.1. Conclusions

The scope of this study was to investigate the possibility of reducing pluvial and coastal flooding of urban areas in Guayaquil. The solution must be able to retain the incoming tide and create storage for excessive rainfall. Closing off one or multiple sea branches and local storage in parks and playgrounds around the city are considered. The main conclusions of this study are:

- Temporary storage of stormwater behind a barrier in a sea branch is a suitable solution to prevent both pluvial and coastal flooding.
- A combination of barriers at location 5, 8 and 9 (see Figure 4.4) is most opportune to withhold the stormwater volume of the 10-year design rainfall from their corresponding catchment areas. In order for these barriers to be effective, they must be closed during low tide prior to heavy rainfall. Even in the event of the highest possible water level during low tide, being neap tide in combination with the storm surge of El Niño, the storage capacities are sufficiently large.
- Local stormwater storage in parks and playgrounds is a small-scale solution to reduce pluvial flooding. The storage capacity of these areas is much smaller than the storage capacity behind a barrier, but it is a solution for low-lying urban areas that are not adjacent to a sea branch or river.
- The impact of the river discharge and the construction of a barrier on the flow and water levels in the sea branches is negligibly small.

9.2. Recommendations

Based on the drawn conclusions, the following recommendations are given to reduce the flood risk in the urban areas of Guayaquil:

- Besides the large-scale and small-scale solutions that are currently considered by the local authorities, they are advised to also consider the intermediate-scale solution presented in this study.
- Parks and playgrounds in Guayaquil can be adapted to local storage areas using the principle already used in The Netherlands, where such areas have already proven themselves useful.
- When the storage capacity of parks and playgrounds in some catchment areas is not sufficient, underground storage basins can be considered as local storage areas.

Several simplifications and assumptions were made throughout this research, as discussed in Chapter 8. Therefore, the following recommendations are given to increase the quality, integrality and reliability of further research.

- The local authorities are advised to set up regulations on return periods for designing flood risk-reducing structures.

- The local authorities are advised to assess the economic losses due to floods in urban areas, in order to be able to estimate acceptable costs of flood risk-reducing structures.
- A technical feasibility study on the barriers is not conducted in this report. An optimisation study on the location, type and height of the barrier must be executed.
- Local authorities are advised to further investigate the distribution of rainfall over the city of Guayaquil due to the presence of microclimates. Detailed insight into accurate rainfall pattern will contribute to an optimal barrier design.
- When the number of years of measurements is increased, the local authorities are advised to calculate accurate precipitation rates during El Niño. Also, the impacts of climate change on the rainfall pattern and mean sea level should be assessed.
- Currently, research on subsidence of landfills in Guayaquil is being executed. Potentially increased flood vulnerability due to subsidence should be taken into account in further studies.
- The impact of a barrier on the morphology and the water quality in the estuary should be considered in further studies.

Bibliography

Amsterdam Rainproof (2014). Waterpleinen. https://www.rainproof.nl/toolbox/maatregelen/waterpleinen. Accessed: 2018-03-20.

API (2016). Flooding guayaquil 2016-01-25 [Photograph]. http://www.ecuavisa.com/articulo/televistazo/noticias/126740-lluvia-mas-12-horas-desato-congestion-vehicular-guayaquil.

Axler, R., Kleist, C., Host, G., C.Hagley, M.Lonsdale, Reed, J., Schomberg, J., Will, N., Henneck, J., Sjerven, G., E.Ruzycki, T.Carlson, Munson, B., and Richards, C. (2009). Lakesuperiorstreams. http://lakesuperiorstreams.org. Accessed: 2018-04-03.

Barrera Crespo, P. (2016). Delft3D Flexible Mesh modelling of the Guayas River and estuary system in Ecuador. Master's thesis, Delft University of Technology and National University of Singapore.

Betancourt, A. M., Tucci, C. E. M., Bertoni, J. C., and Vélez, G. C. (2013). La inundación de Guayaquil en Marzo 2013.

Bosboom, J. and Stive, M. (2013). *Coastal Dynamics 1: Delft*. Delft Academic Press, 0.4 edition.

Brinkhoff, T. (2018). City population. https://www.citypopulation.de/php/ecuador-parish-admin.php?adm2id=090150. Accessed: 2018-02-21.

Butler, D. and Davies, J. (2004). *Urban drainage*. Crc Press.

CAF (2000). El fenomeno el niÑo 1997-1998 memoria, retos y soluciones volumen 4: Ecuador.

CAF (2013). La Inundación de Guayaquil en marzo 2013.

CAF (2017). Diagnóstico y proyección de vulnerabilidades frente a la variabilidad y cambio climático en la ciudad de Guayaquil.

Castro, B. et al. (2009). Sedimentation processes at the confluence of the daule and babahoyo rivers, guayaquil, ecuador. el palmar island. Master's thesis, The University of Birmingham.

Cedeño, P. (2018). Flooding guayaquil 2018-02-19 [Photograph]. https://www.eluniverso.com/guayaquil/2018/02/19/nota/6631615/lluvia-anega-avenidas-norte-guayaquil.

Centre for Ecology & Hydrology (1999). *Flood Estimation Handbook*, volume 3.

De Urbanisten (2013). Water Square Benthemplein. http://www.urbanisten.nl/wp/?portfolio=waterplein-benthemplein. Accessed: 2018-03-20.

Deltares (2015). *Delft3D Flexible Mesh user manual*.

District, P. C. R. F. C. (2014). Design standards for stormwater detention and retention.

DP World (2016). DP World wins concession agreement for Greenfield port in Ecuador.

Garcés Santander, S. (2017). Exploring combination of urban flood risk management measures.

Gemeente Rotterdam (2012). Bellamyplein - waterplein.

Gemeente Rotterdam & dS+V (2011). Vasthouden van regenwater in de openbare ruimte van Rotterdam.

González, J. (2017). El proyecto las esclusas se suma al desarrollo portuario. http://www.elcomercio.com/actualidad/lasesclusas-guayaquil-esterosalado-rioguayas-navegabilidad.html. Accessed: 2018-02-22.

Google (n.d.a). Google Earth historic maps of Guayaquil. Accessed: 2018-02-21.

Google (n.d.b). Google Maps map of Guayaquil. https://goo.gl/o4BiFq. Accessed: 2018-02-14.

Hoogheemraadschap van Delfland (2012). Waterplein Delfshaven, agendapunt 3.b.8.

INAMHI (2018). Official INAMHI website. http://www.serviciometeorologico.gob.ec/. Accessed: 2018-03-15.

INOCAR (2011). El Niño - la Niña. http://www.inocar.mil.ec/modelamiento/elnino/index.php. Accessed: 2018-03-09.

INOCAR (2016). El Niño, La Niña, ENSO, ENOS, El Niño Modoki, El Niño Canónico, El Niño Extraordinario, El Niño Godzilla, El Niño Costero, El Niño Oriental ¿En qué consisten realmente y cómo afectan al Ecuador?

INOCAR (2018a). Official INOCAR website. http://www.inocar.mil.ec/web/index.php/institucion/mision-y-funciones. Accessed: 2018-03-15.

INOCAR (2018b). Tabla de mareas puertos del Ecuador. http://www.inocar.mil.ec/web/index.php/productos/tabla-mareas. Accessed: 2018-03-12.

Interagua (2010a). Ajuste y revision del plan maestroagua potable;alcantarillado sanitario y alcantarillado pluvial tomo I. page 321.

Interagua (2010b). Ajuste y revision del plan maestroagua potable;alcantarillado sanitario y alcantarillado pluvial tomo I. page 273.

José Morán, E. T. (2016). Flooding guayaquil 2016-02-05 [Photograph]. https://www.eltelegrafo.com.ec/noticias/guayaquil/1/la-marea-del-rio-estuvo-baja-pero-guayaquil-se-inundo-nuevamente.

Kernkamp, H. W., Van Dam, A., Stelling, G. S., and de Goede, E. D. (2011). Efficient scheme for the shallow water equations on unstructured grids with application to the continental shelf. *Ocean Dynamics*, 61(8):1175–1188.

LeighFisher (n.d.). Greenfield airport master plan and strategic development plan for guayaquil, ecuador. http://www.leighfisher.com/global-experience/greenfield-airport-master-plan-and-strategic-development-plan-guayaquil-ecuador. Accessed: 2018-04-05.

Minnesota Stormwater Steering Committee (2017a). Minnesota Stormwater Manual. https://stormwater.pca.state.mn.us/index.php?title=Design_infiltration_rates. Accessed: 2018-03-21.

Minnesota Stormwater Steering Committee (2017b). Minnesota Stormwater Manual. http://www.lakesuperiorstreams.org/stormwater/toolkit/underground.html. Accessed: 2018-04-03.

Municipalidad de Guayaquil (2015). Mapa de Zonas Propensas a Inundaciones. http://guayaquil.gob.ec/mapas. Accessed: 2018-03-22.

NOAA (2017). El Niño theme page; pacific marine environmental laboratory. https://www.pmel.noaa.gov/elnino/. Accessed: 2018-02-26.

Rijksoverheid (2016). Jaarlijkse hoeveelheid neerslag in Nederland. http://www.clo.nl/indicatoren/nl0508-jaarlijkse-hoeveelheid-neerslag-in-nederland. Accessed: 2018-02-16.

Roman, J. (2016). Development of a strategic plan for port authority of guayaquil-case of guayaquil. Master's thesis, Erasmus University Rotterdam.

Rotterdam Climate Initiative (n.d.). Waterplein op bellamyplein. http://www.rotterdamclimateinitiative.nl/nl/stad/lopende-projecten/waterplein-op-bellamyplein?project_id=196&global_subcategory_id=3&p=1. Accessed: 2018-03-19.

Schiereck, G. J. (2012). *Introduction to bed, bank and shore protection*. VSSD.

Stenfert, J., Bouman, R. R., Nolthenius, R. T., and Joosten, S. (2017). Flood risk Guayaquil. *Netherlands Centre for River Studies*.

Stormtrap (2016). Stormtrap. http://stormtrap.com/solutions/detention/. Accessed: 2018-04-03.

Straatbeeld (2014). Bellamyplein: speelplezier en bittere noodzaak. https://www.straatbeeld.nl/project/180614/bellamyplein-speelplezier-en-bittere-noodzaak. Accessed: 2018-03-20.

Suárez Changuán, P. (2010). Muelle de servicio isla santay. estudios y diseños. *Ministero del Ambiente*.

Takahashi, K. (2017). Tokyobasin. https://www.nytimes.com/2017/10/06/climate/tokyo-floods.html. Accessed: 2018-04-03.

Twilley, R., Cárdenas, W., Rivera-Monroy, V., Espinoza, J., Suescum, R., Armijos, M., and Solórzano, L. (2001). The Gulf of Guayaquil and the Guayas river estuary, Ecuador. In *Coastal Marine Ecosystems of Latin America*, volume 144, pages 245–263. Springer.

Urban Water Resources Council (1992). *Design and Construction of Urban Stormwater Management Systems*, volume 77.

Vera-Grunauer, X., Bray, J., Pestana, J., Kayen, R., Tandazo, E., Ramirez, J., Vera-Grunauer, J., and Mera-Ortiz, W. (2006). Site characterization and seismic zonation of Guayaquil City, Ecuador. In *8th US National Conference on Earthquake Engineering*.

Visscher, R. (2013). Waterplein maakt Rotterdam regenproof.

A

Flood-prone areas

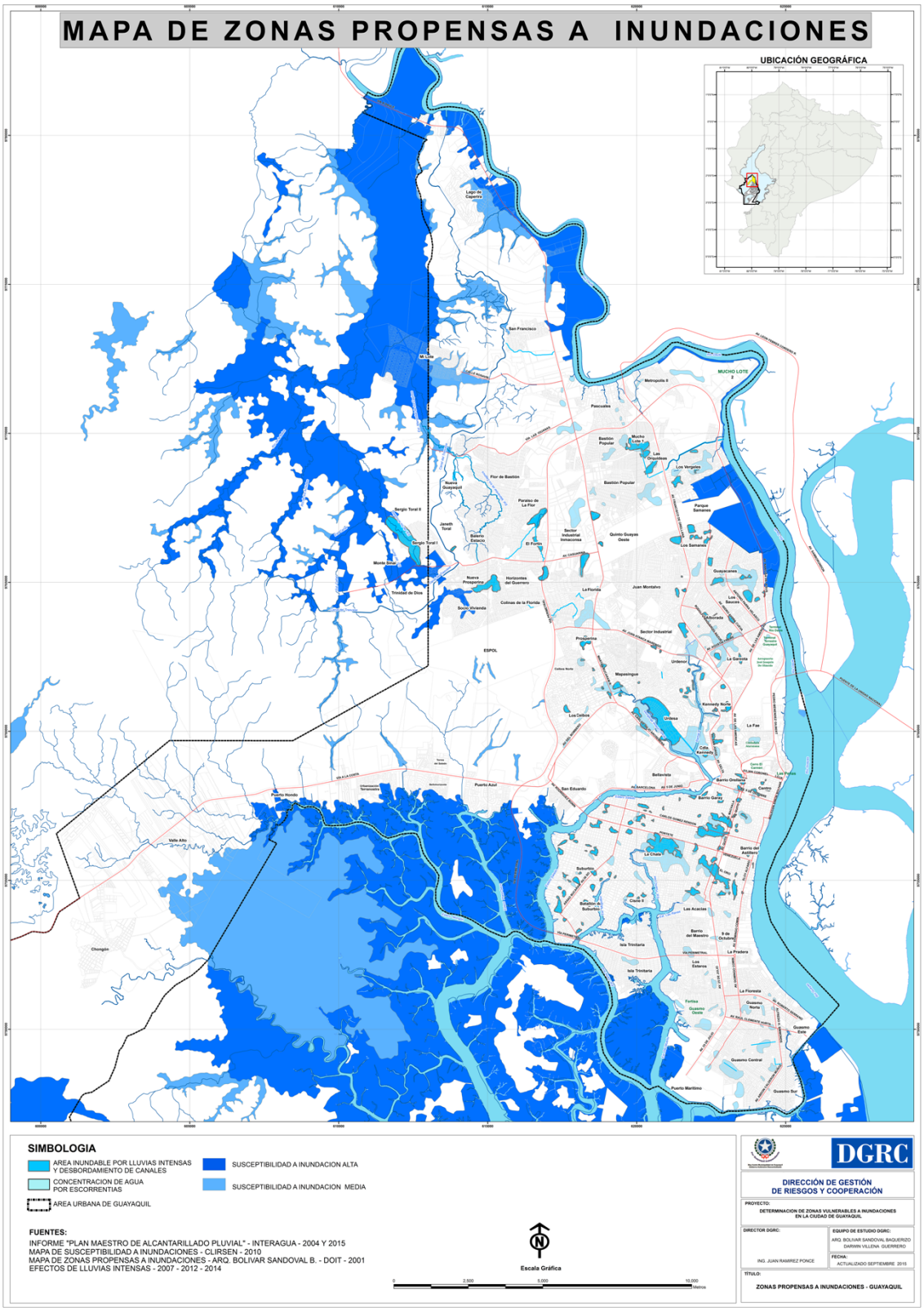

Figure A.1: Areas prone to flooding (Municipalidad de Guayaquil, 2015)

B

Satellite Images

B.1. Guayaquil

Figure B.1: Old satellite images of Guayaquil. (a) 1984, (b) 2016 (Google, nda)

B.2. La Trinitaria

Figure B.2: Old satellite images of La Trinitaria district. (a) 2000, (b) 2016 (Google, nda)

C

Catchment areas

C.1. Typical runoff parameters

To determine the total runoff that arises per catchment area, the ground coverage is characterised by three types. The covering determines the amount of water that can infiltrate into the ground and the amount of water that will be drained over the land.

Table C.1: Typical values of runoff coefficient in urban areas (Urban Water Resources Council, 1992)

Area description	Runoff Coefficient	Surface types	Runoff Coefficient
City centre	0.70-0.95	Asphalt and concrete paving	0.70-0.95
Suburban business	0.50-0.70	Roofs	0.75-0.95
Industrial	0.50-0.90	Lawns	0.05-0.35
Residential	0.30-0.70		
Parks and gardens	0.05-0.30		

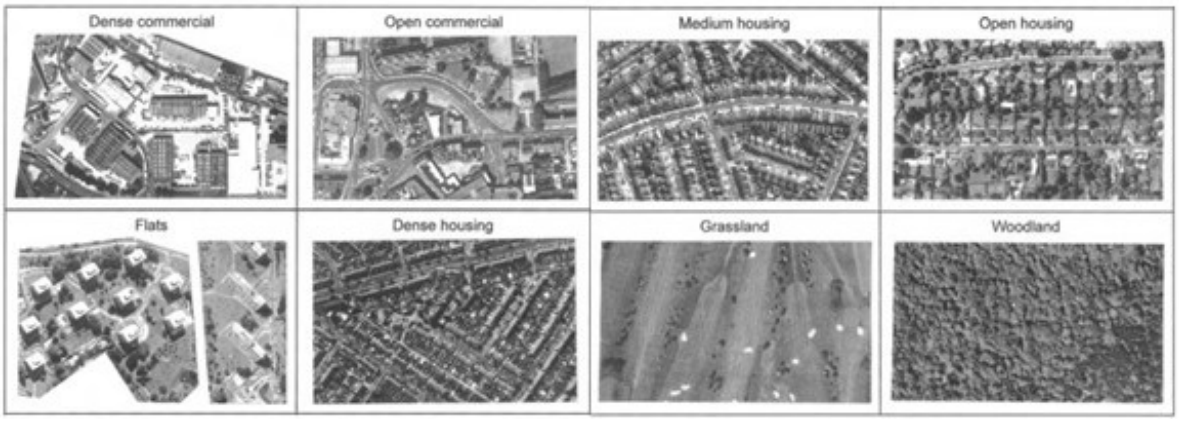

Figure C.1: Characterisation of ground cover in urban areas (Butler and Davies, 2004)

Table C.2: Runoff coefficient per catchment area. Green = green areas, cc = city centre and dense housing, res = residential areas

Catchment Area	Area $[km^2]$	Areal Percentage	Type of Coverage	Runoff Coefficient	Areal Contribution	Average Runoff Coefficient
1	12	0.2	green	0.15	0.03	
		0.55	cc	0.85	0.4675	
		0.25	res	0.6	0.15	0.65
2	11.4	0.1	green	0.15	0.015	
		0.8	cc	0.85	0.68	
		0,1	res	0,6	0,06	0.76
3	11.9	0.3	green	0.15	0.045	
		0.5	cc	0.85	0.425	
		0.2	res	0.6	0.12	0.59
4	10.6	0.2	green	0.15	0.03	
		0.65	cc	0.85	0.5525	
		0.15	res	0.6	0.09	0.67
5	4.37	0.6	cc	0.85	0.51	
		0.4	res	0.6	0.24	0.75
6	2.85	0.7	cc	0.85	0.595	
		0.3	res	0.6	0.18	0.78
7	3.3	0.75	cc	0.85	0.64	
		0.25	res	0.6	0.15	0.79
8	5.1	0.6	cc	0.85	0.51	
		0.4	res	0.6	0.24	0.75
9	8.51	0.3	green	0.15	0.045	
		0.4	cc	0.85	0.34	
		0.3	res	0.6	0.18	0.57
10	2.66	0.1	green	0.15	0.015	
		0.8	cc	0.85	0.68	
		0.1	res	0.6	0.06	0.76
11	2.48	0.5	cc	0.85	0.425	
		0.2	res	0.6	0.12	0.59
12	4.34	0.1	green	0.15	0.015	
		0.6	cc	0.85	0.51	
		0.3	res	0.6	0.18	0.71
13	4.79	0.6	cc	0.85	0.51	
		0.4	res	0.6	0.24	0.75
14	4.39	0.1	green	0.15	0.015	
		0.7	cc	0.85	0.595	
		0.2	res	0.6	0.12	0.73
15	11.6	0.1	green	0.15	0.015	
		0.6	cc	0.85	0.51	
		0.3	res	0.6	0.18	0.71

C.2. Pipelines

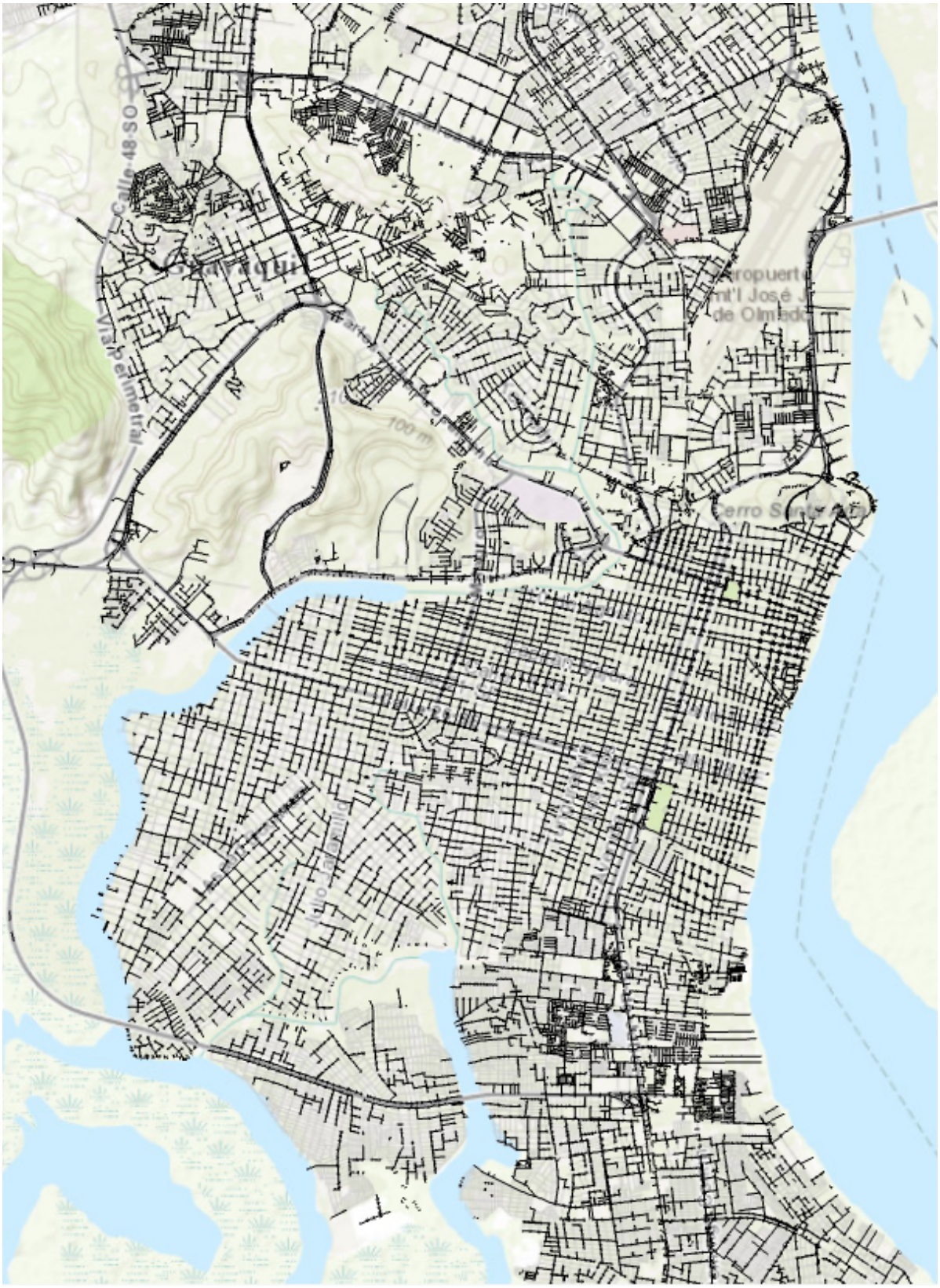

Figure C.2: Part of the system of pipelines in Guayaquil (based on ArcGIS Pro render). This shapefile was used to determine the partial catchment areas along the sea branches.

D

Local authorities

During the project, some interviews have been carried out with local authorities to gain insight into their visions on the inundations in Guayaquil. Asked questions are related to the causes of the floods, possible solutions and their vision on our proposed solution. It must be noted that the people interviewed can in no way be held responsible for their statements within our report. Parts may be lost or misinterpreted due to translation errors.

D.1. Instituto Nacional de Meteorología e Hidrología (INAMHI)

"INAMHI is the National Meteorological and Hydrological Service of Ecuador. It is the National Meteorological and Hydrological Service of Ecuador created by Law, as a necessity and a fundamental right of the community, with capacity and the obligation to provide vital information on the weather, climate and water resources of the past, present and future, who needs to know the country for the protection of human life and material goods. It is an institution with national and international representation, member of the World Meteorological Organization, WMO, a specialised intergovernmental organization of the United Nations for Meteorology (weather and climate), Operational Hydrology and related sciences. It is a technical body that in the national context is assigned to the Risk Management Secretariat; with technical and professional personnel specialised in Meteorology and Hydrology, which contributes to the economic and social development of the country." (INAMHI, 2018)

A meeting took place on 3/5/2018 with:
Local Director ing. Raúl Mejía

D.2. Instituto Oceanográfico de la Armada (INOCAR)

INOCAR is the oceanographic research Institute of the Navy and has the following mission: "Plan, direct, coordinate and control the technical and administrative activities related to the Service of Hydrography, Navigation, Oceanography, Meteorology, Marine Sciences, Nautical Signaling, as well as the administration of the specialised material with its activity." (INOCAR, 2018a)

The institution provides data and knowledge in the field of water-related measurements to the government and has research programs to study the effects of climate change in the future, seismic activity for risk management, and precipitation.

A meeting took place on 3/14/2018 with:
Technical Director Commander Edwin Pinto
Environmental and Meteorological Engineer Jaime Fuentes
Oceanographer Miriam Lucero
Oceanographer Sharl Noboa

D.3. Risk Management Department of the Municipality of Guayaquil

The risk management department is part of the municipality of Guayaquil. They are in charge of natural risk prevention in the city of Guayaquil and along the coast of Ecuador. Fields of interest are for example seismic activities, flooding problems and landslides. The department initiates research questions to authorities like INOCAR or EMAPAG and based on their reports contacts other authorities to take measures. When seismic activities are measured, they are the ones who decide when to sound the alarm or evacuate.

A meeting took place on 3/14/2018 with:
Director ing. Juan Antonio Ramírez Ponce, MSc.
Subdirector Mónica Menéndez V.

D.4. Empresa Pública Municipal de Agua Potable y Alcantarillado de Guayaquil (EMAPAG-EP)

EMAPAG is a public company, governed by the municipality of Guayaquil, in charge of water resources, sewerage and stormwater system. The company controls and regulates the drinking water, the sewage system and the stormwater system services that are operated by concessionaire Interagua. EMAPAG is responsible for long term visions and strategies for the municipality considering water resources. They co-orporate with INOCAR and the Risk Management department.

A meeting took place on 3/27/2018 with:
Technical Director Martha Orta

E

Probability distributions

Three General Extreme Value distributions (GEV) are used: Gumbel, Weibull, and Fréchet. Formulas for the probability density function (PDF) and the cumulative density function (CDF) are shown below.

Gumbel

The Gumbel distribution on the given rainfall data gives a fairly good fit. Although the Fréchet fit has a smaller RMSE, the Gumbel distribution is chosen to be the best fit. This is based on the fact that the Gumbel distribution takes the highest peaks into account better, in contrast to the Fréchet distribution.

$$PDF: f_x(x) = \alpha \exp\left\{-\alpha(x-u) - e^{-\alpha(x-u)}\right\} \tag{E.1}$$

$$CDF: F_x(x) = \exp\left\{-e^{-\alpha(x-u)}\right\} \tag{E.2}$$

Fréchet

Based on the RMSE of the distributions, the Fréchet distribution appears to show the best fit. After analysing the fits visually, the Gumbel distribution is preferred over the Fréchet, since the Fréchet distribution accounts for the highest values in a disproportional way.

$$PDF: f_x(x) = \left(\frac{k}{\alpha}\right)\left(\frac{x-u}{\alpha}\right)^{-k-1} \exp\left\{\left(\frac{-(x-u)}{\alpha}\right)^{-k}\right\} \tag{E.3}$$

$$CDF: F_x(x) = \exp\left\{(-(x-u)/\alpha)^{-k}\right\} \tag{E.4}$$

Weibull

The Weibull distribution on the given rainfall data does not fit the data well. Especially the highest peaks are neglected and therefore not taken into account sufficiently.

$$PDF: f_x(x) = -\left(\frac{k}{\alpha}\right)\left(\frac{x-u}{\alpha}\right)^{k+1} \exp\left\{\left(\frac{-(x-u)}{\alpha}\right)^{k}\right\} \tag{E.5}$$

$$CDF: F_x(x) = \exp\left\{(-(x-u)/\alpha)^{k}\right\} \tag{E.6}$$

F

Design rainfall

F.1. Locations meteorologic measuring stations

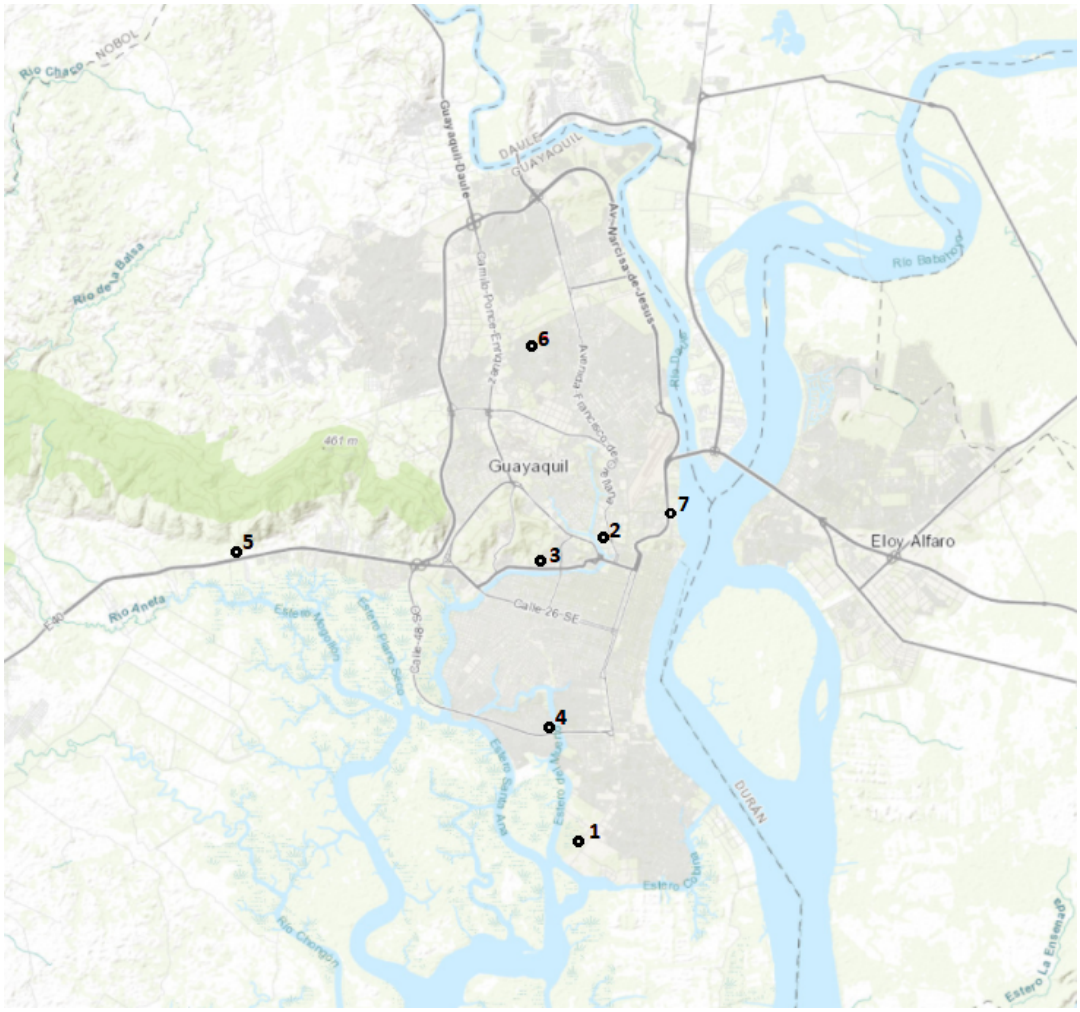

Figure F.1: Locations of used rainfall stations. (1) INOCAR, (2) INAMHI, (3) Bellavista (Interagua), (4) Trinitaria (Interagua), (5) Via a la Costa (Interagua), (6) Juan Montalvo (Interagua), (7) Planta Progreso (Interagua). (based on ArcGIS Pro render)

F.2. Intensity per 24 hours

Measured data per 24 hours (from 0.00-24.00) is provided by INOCAR and INAMHI. The data starts in 1962 for INOCAR and 1992 for INAMHI. Since rainfall is only measured on a daily basis, no conclusion can be stated about shorter time steps. For these stations the daily design rainfall according to return period is determined. Data provided by Interagua is recorded automatically, and therefore more specific. This data is also accumulated to 24-hour data (0.00-24.00) to be able to make a comparison between the institutions. Both methods with one peak and five peaks on average per year are analysed. Five peaks are assumed to give better results, as rainfall events are independent and intensities can vary per year. All of the highest peaks are of most interest to this research.

Table F.1: Daily maximum rainfall per return period

Intensity (mm/h)	INOCAR		INAMHI		INTERAGUA	
Return T	1 peak	5 peaks	1 peak	5 peaks	1 peak	5 peaks
2 years	3.40	4.00	4.27	4.74	-	4.45
5 years	4.71	4.71	5.92	5.57	-	5.35
10 years	5.57	5.23	7.01	6.19	-	6.03
25 years	6.66	5.91	8.38	6.99	-	6.90
50 years	7.47	6.42	9.41	7.60	-	7.56
100 years	8.27	6.93	10.42	8.21	-	8.22

F.3. Intensity per duration

Based on the data of five rainfall measuring stations in Guayaquil (See Appendix F.1) provided by Interagua, the intensity duration frequency curve is determined. To be able to determine this, Gumbel, Weibull and Fréchet distributions are fitted on the histograms of the maximum peak analysis. At first, the root-mean-square error (RMSE) was calculated to determine the best fit (Table F.2). However, in many cases, the best fit did not take the highest peaks into account leading to an underestimation (for example, see Weibull in Figure F.2). Therefore, based on appearance the Gumbel distribution is chosen as the best fit. The fitted curves and RMSE for Bellavista are shown in the figures at the end of this appendix. This analysis is repeated for five stations in total, having Gumbel to be determined to be the best fit for all of the stations.

Table F.2: RMSE per duration for Bellavista rainstation

Distribution \Duration (hours)	1	2	4	8	12	24
Gumbel	0.01308	0.01436	0.01391	0.03250	0.01582	0.02826
Weibul	0.01402	0.01507	0.01386	0.03266	0.01587	0.02837
Fréchet	0.01278	0.01456	0.01409	0.03549	0.01589	0.02820

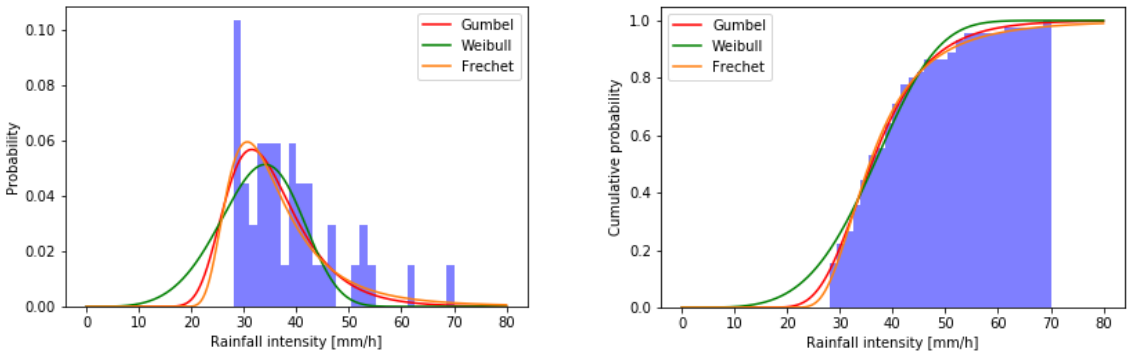

Figure F.2: PDF and CDF of Bellavista (1 hour)

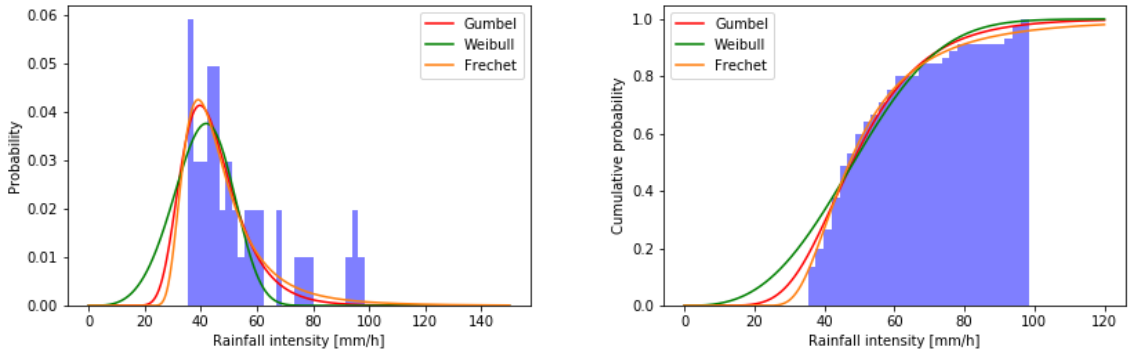

Figure F.3: PDF and CDF of Bellavista (2 hour)

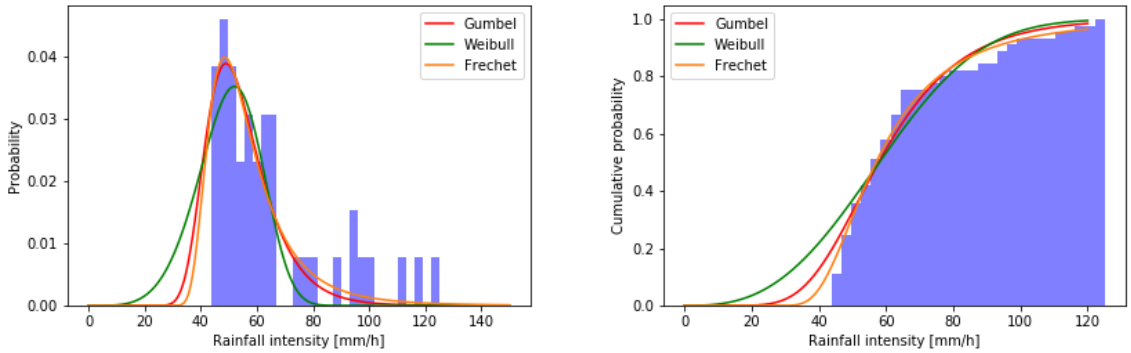

Figure F.4: PDF and CDF of Bellavista (4 hour)

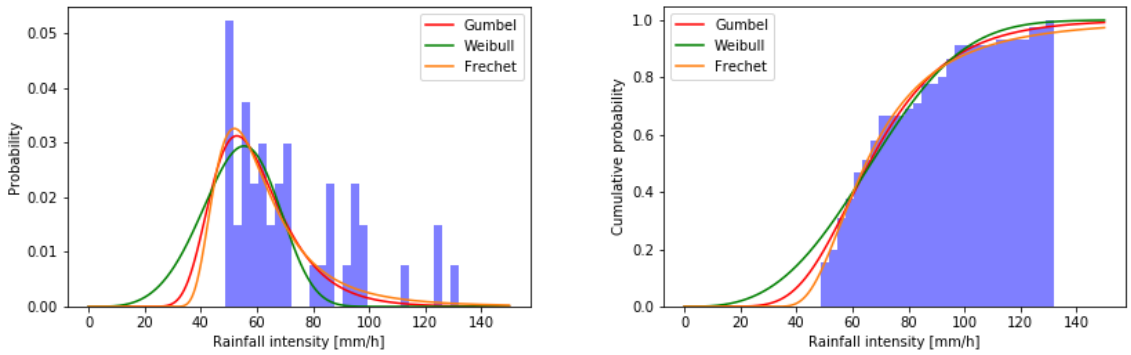

Figure F.5: PDF and CDF of Bellavista (8 hour)

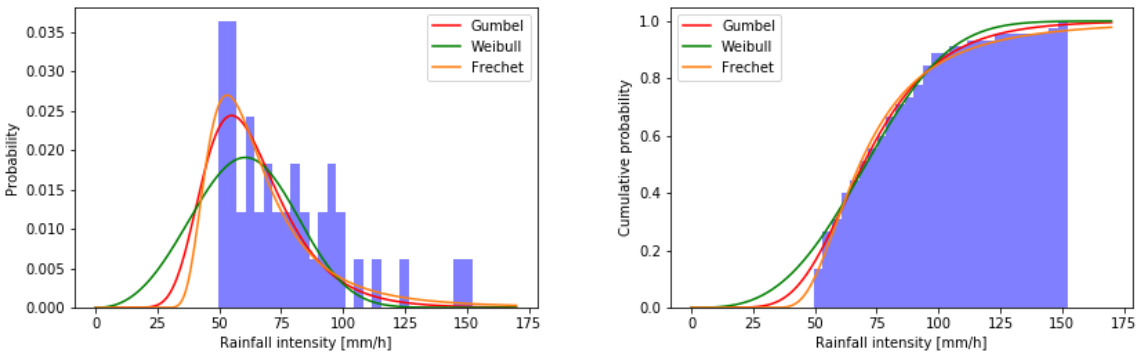

Figure F.6: PDF and CDF of Bellavista (12 hour)

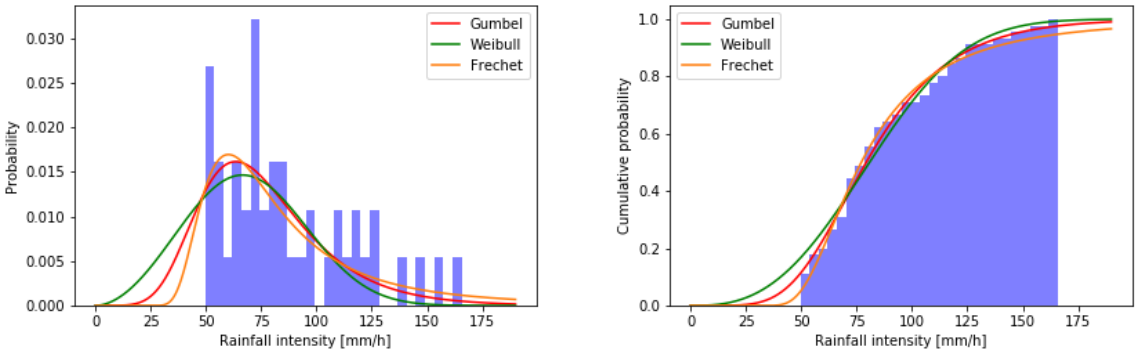

Figure F.7: PDF and CDF of Bellavista (24 hour)

With a Gumbel fit, the rainfall intensities are determined per return periods. The result per station for a return period of 10 years can be found in Figure F.8. The final averaged result is shown in Table 4.1.

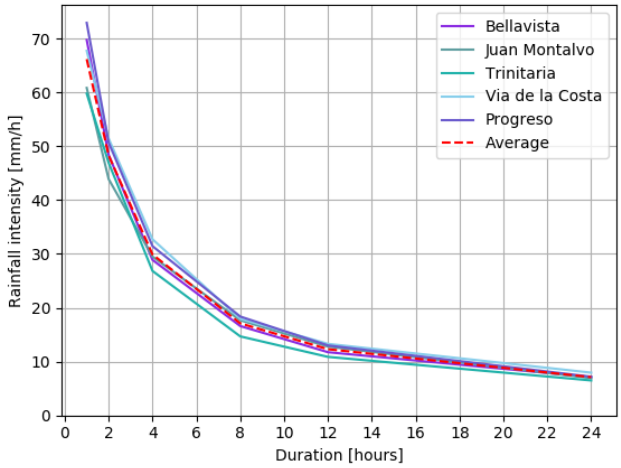

Figure F.8: IDF curves per measuring station

G

Design discharge

The Gumbel, Weibull and Fréchet distributions are fitted onto annual maximum discharge. At first, the root-mean-square error (RMSE) was calculated to determine the best fit. However, in some cases, this leads to an over-or underestimation of the data and therefore a visual analysis is also taken into account to determine the best fit. The discharge per return period is determined based on the distribution with the best fit. This procedure is repeated for all five gauging stations. The fitted PDF- and CDF-curves are shown in the figures below.

In Table G.1 the RMSE for all three distributions is shown. In case of the Vinces, San Pablo and Chimbo rivers the distribution leading to the lowest RMSE is chosen, but not in case of the Daule and Zapotal rivers. A brief explanation for the chosen distribution for each river is given:

Daule: The maximum daily discharge per year is used. It turns out that the errors of the three distributions are close to each other, with Fréchet as the lowest RMSE. However, fitting the Fréchet distribution did not lead to a good fit because it overestimates the discharge for the higher return periods, leading to unreasonable high discharges. Therefore, the Weibull distribution is preferred.

Zapotal: Using the maximum daily discharge per year, the Fréchet distribution gives the best fit. The Weibull fit leads to a slightly smaller RMSE but does underestimate the higher discharges. The Fréchet distribution is therefore used for the fit.

Vinces: In case of the Vinces river, the Weibull distribution gives the lowest RMSE and the best fit and is therefore chosen to determine the discharges.

San Pablo: Using the maximum daily discharge per year the Fréchet distribution leads to the best fit and the smallest error.

Chimbo: For the Chimbo river, only 13 years of reliable data is available, which implies that using the maximum daily discharge per year leads to an insufficient amount of data for a statistical analysis. Because of the small size of the Chimbo river, this will not have a large influence on the results. The Weibull distribution is chosen as the best fit.

Table G.1: RMSE discharge

	Daule	Zapotal	Vinces	San Pablo	Chimbo
Fréchet	0.0003503	0.0007114	0.0010484	0.0018610	0.0018279
Gumbel	0.0003628	0.0007163	0.0010233	0.0019094	0.0017727
Weibull	0.0003619	0.0006827	0.0009295	0.0024582	0.0015581
Lowest MRSE	Fréchet	Weibull	Fréchet	Weibull	Weibull
Best fit	Weibull	Fréchet	Fréchet	Weibull	Weibull

The PDF and CDF curves for each river are shown below.

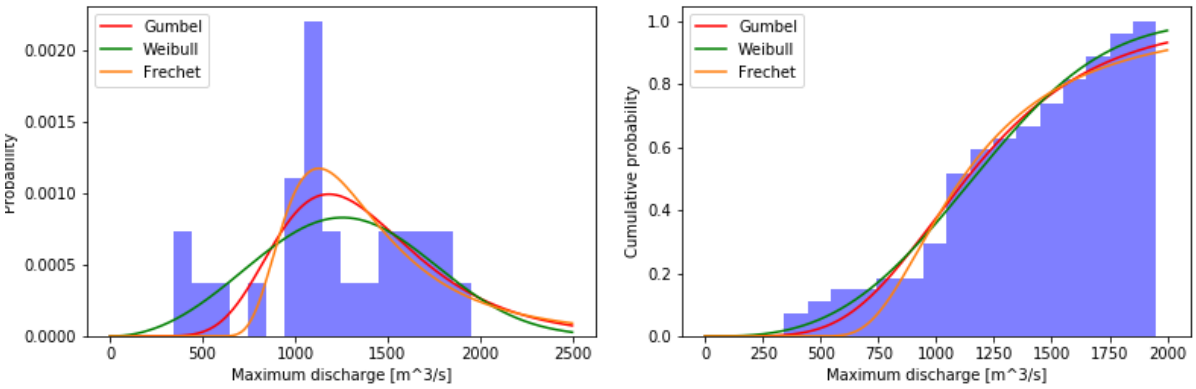

Figure G.1: PDF and CDF of Daule river

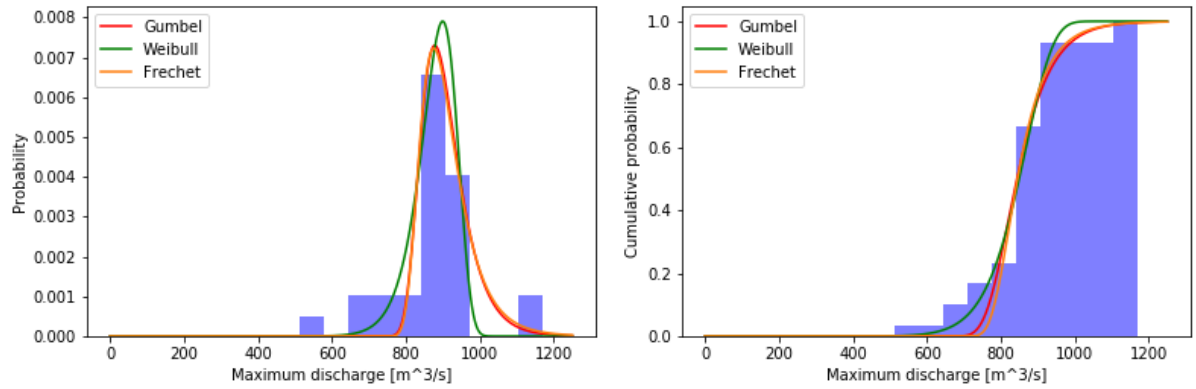

Figure G.2: PDF and CDF of Zapotal river

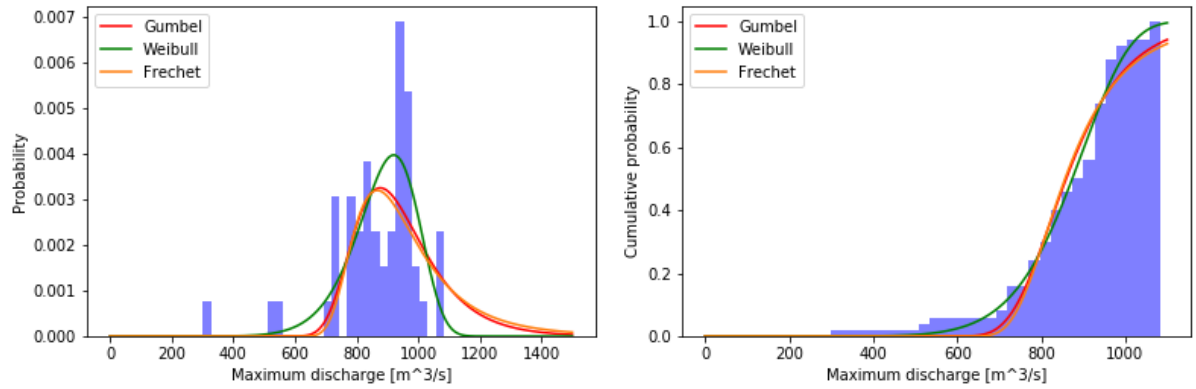

Figure G.3: PDF and CDF of Vinces River

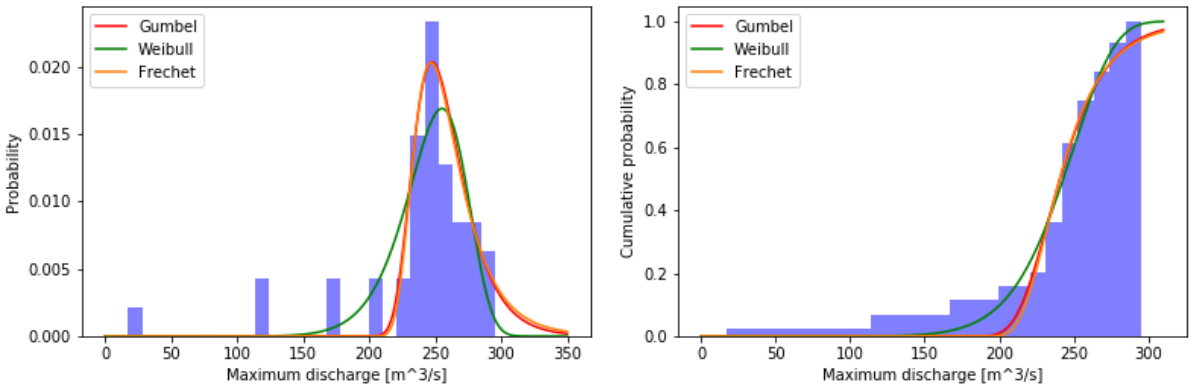

Figure G.4: PDF and CDF of San Pablo river

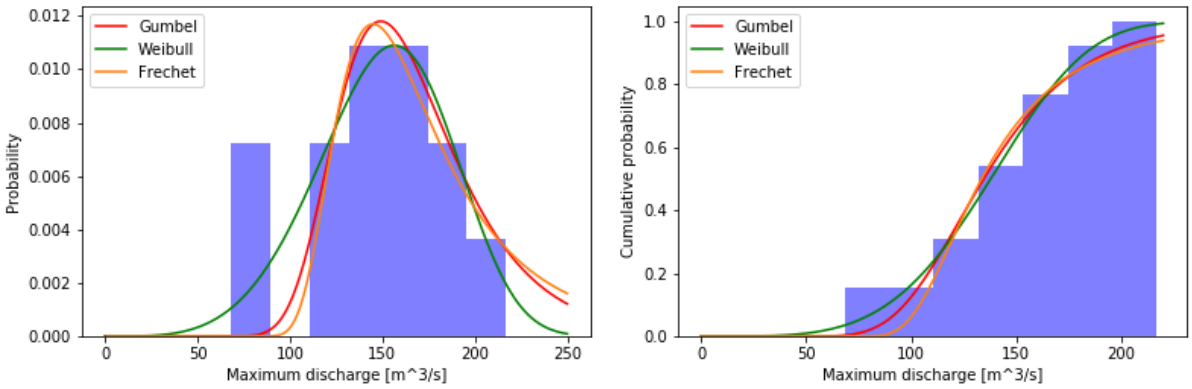

Figure G.5: PDF and CDF of Chimbo river

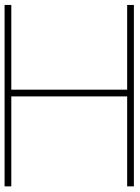

Local storage

H.1. Locations and sizes of possible local storage areas

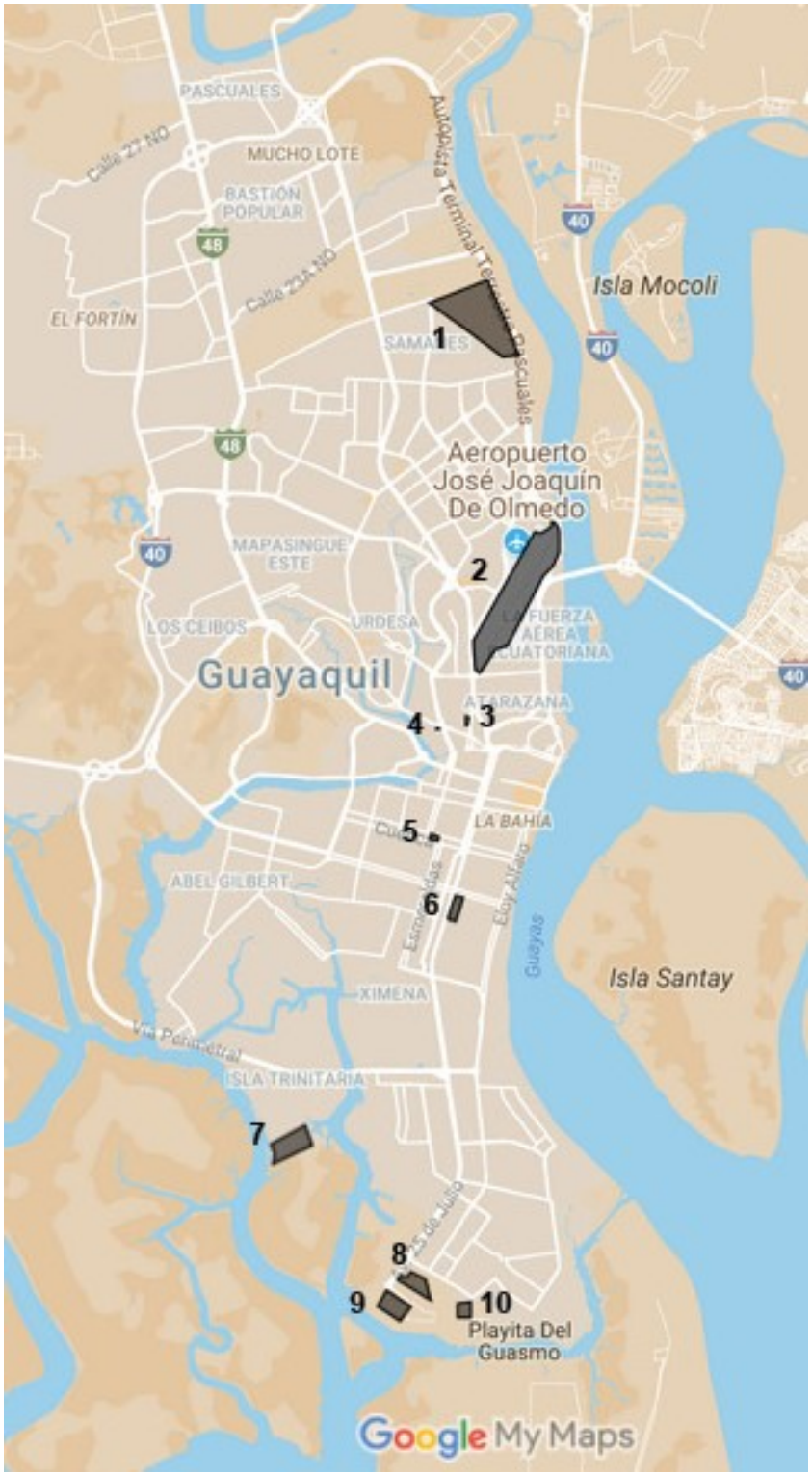

Figure H.1: Locations of possible underground basins (Google, ndb)

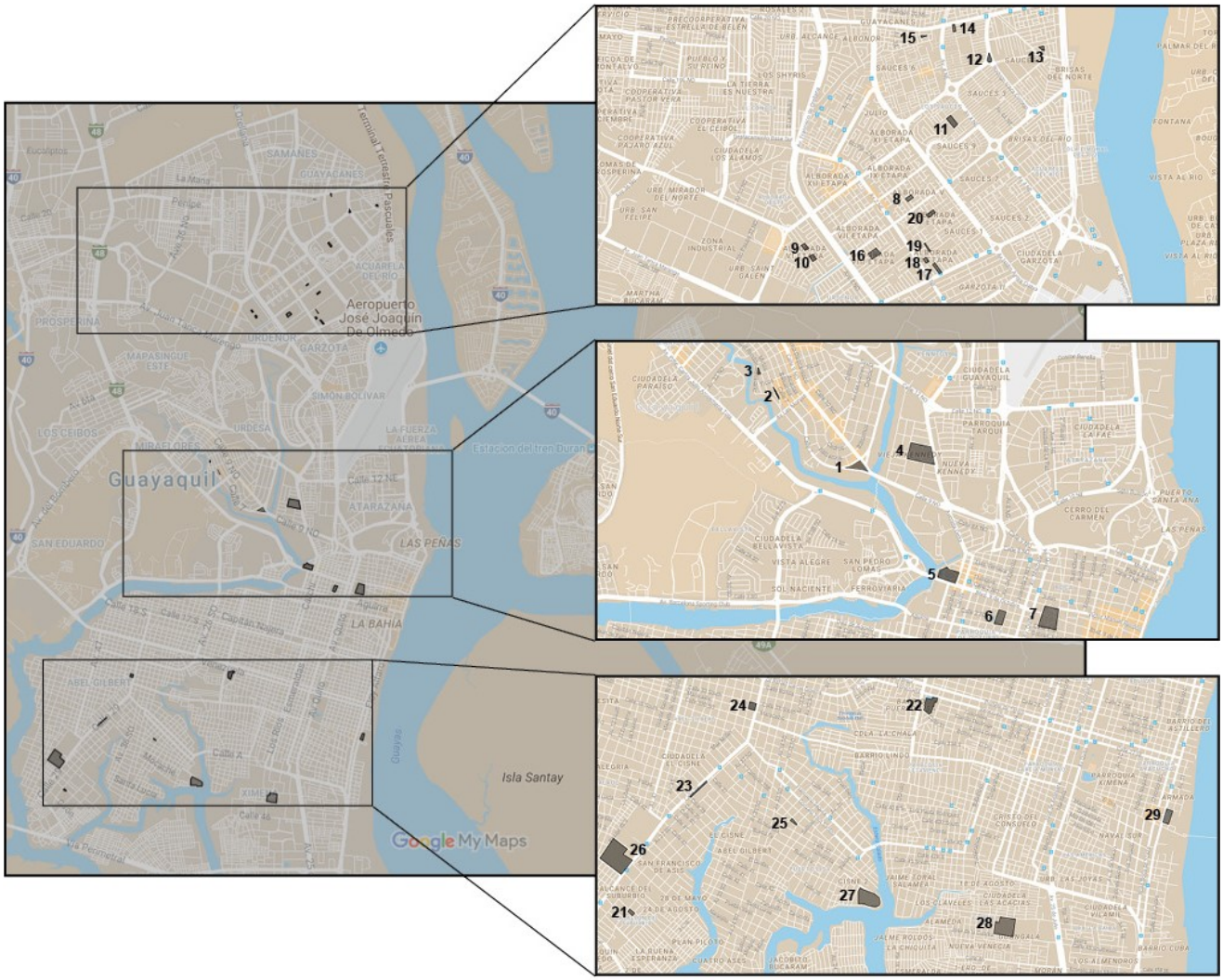

Figure H.2: Locations of possible water squares (Google, ndb)

Table H.1: Sizes of possible water squares

Location [#]	Size [m^2]	Location [#]	Size [m^2]
1	10500	16	8430
2	1950	17	4690
3	1460	18	2330
4	43700	19	1970
5	23100	20	4110
6	12500	21	3180
7	36500	22	16800
8	3220	23	5620
9	3510	24	6820
10	3390	25	2440
11	7640	26	71300
12	3480	27	35400
13	2500	28	39300
14	2520	29	11100
15	1210		

H.2. Soil profiles of park locations

Table H.2: Coordinates of soil profiles (in PSAD56 and WGS84 coordinate system)

	PSAD56		WGS84	
ID	x-coordinate	y-coordinate	x-coordinate	y-coordinate
39	623798.71	9758299.59	623515.63	9757923.41
49	621219.96	9760619.75	620962.09	9760245.35
115	623205.17	9755678.84	622947.28	9755304.48
132	621606.68	9756946.99	621348.80	9756572.62
174	618224.73	9755090.23	617966.87	9754715.88
204	624635.63	9765593.90	624377.74	9765219.46
209	623826.55	9761767.23	623543.47	9761391.02
220	622858.48	9759934.78	622600.59	9759560.39
244	622757.76	9754078.43	622474.68	9753702.28
254	622830.16	9763633.98	622572.28	9763259.56
303	617863.01	9754961.57	617579.97	9754585.42
307	618520.73	9755887.27	618262.87	9755512.91
313	619670.98	9756667.10	619413.11	9756292.74
348	623979.17	9755452.03	623696.08	9755075.87
359	619954.85	9755302.13	619696.98	9754927.78
360	619925.92	9755275.98	619642.86	9754899.82
381	623483.60	9758334.66	623200.52	9757958.48
403	621603.01	9763679.57	621345.14	9763305.15
412	623249.56	9764244.63	622991.68	9763870.20
449	622079.52	9759755.38	621821.64	9759380.99
545	622978.36	9758556.44	622695.28	9758180.25
585	623252.49	9765314.10	622994.61	9764939.67

Table H.3: Soil profiles near the possible water square locations

			Liquid Limit (%)					Plastic Limit (%)					Plasticity Index					Sand (4.75-0.075 mm)					Fines <0.075 mm						
Park	ID	Distance [m]	LL0_2	LL2_4	LL4_6	LL6_8	LL8_10	IP0_2	IP2_4	IP4_6	IP6_8	IP8_10	PI_2	PI_4	PI_6	PI_8	PI_10	ARE0_2	ARE2_4	ARE4_6	ARE6_8	ARE8_10	FIN0_2	FIN2_4	FIN4_6	FIN6_8	FIN8_10	Soil classification	Infiltration rate [mm/hour]
1	449	0	116	115	112	111	105	76	69	66	70	55	40	46	46	41	50	0	0	0	0	0	100	100	100	100	100	Highly plastic clay	15
2	49	128	84.35	67.18		90.8	70.06	60.42	43.52	n/a	55.99	40.85	23.93	23.66		34.81	27.87	1.54	1.52	n/a	3.58	1.69	98.46	98.48		96.42	98.31	Plastic clay	15
3	49	229	84.35	67.18		90.8	70.06	60.42	43.52	n/a	55.99	40.85	23.93	23.66		34.81	29.21	1.54	1.52	n/a	3.58	1.69	98.46	98.48		96.42	98.31	Plastic clay	15
4	220	208																0.71	5.43	31.01	39.15	41.48	99.29	94.57	68.99	60.85	58.52	Clay	15
5	545	133	86	69.5	53.5	0	43.5	47	36.5	26	0	16	39	33		0	33	5	1.5	2.5	51.55	15.7	95	98.5	97.5	48.45	84.3	Plastic clay	15
6	381	75	87	72	69.21	40		67.52	53.44	54.83	23.12		19.48	18.56		16.88	0	16.4	1.62	5.6	10.8	56.23	83.6	98.38	94.4	89.2	43.77	Sandy clay	15
7	39	152	56.85	86.58	95.53	0	41.95	36.53	62.76	61.73	0	22.3	20.32	23.82	33.8	0	19.65	6.21	0	0.7	89.73	4.76	93.79	100	99.3	10.27	95.24	Plastic clay	15
8	412	350	26					11					15					90					10					Not enough data	–
9	403	245	37					18					19					72					28					Not enough data	–
10	403	354	37					18					19					72					28					Not enough data	–
11	585	430		62	60				38	35.3				24	24.7				46	38				54	62			Clayey sand	51
12	585	526		62	60				38	35.3				24	24.7				46	38				54	62			Clayey sand	51
13	204	357	83.2	100.95	103.8	101.3	61.9	56.65	62.96	62.32	61.69	34.2	26.55	37.99	41.48	39.61	10.53	0.44	0.83	0.46	1.09	12.92	99.56	99.17	99.54	98.91	87.08	Plastic clay	15
14	585	640		62	60				38	35.3				24	24.7				46	38				54	62			Clayey sand	51
15	585	500		62	60				38	35.3				24	24.7				46	38				54	62			Clayey sand	51
16	254	280	63.47	106.74	132.38	131.13	73.29	39.36	73.52	89.42	93.34	47.39	24.11	33.22	42.96	37.79	25.9	15.25	0.95	4.91	2.21	32.27	84.75	99.05	95.09	97.79	67.74	Sandy clay	15
17	254	437	63.47	106.74	132.38	131.13	73.29	39.36	73.52	89.42	93.34	47.39	24.11	33.22	42.96	37.79		15.25	0.95	4.91	2.21	32.27	84.75	99.05	95.09	97.79	67.74	Sandy clay	15
18	254	303	63.47	106.74	132.38	131.13	73.29	39.36	73.52	89.42	93.34	47.39	24.11	33.22	42.96	37.79	25.9	15.25	0.95	4.91	2.21	32.27	84.75	99.05	95.09	97.79	67.74	Sandy clay	15
19	254	270	63.47	106.74	132.38	131.13	73.29	39.36	73.52	89.42	93.34	47.39	24.11	33.22	42.96	37.79		15.25	0.95	4.91	2.21	32.27	84.75	99.05	95.09	97.79	67.74	Sandy clay	15
20	412	311	26					11					15					90					10					Not enough data	–
21	174	708	75.7	102.3	75.72			48.26	71.4	47.59			27.44	30.9	28.13			0.36	2.7	16.45			99.74	97.3	83.55			Plastic clay	15
22	132	380	128.3	152.8	111	104.7		96.06	117.1	81.67	68.57		32.24	35.7	29.33	36.13		0.35	0.22	0.3	1.19		99.65	99.78	99.71	98.81		Highly plastic clay	15
23	307	444	61	45	49			33	24.5	25			28	20.5	24			0.62	0.63	1.44	n/a		99.38	99.37	98.56			Plastic clay	15
24	313	192	89	69	72.5	66		57	34	36.75	31		32	35	35.75	35		0.18	0.77	1.43	1.63		99.82	99.23	98.57	98.37		Plastic clay	15
25	359	60	97	108	117.5	123	123.5	66	74	84	88	89	31	34	33.5	35	34.5											Not enough data	–
26	303	195	56	46	53.67			29	23.75	30.67			27	22.25	23	0	0	0.36	0.72	4.05			99.64	99.28	95.95			Plastic clay	15
27	360	1151	101	115		124	110	64	78		85	72		37	0													Not enough data	–
28	244	566	49.49	97.73	106.94	95.66	117.81	27.08	62.43	70.69	61.51	78.67		35.3	36.25			83.15	0.84	2.15	3.6	2	16.85	99.16	97.85	96.4	98	Plastic clay	15
29	348	0	78	87.5	85	75.5	83	49	55	53.67	46.5	61.5	29	32.5	31.33	29	21.5	1.08	0	2.36	10.12	8.81	98.92	100	97.64	89.89	91.19	Sandy clay	15